Persoonia 41, 2018: 142–174
www.ingentaconnect.com/content/nhn/pimj

RESEARCH ARTICLE

ISSN (Online) 1878-9080
https://doi.org/10.3767/persoonia.2018.41.08

Unravelling species boundaries in the *Aspergillus viridinutans* complex (section *Fumigati*): opportunistic human and animal pathogens capable of interspecific hybridization

V. Hubka[1,2,3]*, V. Barrs[4#], Z. Dudová[1,3#], F. Sklenář[1,2#], A. Kubátová[1], T. Matsuzawa[5], T. Yaguchi[6], Y. Horie[6], A. Nováková[2], J.C. Frisvad[7], J.J. Talbot[4], M. Kolařík[2]

Key words

Aspergillus felis
Aspergillus fumigatus
invasive aspergillosis
mating-type genes
multispecies coalescence model
Neosartorya udagawae
scanning electron microscopy
soil fungi

Abstract Although *Aspergillus fumigatus* is the major agent of invasive aspergillosis, an increasing number of infections are caused by its cryptic species, especially *A. lentulus* and the *A. viridinutans* species complex (AVSC). Their identification is clinically relevant because of antifungal drug resistance and refractory infections. Species boundaries in the AVSC are unresolved since most species have uniform morphology and produce interspecific hybrids *in vitro*. Clinical and environmental strains from six continents (n = 110) were characterized by DNA sequencing of four to six loci. Biological compatibilities were tested within and between major phylogenetic clades, and ascospore morphology was characterised. Species delimitation methods based on the multispecies coalescent model (MSC) supported recognition of ten species including one new species. Four species are confirmed opportunistic pathogens; *A. udagawae* followed by *A. felis* and *A. pseudoviridinutans* are known from opportunistic human infections, while *A. felis* followed by *A. udagawae* and *A. wyomingensis* are agents of feline sino-orbital aspergillosis. Recently described human-pathogenic species *A. parafelis* and *A. pseudofelis* are synonymized with *A. felis* and an epitype is designated for *A. udagawae*. Intraspecific mating assay showed that only a few of the heterothallic species can readily generate sexual morphs *in vitro*. Interspecific mating assays revealed that five different species combinations were biologically compatible. Hybrid ascospores had atypical surface ornamentation and significantly different dimensions compared to parental species. This suggests that species limits in the AVSC are maintained by both pre- and post-zygotic barriers and these species display a great potential for rapid adaptation and modulation of virulence. This study highlights that a sufficient number of strains representing genetic diversity within a species is essential for meaningful species boundaries delimitation in cryptic species complexes. MSC-based delimitation methods are robust and suitable tools for evaluation of boundaries between these species.

Article info Received: 28 September 2017; Accepted: 14 March 2018; Published: 21 June 2018.

INTRODUCTION

Aspergillus is a speciose genus with almost 400 species classified into six subgenera and approximately 25 sections (Samson et al. 2014, Jurjević et al. 2015, Hubka et al. 2016a, 2017, Chen et al. 2016a, b, 2017, Kocsubé et al. 2016, Sklenář et al. 2017, Tanney et al. 2017). The species are widely distributed in nature and have a significant economic impact in human and animal health (causative agents of aspergillosis; allergies and respiratory problems associated with presence of fungi in the indoor environment), the food industry (source of enzymes and organic acids for fermentation, food and feed spoilage, production of hazardous mycotoxins), biotechnology and pharmacology (production of bioactive substances, heterologous proteins) (Pitt & Hocking 2009, Meyer et al. 2011, Frisvad & Larsen 2015b, Sugui et al. 2015, Gautier et al. 2016).

Aspergillus sect. *Fumigati* includes approximately 60 species occurring predominantly in soil (Hubka et al. 2017). Many are of considerable medical importance as they cause human and animal infections (Balajee et al. 2005b, 2009, Katz et al. 2005, Yaguchi et al. 2007, Hubka et al. 2012, Talbot & Barrs 2018). *Aspergillus fumigatus* is usually reported as both the most common member of the section in soil worldwide and the most common cause of aspergillosis (Klich 2002, Domsch et al. 2007, Mayr & Lass-Flörl 2011). A series of recent studies highlighted the high prevalence (11–19 %) of so-called cryptic *Aspergillus* species in clinical samples (Balajee et al. 2009, Alastruey-Izquierdo et al. 2013, Negri et al. 2014, Sabino et al. 2014). Their identification is clinically relevant since many demonstrate drug resistance to commonly used antifungals, thus their recognition influences therapeutic management. Reliable identification of clinical isolates to the species level and susceptibility testing by reference methods is thus warranted (Lyskova et al. 2018). Many of these less common pathogens belong to sect. *Fumigati* and the highest numbers of infections are attributed to *A. lentulus*, *A. thermomutatus* (syn. *Neosartorya pseudofischeri*) and species from *A. viridinutans* species complex (AVSC) (Balajee et al. 2005a, 2006, Sugui et al. 2010, 2014, Barrs et al. 2013, Talbot & Barrs 2018).

[1] Department of Botany, Faculty of Science, Charles University, Benátská 2, 128 01 Prague 2, Czech Republic.
[2] Laboratory of Fungal Genetics and Metabolism, Institute of Microbiology of the CAS, v.v.i, Vídeňská 1083, 142 20 Prague 4, Czech Republic.
[3] First Faculty of Medicine, Charles University, Kateřinská 32, 121 08 Prague 2, Czech Republic.
[4] Sydney School of Veterinary Science, Faculty of Science, and Marie Bashir Institute of Infectious Diseases & Biosecurity, University of Sydney, Camperdown, NSW, Australia.
[5] University of Nagasaki, 1-1-1 Manabino, Nagayo-cho, Nishi-Sonogi-gun, Nagasaki 851-2195, Japan.
[6] Medical Mycology Research Center, Chiba University, 1-8-1, Inohana, Chuo-ku, Chiba 260-8673, Japan.
[7] Department of Biotechnology and Biomedicine, Technical University of Denmark, Kongens Lyngby, Denmark.
* corresponding author e-mail: hubka@biomed.cas.cz.
# These co-authors contributed equally to this work.

Table 1 List of *Aspergillus* strains, information on isolation source and reproductive strategy.

Species / Culture collection nos.[1,2]	Locality, substrate, year of isolation[3]	*MAT* locus[4,5]
Aspergillus acrensis		
IFM 57291^T = CCF 4670^T (01-BA-462-5)	Brazil, Acre, Xapuri, grassland soil in cattle farm, 2001	MAT1-1-1
IFM 57290 = CCF 4666 (01-BA-666-5)	Brazil, Amazonas, Manaus, tropical rain forest soil, 2001	MAT1-2-1
CCF 4959 (S973)	Romania, Movile cave, above the Lake Room, cave sediment, 2014	MAT1-2-1
CCF 4960 (S974)	Romania, Movile cave, cave sediment, 2014	MAT1-2-1
CCF 4961 (S975)	Romania, Movile cave, Lake Room, cave sediment, 2014	MAT1-1-1
A. arcoverdensis		
IFM 61334^T = JCM 19878^T = CCF 4900^T (6-2-32)	Brazil, Pernambuco, near Arcoverde, semi-desert soil in a caatinga area, 2011	MAT1-1-1
IFM 61333 = CCF 4899 (10-2-3)	Brazil, Pernambuco, near Arcoverde, semi-desert soil in a caatinga area, 2011	MAT1-1-1
IFM 61337 = JCM 19879 = CCF 4901 (1-1-34)	Brazil, Pernambuco, near Arcoverde, semi-desert soil in a caatinga area, 2011	MAT1-1-1
IFM 61338 = JCM 19880 = CCF 4902 (6-2-3)	Brazil, Pernambuco, near Arcoverde, semi-desert soil in a caatinga area, 2011	MAT1-2-1
IFM 61339 = CCF 4903 (2-1-11)	Brazil, Pernambuco, near Arcoverde, semi-desert soil in a caatinga area, 2011	MAT1-1-1
IFM 61340 = CCF 4904 (7-2-33)	Brazil, Pernambuco, near Arcoverde, semi-desert soil in a caatinga area, 2011	MAT1-1-1
IFM 61345 = CCF 5633 (3-2-2)	Brazil, Pernambuco, near Arcoverde, semi-desert soil in a caatinga area, 2011	MAT1-2-1
IFM 61346 = CCF 4906 (4-2-14)	Brazil, Pernambuco, near Arcoverde, semi-desert soil in a caatinga area, 2011	MAT1-2-1
IFM 61349 = CCF 4907 (4-2-9)	Brazil, Pernambuco, near Arcoverde, semi-desert soil in a caatinga area, 2011	MAT1-2-1
IFM 61362 = CCF 4908 (5-2-2)	Brazil, Pernambuco, near Arcoverde, semi-desert soil in a caatinga area, 2011	MAT1-2-1
IFM 59922 = CCF 4560 (08-SA-2-2)	China, soil, 2008	MAT1-1-1
IFM 59923 = CCF 4569 (08-SA-2-1)	China, soil, 2008	MAT1-1-1
FRR 1266 = CBS 121595 = DTO 019-F2 = CCF 4574	Australia, New South Wales, Warrumbungle National Park, sandy soil, 1971	MAT1-1-1
A. aureolus		
IFM 47021^T = IFM 46935^T = IFM 53589^T = CBS 105.55^T = NRRL 2244^T = IMI 06145^T = KACC 41204^T = KACC 41095^T = CCF 4644^T = CCF 4646^T = CCF 4648^T	Ghana, Tafo, soil, 1950	homothallic
IFM 46584 = IFM 46936 = CBM-FA-0692 = CCF 4645 = CCF 4647	Brazil, São Paulo State, Botucatú, soil, 1993	homothallic
IFM 53615 = CBM-FA-934 = CCF 4571 (ex-type of *A. indohii*)	Brazil, Acre, Cruzeiro do Sul, soil in a grassland in a tropical rain forest, 2001	homothallic
IHEM 22515 (RV 71215)	Peru, Lima, human cornea, < 1995	homothallic
A. felis		
CBS 130245^T = DTO 131-F4^T = CCF 5620	Australia, Sydney, retrobulbar mass, sino-orbital aspergillosis in a 3.5-year-old DSH cat, MN, 2008	MAT1-2-1 (KC797620)
NRRL 62900 = CM-3147 = CCF 4895 (ex-type of *A. parafelis*)	Spain, human oropharyngeal exudate, 2004	MAT1-2-1 (KJ858505)
NRRL 62903 = CM-6087 = CCF 4897 (ex-type of *A. pseudofelis*)	Spain, human sputum, 2010	MAT1-2-1 (KJ858507)
NRRL 62901 = CM-5623 = CCF 4896 = CCF 4557 (Viridi-Pinh)	Portugal, bronchoalveolar lavage, chronic invasive aspergillosis in a 56-year-old male, 2007	MAT1-1-1 (KJ858506)
IFM 59564 = CCF 5612	Japan, human, sputum, 2011	MAT1-2-1
IFM 60053 = CCF 4559	Japan, abscess near thigh bone, 40-year-old man with osteomyelitis, 2012	MAT1-1-1 (HF937392)
IFM 54303 = CCF 4570	Japan, human, clinical material, < 2007	MAT1-1-1
FRR 5679 = CCF 5613 (MK246)	Australia, thoracic mass in a cat, < 2005	MAT1-2-1
FRR 5680 = CCF 5615 (MK284)	Australia, retrobulbar mass, sino-orbital aspergillosis in a cat, < 2005	MAT1-2-1
CCF 2937	Czech Republic, near Kladno, soil of spoil-bank, 1993	MAT1-2-1 (**LT796767**)
CCF 4002 (AK 196/07)	Czech Republic, Markovičky, near Kutná Hora, old silver mine waste dump, 2007	MAT1-2-1
CCF 4003 (AK 27/07)	Czech Republic, Chvaletice, soil crust, abandoned tailing pond, 2007	MAT1-2-1
CCF 4171 = CMF ISB 2162 = IFM 60852 (F39)	USA, Wyoming, Glenrock, soil from coal mine dump, 2010	MAT1-2-1 (**LT796766**)
CCF 4172 (F47)	Spain, Andalusia, Aracena, Gruta de la Maravillas, cave air, 2010	ND
CCF 4148 = CMF ISB 1975 = IFM 60868 (F22)	USA, Wyoming, Glenrock, soil from coal mine dump, 2010	MAT1-1-1 (**LT796760**)
CCF 4376 (AK 102/11)	Czech Republic, Krušné hory, near Abertamy, soil from old dump, 2011	MAT1-1-1
CCF 4497 = CMF ISB 1936 (F6)	USA, Wyoming, Glenrock, soil from coal mine dump, 2010	MAT1-2-1
CCF 4498 = IFM 60853 (F49)	USA, Wyoming, Glenrock, soil from coal mine dump, 2010	MAT1-2-1
DTO 131-E4 = CCF 5609 (2384/07)	Australia, Brisbane, retrobulbar mass, sino-orbital aspergillosis, 7-year-old DSH cat, FN, 2007	MAT1-2-1 (KC797622)
DTO 131-E5 = CCF 5610 (4091/09)	Australia, Brisbane, retrobulbar mass, sino-orbital aspergillosis, 3-year-old Himalayan cat, FN, 2009	MAT1-1-1 (KC797627)
DTO 131-G1 = CCF 5611 (834/07)	Australia, Sydney, retrobulbar mass, sino-orbital aspergillosis, 2-year-old Himalayan cat, MN, 2007	MAT1-2-1 (KC797625)
CCF 5614 (14/4138)	Australia, Sydney, retrobulbar mass, sino-orbital aspergillosis, 5-year-old cat, Ragoll, MN, 2013	ND
CCF 5616 (Felix H. D)	Australia, Canberra, retrobulbar mass, sino-orbital aspergillosis, 8-year-old domestic longhair cat	ND
DTO 131-F1 = CCF 5617 (66/10)	Australia, Brisbane, retrobulbar mass, sino-orbital aspergillosis, 5-year-old DSH cat, FN, 2010	MAT1-1-1 (KC797629)
CCF 5618 (Luigi C.)	Australia, Sydney, retrobulbar mass, sino-orbital aspergillosis, 2-year-old BSH cat, MN, 2012	MAT1-2-1
CBS 130248 = DTO 131-G3 = CCF 5619 (1767/10)	Australia, Brisbane, retrobulbar mass, sino-orbital aspergillosis, 4-year-old DSH cat, FN, 2010	MAT1-2-1 (KC797621)
CBS 130249 = DTO 155-G3 = CCF 5621 (1207/05)	Australia, Sydney, vitreous humor, disseminated invasive apsergillosis 9-year-old Old English Sheepdog, MN, 2005	MAT1-2-1
DTO 131-F2 = CCF 5622 (3532/09)	Australia, Brisbane, retrobulbar mass, sino-orbital aspergillosis, 4.5-year-old Ragdoll cat, MN, 2009	MAT1-2-1
CBS 130247 = DTO 131-G2 = CCF 5623 (1020/07)	Australia, Sydney, retrobulbar mass, sino-orbital aspergillosis, 2-year-old DSH cat, FN, 2007	MAT1-1-1 (KC797632)

Table 1 (cont.)

Species / Culture collection nos.[1,2]	Locality, substrate, year of isolation[3]	*MAT* locus[4,5]
A. felis (cont.)		
DTO 131-E9 = CCF 5624 (1848/08)	Australia, Brisbane, retrobulbar mass, sino-orbital aspergillosis, 1.5-year-old DSH cat, MN, 2008	MAT1-1-1 (KC797628)
DTO 131-E3 = CCF 5625 (3008/08 D)	Australia, Brisbane, retrobulbar mass, sino-orbital aspergillosis, 8-year-old Persian cat, FN, 2008	MAT1-1-1 (KC797634)
DTO 131-F6 = CCF 5626 (8651/09)	Australia, Brisbane, retrobulbar mass, sino-orbital aspergillosis, 8-year-old DSH cat, MN, 2009	MAT1-2-1 (KC797624)
CBS 130244 = DTO 131-E6 = CCF 5627 (4067/09D)	Australia, Sydney, retrobulbar mass, sino-orbital aspergillosis, 5-year-old Cornish Rex cat, FN, 2009	MAT1-1-1 (KC797630)
DTO 131-F3 = CCF 5628 (2188/08)	Australia, Brisbane, retrobulbar mass, sino-orbital aspergillosis, 7-year-old DSH cat, FN, 2008	MAT1-2-1
CBS 130246 = DTO 131-F9 = CCF 5629 (448/08)	Australia, Sydney, nasal cavity, sino-nasal aspergillosis 13-year-old DLH cat, MN, 2008	MAT1-1-1 (KC797631)
A. frankstonensis		
CBS 142233^{T} = IBT 34172^{T} = DTO 341-E7^{T} = CCF 5799^{T}	Australia, Victoria, Frankston, woodland soil, 2015	MAT1-2-1
CBS 142234 = IBT 34204 = DTO 341-F3 = CCF 5798	Australia, Victoria, Frankston, woodland soil, 2015	MAT1-2-1
A. pseudoviridinutans		
NRRL 62904^{T} = CCF 5631 (NIHAV1, 1720)	USA, U.S. National Institutes of Health, mediastinal lymph node, 14-year-old boy with chronic granulomatous disease, 2004	MAT1-1-1 (KJ858509)
CBS 458.75 = KACC 41203 = IHEM 9862 (ex-type of *A. fumigatus* var. *sclerotiorum*)	India, Lucknow, Mohanlalganj, soil, < 1971	MAT1-2-1
IMI 182127 = KACC 41614 = CCF 5630	Srí Lanka, *Pinus caribea*, < 1974	MAT1-2-1
IFM 55266 = CCF 5644	Japan, human, lung, 2004	MAT1-1-1
IFM 57289 = CCF 4665	Brazil, Mato Grosso, soil	MAT1-2-1
IFM 59502 = CCF 4561	Japan, cornea, keratomycosis, 26-year-old woman, 2011	MAT1-1-1
IFM 59503 = CCF 4562	Japan, cornea, keratomycosis, 26-year-old woman, 2011	MAT1-1-1
CCF 5632 (NIHAV2, 2594)	USA, lung biopsy, 8-year-old boy with hyperimmunoglobulin-E syndrome, 2004	MAT1-1-1 (**LT796761**)
A. siamensis		
IFM 59793^{T} = KUFC 6349^{T} = CCF 4685^{T}	Thailand, Chonburi Province, Samaesarn Island, coastal forest soil, 2008	homothallic
IFM 61157 = KUFC 6397 = CCF 4686	Thailand, Chiang Mai, termite nest soil, 2009	homothallic
A. udagawae		
IFM 46972^{T} = CBS 114217^{T} = DTO 157-D7^{T} = CBM-FA 0702^{T} = KACC 41155^{T} = CCF 4558^{T}	Brazil, São Paulo State, Botucatú, Lagoa Seka Avea, plantation soil, 1993	MAT1-1-1
IFM 46973 = CBS 114218 = DTO 157-D8 = CBM-FA 0703 = KACC 41156 = CCF 5672	Brazil, São Paulo State, Botucatú, Lagoa Seka Avea, plantation soil, 1993	MAT1-2-1
IFM 5058 = CCF 4662	Japan, human, eye	MAT1-1-1
IFM 51744 = CCF 4671	Japan, human, clinical material, 2002	MAT1-1-1
IFM 53868 = CCF 4667	Japan, human, clinical material, 2004	MAT1-2-1
IFM 54131 = CBM-FA-0697 = CCF 4663	China, Shaanxi, soil, 1994	MAT1-1-1
IFM 54132 = CBM-FA-0698 = CCF 4664	China, Shaanxi, soil, 1994	MAT1-2-1
IFM 54745 = CBM-FA-694 = CCF 4661	China, Shaanxi, soil, 1994	MAT1-1-1
IFM 55207 = NBRC 31952 = CCF 4660	Russia, soil, 1985	MAT1-2-1
IFM 62155 = CCF 4668	Brazil, soil, 2008	MAT1-1-1
CCF 4475 (F2)	USA, Wyoming, Glenrock, prairie soil, 2010	MAT1-2-1
CCF 4476 (F32)	USA, Wyoming, Glenrock, soil, mine waste dump, 2010	MAT1-1-1
CCF 4478 = CMF ISB 2193 (F66)	USA, Wyoming, Gilette, soil, mine waste dump, 2011	MAT1-2-1
CCF 4479 = CMF ISB 2189 (F70)	USA, Illinois, soil, mine waste dump, 2011	MAT1-2-1
CCF 4481 = CMF ISB 2191 (F83)	USA, Wyoming, Gilette, soil, mine waste dump, 2011	MAT1-2-1
CCF 4491 = CMF ISB 1971 (F3)	USA, Wyoming, Glenrock, prairie soil, 2010	MAT1-2-1
CCF 4492 (F21)	USA, Wyoming, Glenrock, soil, mine waste dump, 2010	MAT1-2-1 (HF937389)
CCF 4494 (F44)	USA, Wyoming, Glenrock, prairie soil, 2010	MAT1-2-1
CMF ISB 1972 = CCF 4502 (F11)	USA, Wyoming, Glenrock, soil, mine waste dump, 2010	MAT1-2-1
CMF ISB 2190 = CCF 5635 (F76)	USA, Indiana, soil, mine waste dump, 2011	MAT1-1-1
CMF ISB 2509 = CCF 5636 (F20)	USA, Wyoming, Glenrock, soil, mine waste dump, 2010	MAT1-2-1
CCF 5637 (F37)	USA, Wyoming, Gilette, soil, mine waste dump, 2008	MAT1-1-1
CCF 5638 (3C8)	USA, Philadelphia, retrobulbar mass, sino-orbital aspergillosis, 4-year-old Persian cat, MN, 2012	MAT1-1-1
DTO 166-D6 = CCF 5639 (11.3356, Milo)	Australia, Sydney, retrobulbar mass, sino-orbital aspergillosis 2-year-old DSH cat, MN, 2011	ND
CCF 5634 (B3)	Czech Republic, Hostěradice, earthworm casts, 2012	MAT1-2-1
A. viridinutans		
IFM 47045^{T} = IFM 47046^{T} = IMI 367415^{T} = IMI 062875^{T} = NRRL 4365^{T} = NRRL 576^{T} = CBS 127.56^{T} = KACC 41142^{T} = CCF 4382^{T} = CCF 4568^{T}	Australia, Victoria, Frankston, rabbit dung, 1954	MAT1-1-1 (HF937390)
A. wyomingensis		
CCF 4417^{T} = CMF ISB 2494^{T} = CBS 135456^{T} (F30)	USA, Wyoming, Glenrock, soil, mine waste dump, 2010	MAT1-1-1 (HF937391)
CCF 4169 = CMF ISB 2486 (F24)	USA, Wyoming, Glenrock, soil, 2010	MAT1-1-1

Table 1 (cont.)

Species / Culture collection nos.[1,2]	Locality, substrate, year of isolation[3]	*MAT* locus[4,5]
A. wyomingensis (cont.)		
CCF 4170 = CMF ISB 2485 (F12)	USA, Wyoming, Glenrock, soil, 2010	MAT1-2-1 (**LT796765**)
CCF 4411 = CMF ISB 1977 = IFM 60854 (F5)	USA, Wyoming, Glenrock, soil, mine waste dump, 2010	MAT1-2-1
CCF 4412 (F9)	USA, Wyoming, Glenrock, soil, mine waste dump, 2010	MAT1-1-1
CCF 4413 = CMF ISB 2317 (F10)	USA, Wyoming, Glenrock, soil, mine waste dump, 2010	MAT1-1-1
CCF 4414 = CMF ISB 1974 = IFM 60856 (F13)	USA, Wyoming, Glenrock, soil, mine waste dump, 2010	MAT1-1-1 (**LT796762**)
CCF 4415 = CMF ISB 2487 (F28)	USA, Wyoming, Glenrock, soil, mine waste dump, 2010	MAT1-1-1
CCF 4416 = CMF ISB 1976 = CBS 135455 (F29)	USA, Wyoming, Glenrock, soil, mine waste dump, 2010	MAT1-2-1 (HF937388)
CCF 4418 = CMF ISB 2162 = IFM 60855 (F31)	USA, Wyoming, Glenrock, soil, mine waste dump, 2010	MAT1-2-1
CCF 4419 = CMF ISB 2495 (F53)	USA, Wyoming, Glenrock, soil, mine waste dump, 2010	MAT1-2-1
CCF 4420 = CMF ISB 2491 (F60)	USA, Wyoming, Glenrock, soil, mine waste dump, 2010	MAT1-1-1
IMI 133982 = CCF 4383	Russia, Moscow, soil, < 1968	MAT1-1-1 (**LT796763**)
IFM 59681 = CCF 4563	China, Urumqi, soil, 2008	MAT1-2-1 (**LT796764**)
DTO 155-G2 = CCF 5640 (Yogurt R.)	Australia, Melbourne, retrobulbar mass in a 1.5-year-old BSH cat, MN, 2010	MAT1-2-1
outgroup		
A. lentulus NRRL 35552^T = CBS 117885^T = IBT 27201^T = KACC 41940^T	USA, human, clinical material	MAT1-2-1

[1] Culture collection acronyms: CBM-FA = Natural History Museum & Institute, Chiba, Japan; CBS = CBS culture collection housed at the Westerdijk Institute, Utrecht, The Netherlands; CCF = Culture Collection of Fungi, Prague, Czech Republic; CM = Filamentous fungus collection of the Spanish National Center for Microbiology, Madrid, Spain; CMF ISB = Collection of Microscopic Fungi, Institute of Soil Biology, Academy of Sciences of the Czech Republic, České Budějovice, Czech Republic; DTO = working collection of the Applied and Industrial Mycology department housed at the Westerdijk Institute, Utrecht, The Netherlands; FRR = Food Fungal Culture Collection, North Ryde, Australia; IBT = culture collection of the DTU Systems Biology, Lyngby, Denmark; IFM = Collection at the Medical Mycology Research Centre, Chiba University, Japan; IHEM = Belgian Coordinated Collections of Micro-organisms (BCCM/IHEM), Brussels, Belgium; IMI = CABI's collection of fungi and bacteria, Egham, UK; JCM = Japan Collection of Microorganisms, Tsukuba, Japan; KACC = Korean Agricultural Culture Collection, Wanju, South Korea; KUFC = Kasetsart University Fungal Collection, Bangkok, Thailand; NBRC (IFO) = Biological Resource Center, National Institute of Technology and Evaluation, Chiba, Japan; NRRL = Agricultural Research Service Culture Collection, Peoria, Illinois, USA.

[2] Original numbers of strains and personal strain designations are given in parentheses.

[3] BSH = British shorthair; DLH = domestic longhair; DSH = domestic shorthair; FN = female neutered (desexed); MN = male neutered; ND = not determined.

[4] When available, sequence number in public database is given in parentheses; in the remaining cases, the MAT idiomorph was confirmed only on the electrophoretogram (specific PCR and length of amplicons).

[5] Sequences generated in this study are in **bold**.

Homothallism is a predominant reproductive mode in sect. *Fumigati* and many species readily produce ascomata (neosartorya-morph) in culture, while others are heterothallic or have an unknown sexual morph (Hubka et al. 2017). Homothallic species are infrequently pathogenic, although *A. thermomutatus* is a notable exception. The majority of clinically relevant species belong to the *A. fumigatus* clade (Balajee et al. 2005b, 2009, Yaguchi et al. 2007, Alcazar-Fuoli et al. 2008) or the AVSC (Sugui et al. 2010, 2014, Barrs et al. 2013, Nováková et al. 2014) and are heterothallic. A cryptic sexual cycle of several of these opportunistic pathogens, including *A. fumigatus* (O'Gorman et al. 2009), *A. lentulus* (Swilaiman et al. 2013) and *A. felis* (Barrs et al. 2013), was discovered recently by crossing opposite mating type isolates *in vitro*.

Molecular methods are routinely used for identification of species from sect. *Fumigati* due to overlapping morphological features of their asexual morph. In contrast, the morphology of the sexual morph, especially of ascospores, is amongst the most informative of phenotypic characteristics in sect. *Fumigati*. The taxonomy of AVSC has developed rapidly since eight of the currently 11 recognized species were described in the last four years (Barrs et al. 2013, Eamvijarn et al. 2013, Nováková et al. 2014, Sugui et al. 2014, Matsuzawa et al. 2015, Talbot et al. 2017). The species boundaries delimitation was usually based on comparison of single-gene phylogenies and principles of genealogical concordance. In addition, some studies supported the species concept by results of *in vitro* mating experiments between opposite mating type strains. With the increasing number of species, available isolates and new mating experiment data, the species boundaries in AVSC became unclear as pointed out by Talbot et al. (2017) who used the designation '*A. felis* clade' for *A. felis* and related species. Importantly, Sugui et al. (2014) and Talbot et al. (2017) identified that interpretation of *in vitro* mating assays in sect. *Fumigati* may be problematic because different phylogenetic species in the AVSC were able to produce fertile ascomata when crossed between themselves. Some even mated successfully with *A. fumigatus* s.str.

Here we present a critical re-evaluation of species boundaries in the AVSC. We examined a large set of clinical and environmental strains collected worldwide. We did not use classical phylogenetic methods or genealogical concordance phylogenetic species recognition rules (GCPSR) for species delimitation due to their unsatisfactory results in previous AVSC studies. Such methods, based predominantly on analysis of concatenated DNA sequence data or comparison of single-gene phylogenies are frequently prone to species over-delimitation or are affected by subjective judgements of species boundaries. Instead, we used recently introduced delimitation techniques based on coalescent theory and the multispecies coalescent model (MSC) (Flot 2015). We followed the approach recommended by Carstens et al. (2013) that combines species delimitation, species tree estimation and species validation steps. Although these methods have already been applied to other groups of organisms such as animals and plants their use in fungi is scarce (Stewart et al. 2014, Singh et al. 2015, Liu et al. 2016, Sklenář et al. 2017, Hubka et al. 2018). Here, the results of MSC methods were taken as a basic hypothesis for species delimitation and then further verified by analysis of intra- and interspecific biological compatibilities, as well as ascospore dimensions and ornamentation.

MATERIAL AND METHODS

Fungal strains

A total of 110 isolates were examined including new isolates and isolates obtained from previously published studies (Katz et

Table 2 List of *Aspergillus* strains and sequences used in phylogenetic analysis; accession numbers in **bold** were generated for this study.

Species	Culture collection nos.[1]	GenBank/ENA/DDBJ accession numbers						
		ITS	*benA*	*CaM*	*RPB2*	*act*	*mcm7*	*tsr1*
Aspergillus acrensis	IFM 57291^T = CCF 4670^T	–	**LT795980**	**LT795981**	**LT795982**	**LT795983**	–	–
	IFM 57290 = CCF 4666	–	**LT795976**	**LT795977**	**LT795978**	**LT795979**	–	–
	CCF 4959	–	**LT795984**	LT558741	**LT795985**	**LT795986**	–	–
	CCF 4960	–	**LT795987**	LT558742	**LT795988**	**LT795989**	–	–
	CCF 4961	–	**LT795990**	LT558743	**LT795991**	**LT795992**	–	–
A. arcoverdensis	IFM 61334^T = JCM 19878^T = CCF 4900^T	–	AB818845	**LT795958**	**LT795959**	AB818867	–	–
	IFM 61333 = CCF 4899	–	**LT795954**	**LT795955**	**LT795956**	**LT795957**	–	–
	IFM 61337 = JCM 19879 = CCF 4901	–	AB818846	**LT795960**	**LT795961**	AB818868	–	–
	IFM 61338 = JCM 19880 = CCF 4902	–	AB818847	**LT795962**	**LT795963**	AB818869	–	–
	IFM 61339 = CCF 4903	–	AB818848	**LT795964**	**LT795965**	AB818870	–	–
	IFM 61340 = CCF 4904	–	AB818849	**LT795966**	**LT795967**	AB818871	–	–
	IFM 61345 = CCF 5633	–	AB818850	**LT795968**	**LT795969**	AB818872	–	–
	IFM 61346 = CCF 4906	–	AB818851	**LT795970**	**LT795971**	AB818873	–	–
	IFM 61349 = CCF 4907	–	AB818852	**LT795972**	**LT795973**	AB818874	–	–
	IFM 61362 = CCF 4908	–	AB818853	**LT795974**	**LT795975**	AB818875	–	–
	IFM 59922 = CCF 4560	–	**LT795944**	**LT795945**	**LT795946**	**LT795947**	–	–
	IFM 59923 = CCF 4569	–	AB818844	**LT795948**	**LT795949**	AB818866	–	–
	FRR 1266 = CBS 121595 = DTO 019-F2 = CCF 4574	JX021672	**LT795950**	**LT795951**	**LT795952**	**LT795953**	–	–
A. aureolus	IFM 47021^T = IFM 46935^T = IFM 53589^T = CBS 105.55^T = NRRL 2244^T = IMI 06145^T = KACC 41204^T = KACC 41095^T = CCF 4644^T = CCF 4646^T = CCF 4648^T	EF669950	EF669808	HG426051	EF669738	DQ094861	KJ914718	KJ914750
	IFM 46584 = IFM 46936 = CBM-FA-0692 = CCF 4645 = CCF 4647	–	**LT796001**	HG426050	**LT796002**	**LT796003**	–	–
	IFM 53615 = CBM-FA-934 = CCF 4571 (ex-type of *A. indohii*)	–	AB488757	**LT795998**	**LT795999**	**LT796000**	–	–
	IHEM 22515	–	**LT796004**	**LT796005**	**LT796006**	**LT796007**	**LT796153**	**LT796756**
A. felis	CBS 130245^T = DTO 131-F4^T = CCF 5620	KF558318	KJ914694	KJ914706	KJ914735	**LT795880**	KJ914724	**LT796745**
	NRRL 62900 = CM-3147 = CCF 4895 (ex-type of *A. parafelis*)	–	KJ914692	KJ914702	**LT795839**	**LT795838**	KJ914720	**LT796734**
	NRRL 62903 = CM-6087 = CCF 4897 (ex-type of *A. pseudofelis*)	–	KJ914697	KJ914705	**LT795891**	**LT795892**	KJ914723	**LT796749**
	NRRL 62901 = CM-5623 = CCF 4896 = CCF 4557	–	KJ914693	**LT795813**	**LT795814**	**LT795815**	**LT796152**	**LT796727**
	IFM 59564 = CCF 5612	–	**LT795801**	**LT795802**	**LT795803**	**LT795804**	**LT796126**	**LT796724**
	IFM 60053 = CCF 4559	–	**LT795856**	**LT795857**	**LT795858**	**LT795859**	**LT796138**	**LT796739**
	IFM 54303 = CCF 4570	AB250780	**LT795860**	**LT795861**	**LT795862**	**LT795863**	**LT796139**	**LT796740**
	FRR 5679 = CCF 5613	–	**LT795805**	**LT795806**	**LT795807**	**LT795808**	**LT796127**	**LT796725**
	FRR 5680 = CCF 5615	–	**LT795844**	**LT795845**	**LT795846**	**LT795847**	**LT796135**	**LT796736**
	CCF 2937	–	**LT795816**	**LT795817**	**LT795818**	**LT795819**	**LT796129**	**LT796728**
	CCF 4002	FR733865	FR775350	**LT795824**	**LT795825**	**LT795826**	**LT796131**	**LT796730**
	CCF 4003	FR733866	FR775349	**LT795827**	**LT795828**	**LT795829**	**LT796132**	**LT796731**
	CCF 4171 = CMF ISB 2162 = IFM 60852	–	**LT795840**	**LT795841**	**LT795842**	**LT795843**	**LT796134**	**LT796735**
	CCF 4172	–	**LT795834**	**LT795835**	**LT795836**	**LT795837**	**LT796133**	**LT796733**
	CCF 4148 = CMF ISB 1975 = IFM 60868	HE578063	**LT795868**	**LT795869**	**LT795870**	**LT795871**	–	**LT796741**
	CCF 4376	–	**LT795872**	**LT795873**	**LT795874**	**LT795875**	**LT796141**	**LT796743**
	CCF 4497 = CMF ISB 1936	–	**LT795820**	**LT795821**	**LT795822**	**LT795823**	**LT796130**	**LT796729**
	CCF 4498 = IFM 60853	–	**LT795830**	**LT795831**	**LT795832**	**LT795833**	–	**LT796732**
	DTO 131-E4 = CCF 5609	JX021673	**LT795789**	**LT795790**	**LT795791**	**LT795792**	**LT796123**	**LT796721**
	DTO 131-E5 = CCF 5610	JX021674	**LT795793**	**LT795794**	**LT795795**	**LT795796**	**LT796124**	**LT796722**
	DTO 131-G1 = CCF 5611	JX021682	**LT795797**	**LT795798**	**LT795799**	**LT795800**	**LT796125**	**LT796723**
	CCF 5614	–	**LT795809**	**LT795810**	**LT795811**	**LT795812**	**LT796128**	**LT796726**
	CCF 5616	–	**LT795848**	**LT795849**	**LT795850**	**LT795851**	**LT796136**	**LT796737**
	DTO 131-F1 = CCF 5617	JX021677	**LT795852**	**LT795853**	**LT795854**	**LT795855**	**LT796137**	**LT796738**
	CCF 5618	–	**LT795864**	**LT795865**	**LT795866**	**LT795867**	**LT796140**	**LT796742**
	CBS 130248 = DTO 131-G3 = CCF 5619	JX021684	**LT795876**	**LT795877**	**LT795878**	**LT795879**	**LT796142**	**LT796744**

Table 2 (cont.)

Species	Culture collection nos.[1]	GenBank/ENA/DDBJ accession numbers						
		ITS	*benA*	*CaM*	*RPB2*	*act*	*mcm7*	*tsr1*
A. felis (cont.)	CBS 130249 = DTO 155-G3 = CCF 5621	JX021686	JX021711	JX021713	**LT795881**	**LT795882**	**LT796143**	**LT796746**
	DTO 131-F2 = CCF 5622	JX021678	**LT795883**	**LT795884**	**LT795885**	**LT795886**	**LT796144**	**LT796747**
	CBS 130247 = DTO 131-G2 = CCF 5623	JX021683	**LT795887**	**LT795888**	**LT795889**	**LT795890**	**LT796145**	**LT796748**
	DTO 131-E9 = CCF 5624	JX021676	**LT795893**	**LT795894**	**LT795895**	**LT795896**	**LT796146**	**LT796750**
	DTO 131-E3 = CCF 5625	JX021671	**LT795897**	**LT795898**	**LT795899**	**LT795900**	**LT796147**	**LT796751**
	DTO 131-F6 = CCF 5626	JX021680	**LT795901**	**LT795902**	**LT795903**	**LT795904**	**LT796148**	**LT796752**
	CBS 130244 = DTO 131-E6 = CCF 5627	JX021675	**LT795905**	**LT795906**	**LT795907**	**LT795908**	**LT796149**	**LT796753**
	DTO 131-F3 = CCF 5628	JX021679	**LT795909**	**LT795910**	**LT795911**	**LT795912**	**LT796150**	**LT796754**
	CBS 130246 = DTO 131-F9 = CCF 5629	JX021681	**LT795913**	**LT795914**	**LT795915**	**LT795916**	**LT796151**	**LT796755**
A. frankstonensis	CBS 142233^T = IBT 34172^T = DTO 341-E7^T = CCF 5799^T	KY808756	KY808594	KY808724	KY808948	KY808549	KY808901	**LT904842**
	CBS 142234 = IBT 34204 = DTO 341-F3 = CCF 5798	KY808761	KY808599	KY808729	KY808953	KY808554	KY808906	–
A. pseudoviridinutans	NRRL 62904^T = CCF 5631	–	KJ914690	KJ914708	**LT795930**	**LT795931**	**LT796119**	**LT796717**
	CBS 458.75 = KACC 41203 = IHEM 9862 (ex-type of *A. fumigatus* var. *sclerotiorum*)	–	**LT795925**	HG426048	**LT795926**	DQ094853	**LT796117**	**LT796715**
	IMI 182127 = KACC 41614 = CCF 5630	–	**LT795927**	**LT795928**	**LT795929**	DQ094850	**LT796118**	**LT796716**
	IFM 55266 = CCF 5644	–	**LT795917**	**LT795918**	**LT795919**	**LT795920**	**LT796115**	**LT796713**
	IFM 57289 = CCF 4665	–	**LT795921**	**LT795922**	**LT795923**	**LT795924**	**LT796116**	**LT796714**
	IFM 59502 = CCF 4561	–	**LT795936**	**LT795937**	**LT795938**	**LT795939**	**LT796121**	**LT796719**
	IFM 59503 = CCF 4562	–	**LT795940**	**LT795941**	**LT795942**	**LT795943**	**LT796122**	**LT796720**
	CCF 5632	–	**LT795932**	**LT795933**	**LT795934**	**LT795935**	**LT796120**	**LT796718**
A. siamensis	IFM 59793^T = KUFC 6349^T = CCF 4685^T	–	AB646989	**LT795993**	**LT795994**	AB776703	–	–
	IFM 61157 = KUFC 6397 = CCF 4686	–	AB776701	**LT795995**	**LT795996**	**LT795997**	–	–
A. udagawae	IFM 46972^T = CBS 114217^T = DTO 157-D7^T = CBM-FA 0702^T = KACC 41155^T = CCF 4558^T	AB185265	**LT796063**	**LT796064**	**LT796065**	**LT796066**	–	–
	IFM 46973 = CBS 114218 = DTO 157-D8 = CBM-FA 0703 = KACC 41156 = CCF 5672	JN943591	**LT796067**	**LT796068**	**LT796069**	**LT796070**	–	–
	IFM 5058 = CCF 4662	AB250402	**LT796075**	**LT796076**	**LT796077**	**LT796078**	–	–
	IFM 51744 = CCF 4671	AB250403	**LT796079**	**LT796080**	**LT796081**	**LT796082**	–	–
	IFM 53868 = CCF 4667	AB250405	**LT796111**	**LT796112**	**LT796113**	**LT796114**	–	–
	IFM 54131 = CBM-FA-0697 = CCF 4663	–	**LT796083**	**LT796084**	**LT796085**	**LT796086**	–	–
	IFM 54132 = CBM-FA-0698 = CCF 4664	–	**LT796087**	**LT796088**	**LT796089**	**LT796090**	–	–
	IFM 54745 = CBM-FA-694 = CCF 4661	–	**LT796091**	**LT796092**	**LT796093**	**LT796094**	–	–
	IFM 55207 = NBRC 31952 = CCF 4660	–	**LT796095**	**LT796096**	**LT796097**	**LT796098**	–	–
	IFM 62155 = CCF 4668	–	**LT796099**	**LT796100**	**LT796101**	**LT796102**	–	–
	CCF 4475	–	HF933366	HF933407	**LT796037**	**LT796038**	–	–
	CCF 4476	–	HF933371	HF933412	**LT796043**	**LT796044**	–	–
	CCF 4478 = CMF ISB 2193	–	HF933376	HF933416	**LT796045**	**LT796046**	–	–
	CCF 4479 = CMF ISB 2189	–	HF933377	HF933417	**LT796047**	**LT796048**	–	–
	CCF 4481 = CMF ISB 2191	–	HF933379	HF933419	**LT796049**	**LT796050**	–	–
	CCF 4491 = CMF ISB 1971	–	HF933370	HF933411	**LT796051**	**LT796052**	–	–
	CCF 4492	–	HF933368	HF933409	**LT796053**	**LT796054**	–	–
	CCF 4494	–	HF933373	HF933413	**LT796055**	**LT796056**	–	–
	CMF ISB 1972 = CCF 4502	HE578061	HE578075	HF933405	**LT796057**	**LT796058**	–	–
	CMF ISB 2190 = CCF 5635	–	HG426055	HG426049	**LT796059**	**LT796060**	–	–
	CMF ISB 2509 = CCF 5636	–	HF933367	HF933408	**LT796061**	**LT796062**	–	–
	CCF 5637	–	**LT796071**	**LT796072**	**LT796073**	**LT796074**	–	–
	CCF 5638	–	**LT796103**	**LT796104**	**LT796105**	**LT796106**	**LT796156**	**LT796758**
	DTO 166-D6 = CCF 5639	–	**LT796107**	**LT796108**	**LT796109**	**LT796110**	**LT796155**	**LT796759**
	CCF 5634	–	**LT796039**	**LT796040**	**LT796041**	**LT796042**	–	–
A. viridinutans	IFM 47045^T = IFM 47046^T = IMI 367415^T = IMI 062875^T = NRRL 4365^T = NRRL 576^T = CBS 127.56^T = KACC 41142^T = CCF 4382^T = CCF 4568^T	EF669978	EF669834	EF669904	EF669765	DQ094862	KJ914717	KJ914751

Table 2 (cont.)

Species	Culture collection nos.[1]	GenBank/ENA/DDBJ accession numbers						
		ITS	*benA*	*CaM*	*RPB2*	*act*	*mcm7*	*tsr1*
A. wyomingensis	CCF 4417^{T} = CMF ISB 2494^{T} = CBS 135456^{T}	HG324081	HF933359	HF933397	HF937378	HF937382	–	–
	CCF 4169 = CMF ISB 2486	–	HF933354	HF933394	**LT796009**	**LT796008**	–	–
	CCF 4170 = CMF ISB 2485	–	HF933356	HF933392	**LT796011**	**LT796010**	–	–
	CCF 4411 = CMF ISB 1977 = IFM 60854	HE578062	HE578077	HF933389	**LT796016**	**LT796015**	–	–
	CCF 4412	–	HF933352	HF933390	**LT796018**	**LT796017**	–	–
	CCF 4413 = CMF ISB 2317	–	HF933360	HF933391	**LT796019**	**LT796020**	–	–
	CCF 4414 = CMF ISB 1974 = IFM 60856	–	HF933353	HF933393	**LT796021**	**LT796022**	–	–
	CCF 4415 = CMF ISB 2487	–	HF933357	HF933395	**LT796023**	**LT796024**	–	–
	CCF 4416 = CMF ISB 1976 = CBS 135455	–	HF933358	HF933396	HF937377	HF937381	–	–
	CCF 4418 = CMF ISB 2162 = IFM 60855	–	HF933355	HF933398	**LT796025**	**LT796026**	–	–
	CCF 4419 = CMF ISB 2495	–	HF933361	HF933399	**LT796027**	**LT796028**	–	–
	CCF 4420 = CMF ISB 2491	–	HF933362	HF933400	**LT796029**	**LT796030**	–	–
	IMI 133982 = CCF 4383	–	**LT796012**	**LT796013**	**LT796014**	DQ094860	–	–
	IFM 59681 = CCF 4563	–	HG426056	HG426053	**LT796031**	**LT796032**	–	–
	DTO 155-G2 = CCF 5640	–	**LT796033**	**LT796034**	**LT796035**	**LT796036**	**LT796154**	**LT796757**
outgroup								
A. lentulus	NRRL 35552^{T} = CBS 117885^{T} = IBT 27201^{T} = KACC 41940^{T}	EF669969	EF669825	EF669895	EF669756	DQ094873	KJ914712	KJ914746

[1] Culture collection acronyms: CBM-FA = Natural History Museum & Institute, Chiba, Japan; CBS = CBS culture collection housed at the Westerdijk Institute, Utrecht, The Netherlands; CCF = Culture Collection of Fungi, Prague, Czech Republic; CM = Filamentous fungus collection of the Spanish National Center for Microbiology, Madrid, Spain; CMF ISB = Collection of Microscopic Fungi, Institute of Soil Biology, Academy of Sciences of the Czech Republic, České Budějovice, Czech Republic; DTO = working collection of the Applied and Industrial Mycology department housed at the Westerdijk Institute, Utrecht, The Netherlands; FRR = Food Fungal Culture Collection, North Ride, Australia; IBT = culture collection of the DTU Systems Biology, Lyngby, Denmark; IFM = Collection at the Medical Mycology Research Centre, Chiba University, Japan; IHEM = Belgian Coordinated Collections of Micro-organisms (BCCM/IHEM), Brussels, Belgium; IMI = CABI's collection of fungi and bacteria, Egham, UK; JCM = Japan Collection of Microorganisms, Tsukuba, Japan; KACC = Korean Agricultural Culture Collection, Wanju, South Korea; KUFC = Kasetsart University Fungal Collection, Bangkok, Thailand; NBRC (IFO) = Biological Resource Center, National Institute of Technology and Evaluation, Chiba, Japan; NRRL = Agricultural Research Service Culture Collection, Peoria, Illinois, USA.

al. 2005, Vinh et al. 2009, Coelho et al. 2011, Shigeyasu et al. 2012, Barrs et al. 2013, 2014, Eamvijarn et al. 2013, Nováková et al. 2014, Sugui et al. 2014, Matsuzawa et al. 2015, Talbot et al. 2017) and culture collections. The set comprised 38 clinical strains and 72 environmental isolates, including 67 from soil, four from cave environments and one from plant material. The provenance of isolates is detailed in Table 1. Newly isolated strains were deposited into the Culture Collection of Fungi at the Department of Botany, Charles University, Prague, Czech Republic (CCF). Dried herbarium specimens were deposited into the herbaria of the Medical Mycology Research Center, Chiba University, Japan (IFM) and Mycological Department of the National Museum, Prague, Czech Republic (PRM).

Phenotypic studies

The strains were grown on malt extract agar (MEA), Czapek Yeast Autolysate Agar (CYA), Czapek-Dox agar (CZA), yeast extract sucrose agar (YES), CYA supplemented with 20 % sucrose (CY20S), and creatine sucrose agar (CREA), and incubated at 25 °C. Agar media composition was based on that described by Samson et al. (2014). Malt extract and yeast extract were obtained from Oxoid (Basingstoke, UK) and Fluka Chemie GmbH (Switzerland), respectively. Growth at 42, 45 and 47 °C was tested on MEA plates sealed with Parafilm. Colour determination was performed according to the ISCC-NBS (Inter-Society Color Council – National Bureau of Standards) Centroid Colour Charts (Kelly 1964).

Micromorphology was observed on MEA. Lactic acid with cotton blue was used as a mounting medium. Photographs were taken on an Olympus BX-51 microscope (Olympus DP72 camera) using Nomarski contrast. Macromorphology of the colonies was documented using a stereomicroscope Olympus SZ61 (with Olympus Camedia C-5050 Zoom camera) or Canon EOS 500D.

Scanning electron microscopy (SEM) was performed using a JEOL-6380 LV scanning electron microscope (JEOL Ltd. Tokyo, Japan) as described by Hubka et al. (2013b). Briefly, pieces of colony or mature ascomata were fixed in osmium tetroxide vapours for one wk at 5–10 °C and gold coated using a Bal-Tec SCD 050 sputter coater. The specimens were observed using 40 µm spot size and 15–25 kV accelerating voltage.

Molecular studies

ArchivePure DNA yeast and Gram2+ kit (5 PRIME Inc., Gaithersburg, MD) was used for DNA isolation from 7-d-old cultures according to the manufacturer's instructions as updated by Hubka et al. (2015b). The purity and concentration of extracted DNA was evaluated by NanoDrop 1000 Spectrophotometer. ITS rDNA region was amplified using forward primers ITS1 or ITS5 (White et al. 1990) and reverse primers ITS4S (Kretzer et al. 1996) or NL4 (O'Donnell 1993); partial β-tubulin gene (*benA*) using forward primers Bt2a (Glass & Donaldson 1995) or Ben2f (Hubka & Kolařík 2012) and reverse primer Bt2b (Glass & Donaldson 1995); partial calmodulin gene (*CaM*) using forward primers CF1M or CF1L and reverse primer CF4 (Peterson 2008); partial actin gene (*act*) using primers ACT-512F and ACT-783R (Carbone & Kohn 1999); partial RNA polymerase II second largest subunit (*RPB2*) using forward primers fRPB2-5F (Liu et al. 1999) or RPB2-F50-CanAre (Jurjević et al. 2015) and reverse primer fRPB2-7cR (Liu et al. 1999); partial *mcm7* gene encoding minichromosome maintenance factor 7 with primers Mcm7-709for and Mcm7-1348rev (Schmitt et al. 2009); and partial *tsr1* gene encoding ribosome biogenesis protein with primers Tsr1-1453for and Tsr1-2308rev (Schmitt et al. 2009). Terminal primers were used for sequencing.

The PCR reaction volume of 20 µL contained 1 µL (50 ng) of DNA, 0.3 µL of both primers (25 pM/mL), 0.2 µL of MyTaq™ DNA

Polymerase (Bioline, GmbH, Germany) and 4 µL of 5× MyTaq PCR buffer. The ITS rDNA, *benA* and *CaM* fragments were amplified using the following thermal cycle profile: 93 °C/2 min; 30 cycles of 93 °C/30 s; 55 °C/30 s; 72 °C/60 s; 72 °C/10 min. The annealing temperature for amplification of *act* gene was 60 °C (30 cycles); and that for *tsr1* gene 50 °C (37 cycles). Partial *RPB2* gene fragments were amplified using the above-mentioned cycle or touchdown thermal-cycling: 93 °C/2 min; 5 cycles of 93 °C/30 s, 65–60 °C/30 s, 72 °C/60 s; 38 cycles of 93 °C/30 s, 55 °C/30 s, 72 °C/60 s; 72 °C/10 min. The partial *mcm7* gene was amplified using modified touchdown thermal-cycling: 93 °C/2 min; 5 cycles of 93 °C/30 s, 65–60 °C/30 s, 72 °C/60 s; 38 cycles of 93 °C/30 s, 60 °C/30 s, 72 °C/60 s; 72 °C/10 min. PCR product purification followed the protocol of Réblová et al. (2016). Automated sequencing was performed at Macrogen Sequencing Service (Amsterdam, The Netherlands) using both terminal primers. Sequences were deposited into the ENA (European Nucleotide Archive) database under the accession numbers listed in Table 2.

Phylogenetic analysis

Sequences were inspected and assembled using Bioedit v. 7.2.5 (www.mbio.ncsu.edu/BioEdit/bioedit.html). Alignments of the *benA*, *CaM*, *act* and *RPB2* regions were performed using the G-INS-i option implemented in MAFFT v. 7 (Katoh & Standley 2013). Alignments were trimmed, concatenated and then analysed using Maximum likelihood (ML) and Bayesian inference (BI) analyses. Suitable partitioning scheme and substitution models (Bayesian information criterion) for analyses were selected using the greedy algorithm implemented in PartitionFinder v. 1.1.1 (Lanfear et al. 2017) with settings allowing introns, exons and codon positions to be independent partitions. Proposed partitioning schemes and substitution models for each dataset are listed in Table 3. The alignment characteristics are listed in Table 4.

The ML tree was constructed with IQ-TREE v. 1.4.4 (Nguyen et al. 2015) with nodal support determined by non-parametric bootstrapping (BS) with 1000 replicates. Bayesian posterior probabilities (PP) were calculated using MrBayes v. 3.2.6 (Ronquist et al. 2012). The analyses ran for 10^7 generations, two parallel runs with four chains each were used, every 1000th tree was retained, and the first 25 % of trees were discarded as burn-in. The trees were rooted with *Aspergillus clavatus* NRRL 1 and *A. lentulus* NRRL 35552, respectively. All alignments are available from the Dryad Digital Repository (https://doi.org/10.5061/dryad.38889).

Species delimitation and species tree inference

Several species delimitation methods were applied to elucidate the species boundaries within the AVSC. We followed the recommendation of Carstens et al. (2013) and compared the results of several different methods. The analysis was divided into two parts. Four genetic loci were examined in the first analysis which comprised all species from the AVSC while six genetic loci were examined in the second analysis focused on the clade comprising *Aspergillus felis*, *A. pseudofelis*, *A. parafelis* and *A. pseudoviridinutans* (*A. aureolus* was used as an outgroup). The alignment characteristics are listed in Table 4.

Only unique nucleotide sequences, selected with DAMBE v. 6.4.11 (Xia 2017) were used in the analyses. Nucleotide substitution models for particular loci were determined using jModeltest v. 2.1.7 (Posada 2008) based on Bayesian information criterion (BIC) and were as follows: 1st analysis - K80+G (*benA*), K80+I (*CaM*), K80+G (*act*), K80+G (*RPB2*); 2nd analysis - K80+I (*benA*), K80+G (*CaM*), K80 (*act*), K80 (*RPB2*), HKY+I+G (*tsr1*), K80 (*mcm7*).

In the first analysis, only unique sequences of four loci were used, i.e., *benA*, *CaM*, *act* and *RPB2*. The number of isolates of *A. felis* and *A. pseudoviridinutans* was reduced to two, because this clade was examined in detail in the second analysis based

Table 3 Partition-merging results and best substitution model for each partition according to Bayesian information criterion (BIC) as proposed by PartitionFinder v. 1.1.0. for combined dataset of *benA*, *CaM*, *act* and *RPB2* genes.

Dataset	Phylogenetic method	Partitioning scheme (substitution model)
Section *Fumigati* (Fig. 1)	Maximum likelihood	*benA* + *CaM* + *act* introns (TrNef+G); 3rd codon positions of *benA* (GTR+G); 1st codon positions of *benA* + *CaM* + *act* + *RPB2* + 2nd codon positions of *act* + 3rd codon positions of *act* (TIM+I); 2nd codon positions of *benA* + *CaM* + *RPB2* (HKY); 3rd codon positions of *CaM* + *RPB2* (HKY+G)
	Bayesian inference	*benA* + *CaM* + *act* introns (K80+G); 3rd codon positions of *benA* (GTR+G); 1st codon positions of *benA* + *CaM* + *act* + *RPB2* + 2nd codon positions of *act* + 3rd codon positions of *act* (GTR+I); 2nd codon positions of *benA* + *CaM* + *RPB2* (HKY); 3rd codon positions of *CaM* + *RPB2* (HKY+G)
A. viridinutans clade (Fig. 5)	Maximum likelihood	*benA* + *CaM* + *act* introns (K80+G); 3rd codon positions of *benA* + *CaM* + *RPB2* (TrN+G); 1st codon positions of *benA* + *CaM* + *act* + *RPB2* + 3rd codon positions of *act* (TrN); 2nd codon positions of *benA* + *CaM* + *act* + *RPB2* (F81)
	Bayesian inference	*benA* + *CaM* + *act* introns (K80+G); 3rd codon positions of *benA* + *CaM* + *RPB2* (HKY+G); 1st codon positions of *benA* + *CaM* + *act* + *RPB2* + 3rd codon positions of *act* (HKY); 2nd codon positions of *benA* + *CaM* + *act* + *RPB2* (F81)

Table 4 Overview of alignments characteristics used for phylogenetic analyses.

Alignment characteristic	*benA*	*CaM*	*act*	*RPB2*	*mcm7*	*tsr1*	Combined dataset
Section *Fumigati* (Fig. 1)							
Length (bp)	534	697	431	999	–	–	2661
Variable position	268	322	234	280	–	–	1104
Parsimony informative sites	184	226	148	186	–	–	744
A. viridinutans complex (Fig. 5)							
Length (bp)	475	697	344	967	–	–	2483
Variable position	115	168	102	135	–	–	520
Parsimony informative sites	84	114	70	81	–	–	349
A. felis clade (Fig. 3)							
Length (bp)	474	681	329	967	623	761	3835
Variable position	72	73	35	59	38	103	380
Parsimony informative sites	50	49	18	32	24	58	231

on six loci. Three single-locus species delimitation methods, i.e., bGMYC (Reid & Carstens 2012), GMYC (Fujisawa & Barraclough 2013) and PTP (Zhang et al. 2013), and one multilocus species delimitation method STACEY (Jones 2017) were used to find putative species boundaries. The bGMYC and GMYC methods require ultrametric trees as an input, while PTP does not. Therefore, single locus ultrametric trees were constructed using a Bayesian approach in BEAST v. 2.4.5 (Bouckaert et al. 2014) with both Yule and coalescent tree models. We also looked at possible differences between strict and relaxed clock models, but since these parameters had no effect on the number of delimited species, only the results with strict clock model are presented here. Chain length for each tree was 1×10^7 generations with 25 % burn-in. The highest credibility tree was used for the GMYC method and 100 trees randomly sampled throughout the analysis were used for the bGMYC method. Both methods were performed in R v. 3.3.4 (R Core Team 2015) using *bgmyc* (Reid & Carstens 2012) and *splits* (SPecies' LImits by Threshold Statistics) (Fujisawa & Barraclough 2013) packages. The non-ultrametric trees for the PTP method were constructed using the ML approach in RAxML v. 7.7.1 (Stamatakis et al. 2008) and IQ-TREE v. 1.5.3 (Nguyen et al. 2015) with 1 000 bootstrap replicates. The PTP method was performed on the web server http://mptp.h-its.org/ (Kapli et al. 2017) with p-value set to 0.001. The multilocus species delimitation was performed in BEAST v. 2.4.5 with add-on STACEY v. 1.2.2 (Jones 2017). The chain length was set to 5×10^8 generations, priors were set as follows: the species tree prior was set to the Yule model, growth rate prior was set to lognormal distribution (M = 5, S = 2), clock rate priors for all loci were set to lognormal distribution (M = 0, S = 1), PopPriorScale prior was set to lognormal distribution (M = -7, S = 2) and relativeDeathRate prior was set to beta distribution ($\alpha = 1$, $\beta = 1\,000$). The output was processed with SpeciesDelimitationAnalyzer (Jones 2017).

The species tree was inferred using *BEAST (Heled & Drummond 2010) implemented in BEAST v. 2.4.5. The isolates were assigned to a putative species according to the results of the above-mentioned species delimitation methods. The MCMC analysis ran for 1×10^8 generations, 25 % of trees were discarded as a burn-in. The strict molecular clock was chosen for all loci and population function was set as constant. Convergence was assessed by examining the likelihood plots in Tracer v. 1.6 (http://tree.bio.ed.ac.uk/software/tracer). We also constructed the phylogenetic tree based on concatenated alignment of all four loci in IQ-TREE v. 1.5.3 with 1 000 bootstrap replicates and the optimal partitioning scheme determined by PartitionFinder v. 2.1.1 (Lanfear et al. 2017).

The validation of the species hypotheses was performed in BP&P v. 3.3 (Bayesian phylogenetics and phylogeography) (Yang & Rannala 2010). The isolates were assigned to the species based on the results of species delimitation methods and the species tree inferred with *BEAST was used as a guide tree. Three different combinations of the prior distributions of the parameters θ (ancestral population size) and τ_0 (root age) were tested as proposed by Leaché & Fujita (2010), i.e., large ancestral population sizes and deep divergence: θ ~ G (1, 10) and τ_0 ~ G (1, 10); small ancestral population sizes and shallow divergences among species: θ ~ G (2, 2000) and τ_0 ~ G (2, 2000); large ancestral populations sizes and shallow divergences among species: θ ~ G (1, 10) and τ_0 ~ G (2, 2000).

The second analysis with six protein-coding loci, i.e., *benA*, *CaM*, *act*, *RPB2*, *mcm7* and *tsr1*, consisted of the same steps as described above. Instead of PTP, we used the programme mPTP (Kapli et al. 2017) with IQ-TREE and RAxML trees as an input. Within the mPTP programme we used the following settings: Maximum likelihood species delimitation inference (option ML) and a different coalescent rate for each delimited species (option multi). R package *ggtree* (Yu et al. 2017) and the programme densitree (Bouckaert 2010) were used for visualization of the phylogenetic trees.

Mating experiments

The MAT idiomorph was determined using the primer pairs alpha1 and alpha2 located in MAT1-1-1 locus (alpha box domain), and HMG1 and HMG2 primers located in MAT1-2-1 locus (high-mobility-group domain) as described by Sugui et al. (2010). The MAT idiomorphs were differentiated based on the different lengths of PCR products visualized by gel electrophoresis; absence of opposite MAT idiomorph was also verified in all isolates. The identity of PCR products was proved by DNA sequencing in several isolates (accession numbers in Table 1); product purification and sequencing were performed at Macrogen Europe (Amsterdam, The Netherlands) using terminal primers. Selected opposite mating type strains were paired within and between major phylogenetic clades on MEA and oatmeal agar (OA; Difco, La Ponte de Claix, France) plates and incubated at 25, 30 and 37 °C in the dark. The plates were sealed with Parafilm and examined weekly from the third wk of cultivation for two months under a stereomicroscope for the production of ascomata. The presence of ascospores was determined using light microscopy. Width and height of ascospores were recorded at least 35 times for each successful mating pair.

Statistical analysis

Statistical differences in the width and height of the ascospores of particular species and interspecific hybrids were tested with one-way ANOVA followed by Tukey's HSD (honest significant difference) post hoc test in R v. 3.3.4 (R Core Team 2015). R package *multcomp* (Hothorn et al. 2008) was used for the calculation and package *ggplot2* (Wickham 2009) for visualization of the results.

Exometabolite analysis

The extracts were prepared according to Houbraken et al. (2012). High-performance liquid chromatography with diode-array detection was performed according to Frisvad & Thrane (1987, 1993) as updated by Nielsen et al. (Nielsen et al. 2011). Fungi were incubated for 1 wk at 25 °C in darkness on CYA and yeast extract sucrose (YES) agars for exometabolite analysis.

RESULTS

Phylogenetic definition of AVSC

In the phylogenetic analysis, 76 combined *benA*, *CaM*, *act* and *RPB2* sequences were assessed for members of sect. *Fumigati*. The analysis was based on the modified alignment previously used by Hubka et al. (2017) and enriched by taxa from AVSC. In the Bayesian tree shown in Fig. 1, members of sect. *Fumigati* are resolved in several monophyletic clades. The analysis showed that AVSC is a phylogenetically well-defined group and the clade gained full support. Similarly, some other clades are well-supported by both BI and ML analyses including *A. spinosus* clade, *A. brevipes* clade, *A. tatenoi* clade, *A. thermomutatus* clade and *A. fennelliae* clade; *A. spathulatus* forms a single-species lineage distantly related to other clades. Other clades have moderate or low support and the species represented therein may differ based on genetic loci used for phylogenetic reconstruction and taxa included in the analysis. Heterothallic species are dispersed across sect. *Fumigati* (Fig. 1) but the majority of them cluster in AVSC and *A. fumigatus* clades. These two clades also encompass the highest number of human and animal pathogens in sect. *Fumigati* not only in terms of their number but also their clinical relevance.

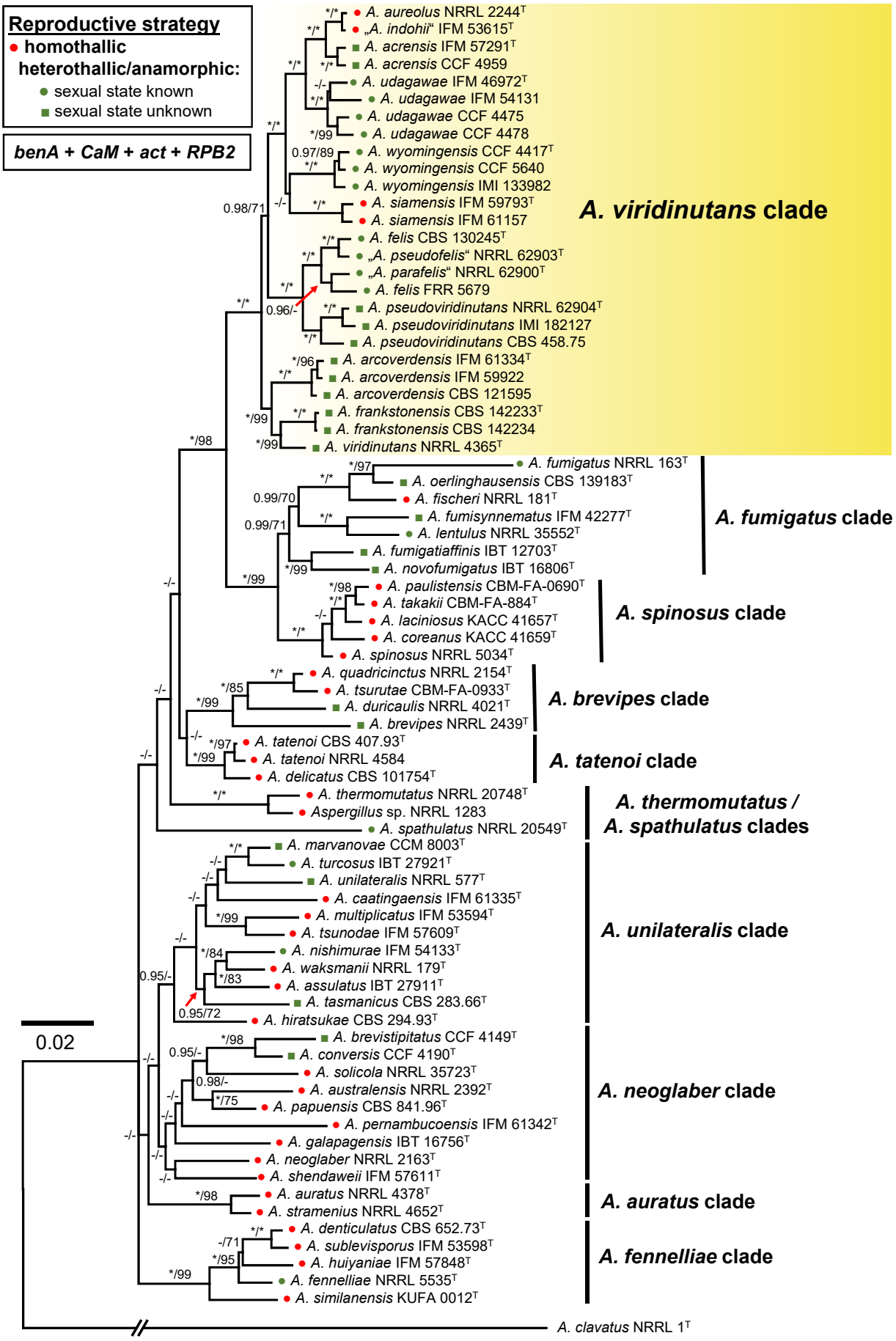

Fig. 1 Phylogenetic relationships of the sect. *Fumigati* members inferred from Bayesian analysis of the combined, 4-gene dataset of β-tubulin (*benA*), calmodulin (*CaM*), actin (*act*) and RNA polymerase II second largest subunit (*RPB2*) genes. Bayesian posterior probabilities (PP) and Maximum likelihood bootstrap supports (BS) are appended to nodes; only PP ≥ 95 % and BS ≥ 70 % are shown; lower supports are indicated with a hyphen, whereas asterisks indicate full support (1.00 PP or 100 % BS); ex-type strains are designated by a superscript ^{T}; species names in quotes are considered synonyms; the bar indicates the number of substitutions per site. The tree is rooted with *Aspergillus clavatus* NRRL 1^{T}. The reproductive mode of each species is designated by icons before the species name (see legend).

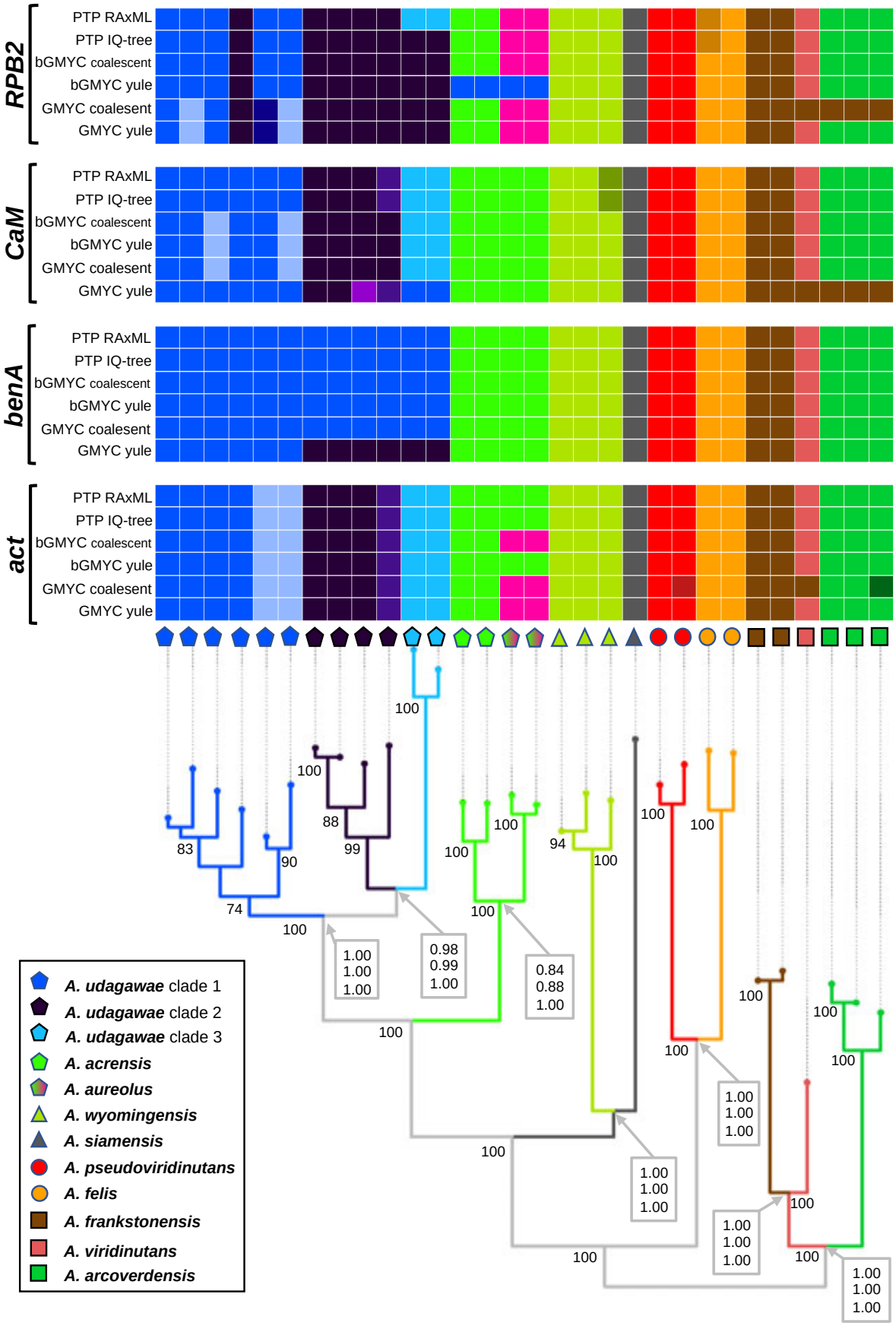

Fig. 2 Schematic representation of results of species delimitation methods in *Aspergillus viridinutans* species complex based on four genetic loci. The results of multilocus method (STACEY) are compared to results of single-locus methods (PTP, bGMYC, GMYC). The results of STACEY are shown as tree branches with different colours, while the results of single-locus methods are depicted with coloured bars highlighting congruence across methods. The displayed tree is derived from IQ-TREE analysis based on a concatenated dataset and is used solely for the comprehensive presentation of the results from different methods. The species validation analysis results (BP&P) are appended to nodes and shown in grey bordered boxes; the values represent posterior probabilities calculated in three scenarios having different prior distributions of parameters θ (ancestral population size) and τ_0 (root age). The top value represents the results of analysis with large ancestral population sizes and deep divergence: θ ~ G (1, 10) and τ_0 ~ G (1, 10); the middle value represents the results of analysis with large ancestral populations sizes and shallow divergences among species: θ ~ G (1, 10) and τ_0 ~ G (2, 2000); and the bottom value small ancestral population sizes and shallow divergences among species: θ ~ G (2, 2000) and τ_0 ~ G (2, 2000).

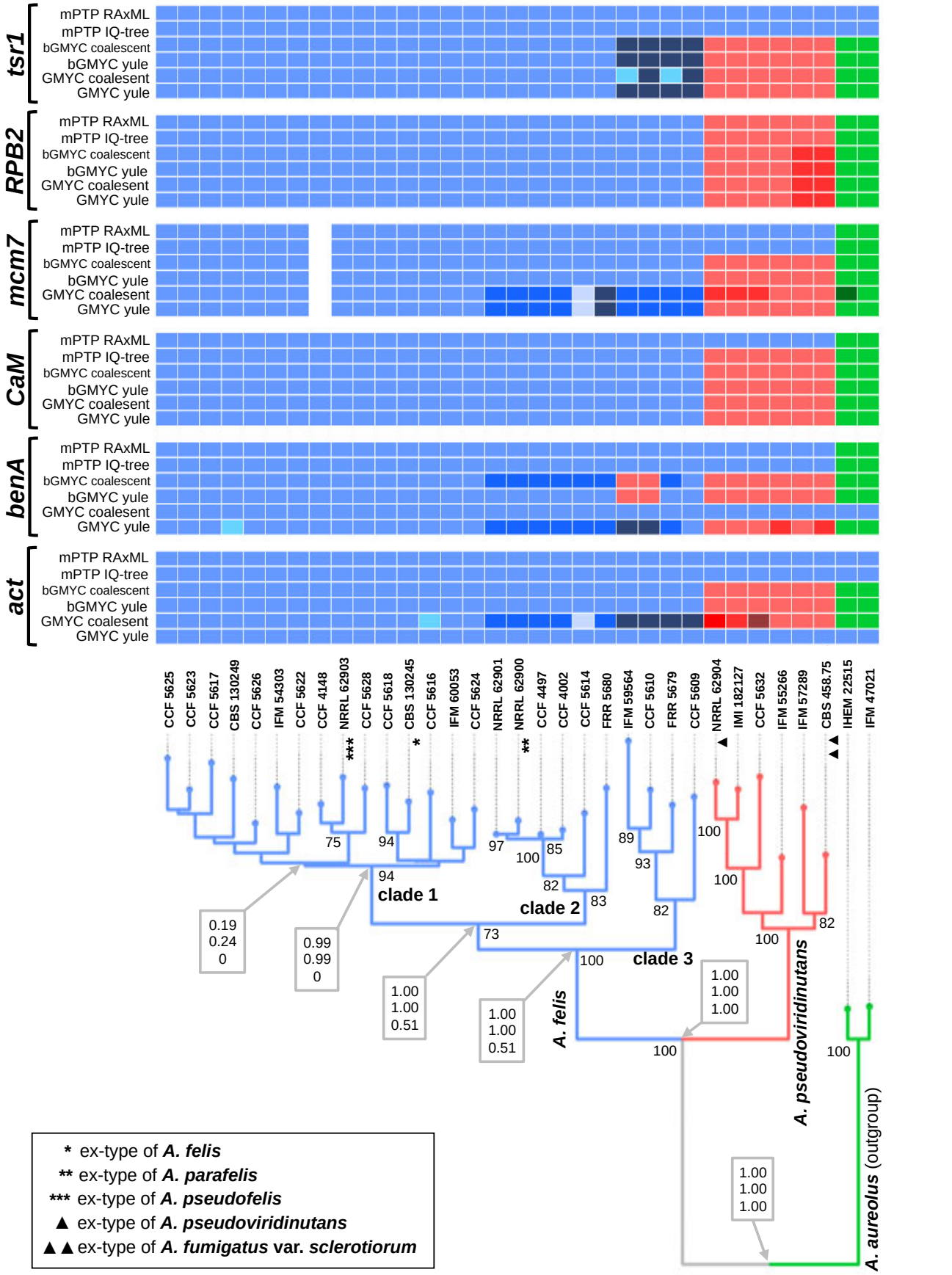

Fig. 3 Schematic representation of results of species delimitation methods in *Aspergillus felis* clade based on six genetic loci. The results of multilocus method (STACEY) are compared to results of single-locus methods (mPTP, bGMYC, GMYC). The results of STACEY are shown as tree branches with different colours, while the results of single-locus methods are depicted with coloured bars highlighting congruence across methods. The displayed tree is derived from IQ-TREE analysis based on a concatenated dataset and is used solely for the comprehensive presentation of the results from different methods. The species validation analysis results (BP&P) are appended to nodes and shown in grey bordered boxes; the values represent posterior probabilities calculated in three scenarios having different prior distributions of parameters θ (ancestral population size) and τ_0 (root age). The top value represents the results of analysis with large ancestral population sizes and deep divergence: θ ~ G (1, 10) and τ_0 ~ G (1, 10); the middle value represents the results of analysis with large ancestral populations sizes and shallow divergences among species: θ ~ G (1, 10) and τ_0 ~ G (2, 2000); and the bottom value small ancestral population sizes and shallow divergences among species: θ ~ G (2, 2000) and τ_0 ~ G (2, 2000).

Species delimitation and validation in AVSC

In the first analysis, four genetic loci were examined across species of AVSC, isolates of *A. felis* and its close relatives were reduced to two individuals, because a separate analysis based on six loci was performed for this clade. Eleven tentative species were delimited in AVSC using STACEY. The results are summarised in Fig. 2, the differences in the colour of the tree branches reflect species delimited by the analysis. The analysis supported recognition of three putative species in *A. udagawae* lineage, delimitation of *A. acrensis* (described below) from *A. aureolus* was not supported, other AVSC species were supported by STACEY without differences from their current concept.

The results derived from STACEY were compared to those from three single-locus species delimitation methods. The consensual results from single-locus species delimitation methods are generally in agreement with the results of STACEY for the majority of species but vary greatly for *A. udagawae*, *A. aureolus* and *A. acrensis* lineages (Fig. 2). Recognition of three putative species in *A. udagawae* lineage was supported only based on the *CaM* locus, while based on *benA* locus, none of these three sublineages gained support. Various delimitation schemes were proposed by different single-locus species delimitation methods in the *A. udagawae* lineage based on the *RPB2* gene (results even varied between the analyses based on different input trees for the PTP and GMYC methods), while five putative species were identically delimited based on the *act* locus. The methods relatively consistently supported delimitation of the *A. acrensis* lineage based on the *RPB2* locus and similarly, bGMYC and GMYC methods supported this species based on the *act* locus. In contrast, lineages of *A. acrensis* and *A. aureolus* were not split by any method when analyzing *benA* and *CaM* loci.

The species validation analysis results are appended to nodes of the tree in Fig. 2. A reasonable support is defined by posterior probabilities ≥ 0.95 under all three scenarios simulated by different prior distributions of parameters θ (ancestral population size) and τ_0 (root age). Delimitation of all putative species (those delimited by STACEY, *A. acrensis* and *A. aureolus*) were supported by the posterior probability 0.98 or higher based on the analysis in BP&P v. 3.1 (Yang & Rannala 2010) under all three scenarios. The only exception was lower support for splitting of *A. acrensis* and *A. aureolus*; this scenario was supported by the posterior probabilities 0.84, 0.88, 1.00, respectively.

Species delimitation and validation in A. felis clade and its relatives

In the second analysis, six genetic loci were examined across isolates of *A. felis*, *A. parafelis*, *A. pseudofelis* and *A. pseudoviridinutans.* Only two tentative species, *A. felis* and *A. pseudoviridinutans*, were delimited in this clade using STACEY. The results are shown as branches designated by different colours in Fig. 3. The analysis did not support separation of *A. pseudofelis* and *A. parafelis* from *A. felis*; *A. fumigatus* var. *sclerotiorum* is included in the lineage of *A. pseudoviridinutans*.

The results of three single-locus species delimitation methods were compared to those from STACEY, and the consensual results showed a general agreement (Fig. 3). Delimitation of *A. pseudofelis* from *A. felis* was not supported by any of the used methods. Only a negligible number of analyses supported delimitation of basal clades in *A. felis* as tentative species (designated as clade 2 and 3 in Fig. 3). But even in these minority scenarios, there were no clear consensual delimitation patterns that would support delimitation of *A. parafelis*. Interestingly, mPTP analysis based on *act*, *benA*, *CaM* (with RAxML trees as an input only), *mcm7* and *tsr1* loci together with GMYC analysis based on *benA* (only input tree based on coalescent tree model) and *act* (only input tree based on Yule tree model) loci did not support delimitation of *A. pseudoviridinutans* from a robust clade of *A. felis*. An incomplete lineage sorting was observed between *A. felis* and *A. pseudoviridinutans* (Fig. 3) evidencing that there was probably an ancestral gene flow between these lineages. Two isolates from *A. felis* lineage (IFM 59564 and CCF 5610) have *benA* sequences that cluster with *A. pseudoviridinutans* while sequences of the remaining 5 loci placed them in the *A. felis* lineage (single-gene trees not shown).

The species validation analysis results are appended to nodes of the tree in Fig. 3. Delimitation of *A. felis* and *A. pseudoviridinutans* gained absolute support in BP&P analysis (Yang & Rannala 2010) under all three scenarios simulated by different prior distributions of parameters θ (ancestral population size) and τ_0 (root age). Delimitation of three putative species within *A. felis* lineage gained no support (posterior probability 0.51) under the scenario with small ancestral population sizes and shallow divergences among species: θ ~ G (2, 2000) and τ_0 ~ G (2, 2000).

Species tree

The species tree topology was inferred with *BEAST (Heled & Drummond 2010) and is shown in Fig. 4. It was used as a guide tree during species validation using BP&P but it also represents the most probable evolutionary relationships between species in the AVSC. The analysis confirmed recombination between three subclades of *A. felis* (Fig. 4) which include also recently proposed species *A. parafelis* and *A. pseudofelis* thus representing the synonyms of *A. felis*. Similarly, the recombination between three subclades of *A. udagawae* rejected the hypothesis that they could be considered separate species (Fig. 4).

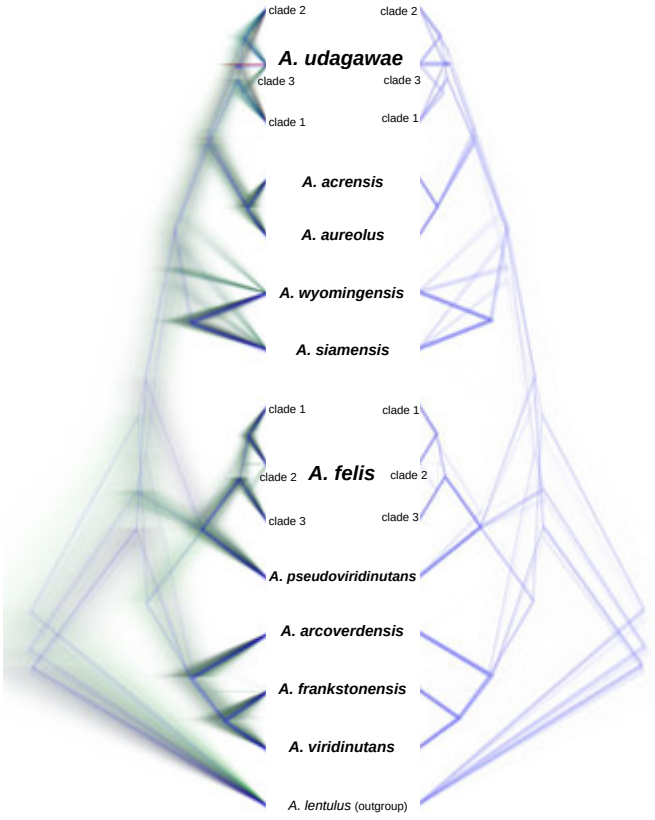

Fig. 4 Species tree inferred with *BEAST visualized by using DensiTree (Bouckaert 2010). All trees created in the analysis (except 25 % burn-in phase) are displayed on the left side. Trees with the most common topology are highlighted by blue, trees with the second most common topology by red, trees with the third most common topology by pale green and all other trees by dark green. On the right side, the consensus trees of the three most common topologies are displayed.

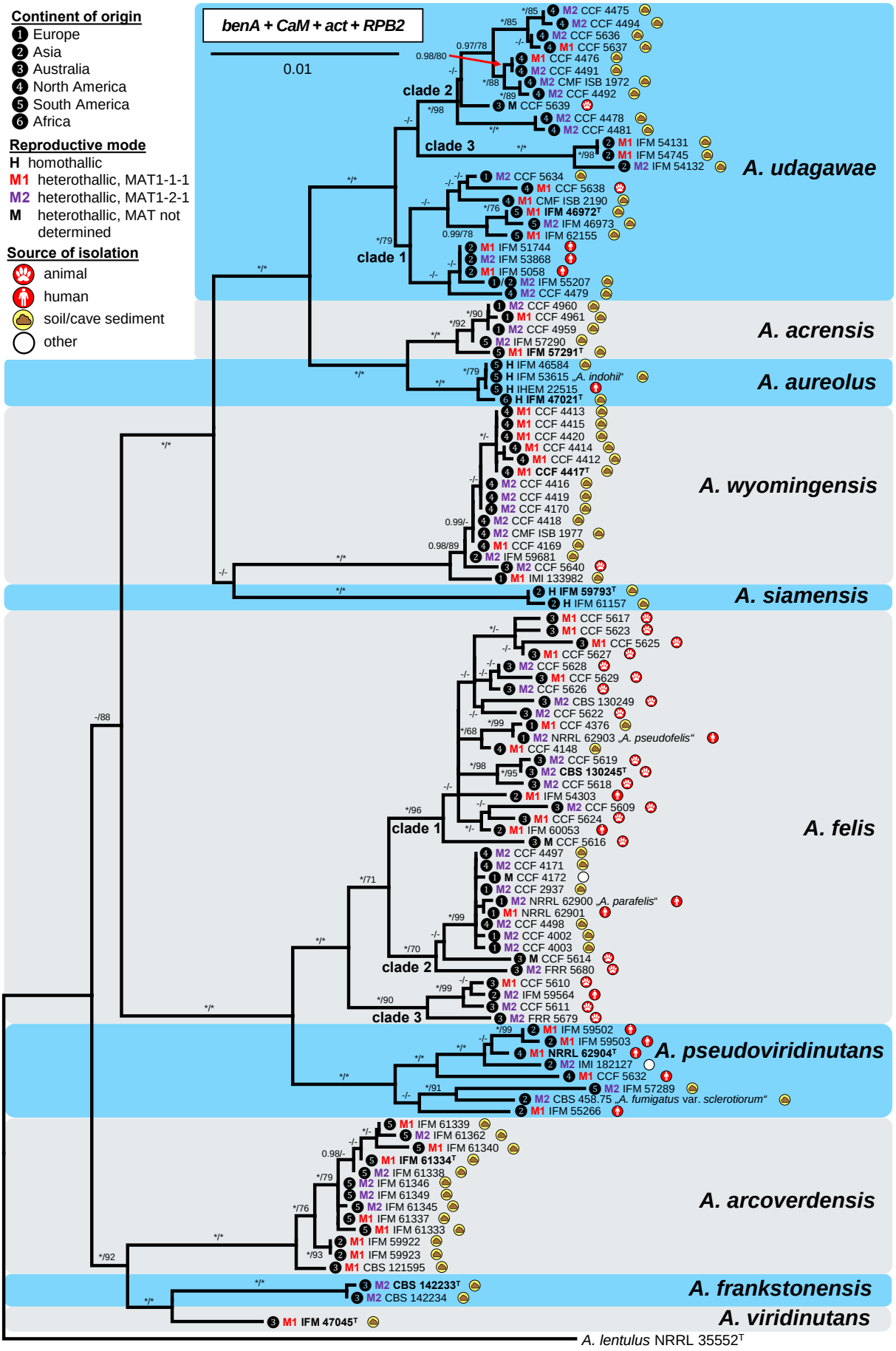

Fig. 5 Phylogenetic relationships of the *Aspergillus viridinutans* species complex members inferred from Bayesian analysis of the combined, 4-gene dataset of β-tubulin (*benA*), calmodulin (*CaM*), actin (*act*) and RNA polymerase II second largest subunit (*RPB2*) genes. Bayesian posterior probabilities (PP) and Maximum likelihood bootstrap supports (BS) are appended to nodes; only PP ≥ 90 % and BS ≥ 70 % are shown; lower supports are indicated with a hyphen, whereas asterisks indicate full support (1.00 PP or 100 % BS); ex-type strains are designated by a superscript ^{T}; species names in quotes are considered synonyms; the bar indicates the number of substitutions per site. The tree is rooted with *Aspergillus lentulus* NRRL 35552^{T}. The geographic origin and reproductive mode with MAT idiomorph (if known) is designated by icons before the isolate number while substrate of origin is designated by icons after isolate number (see legend).

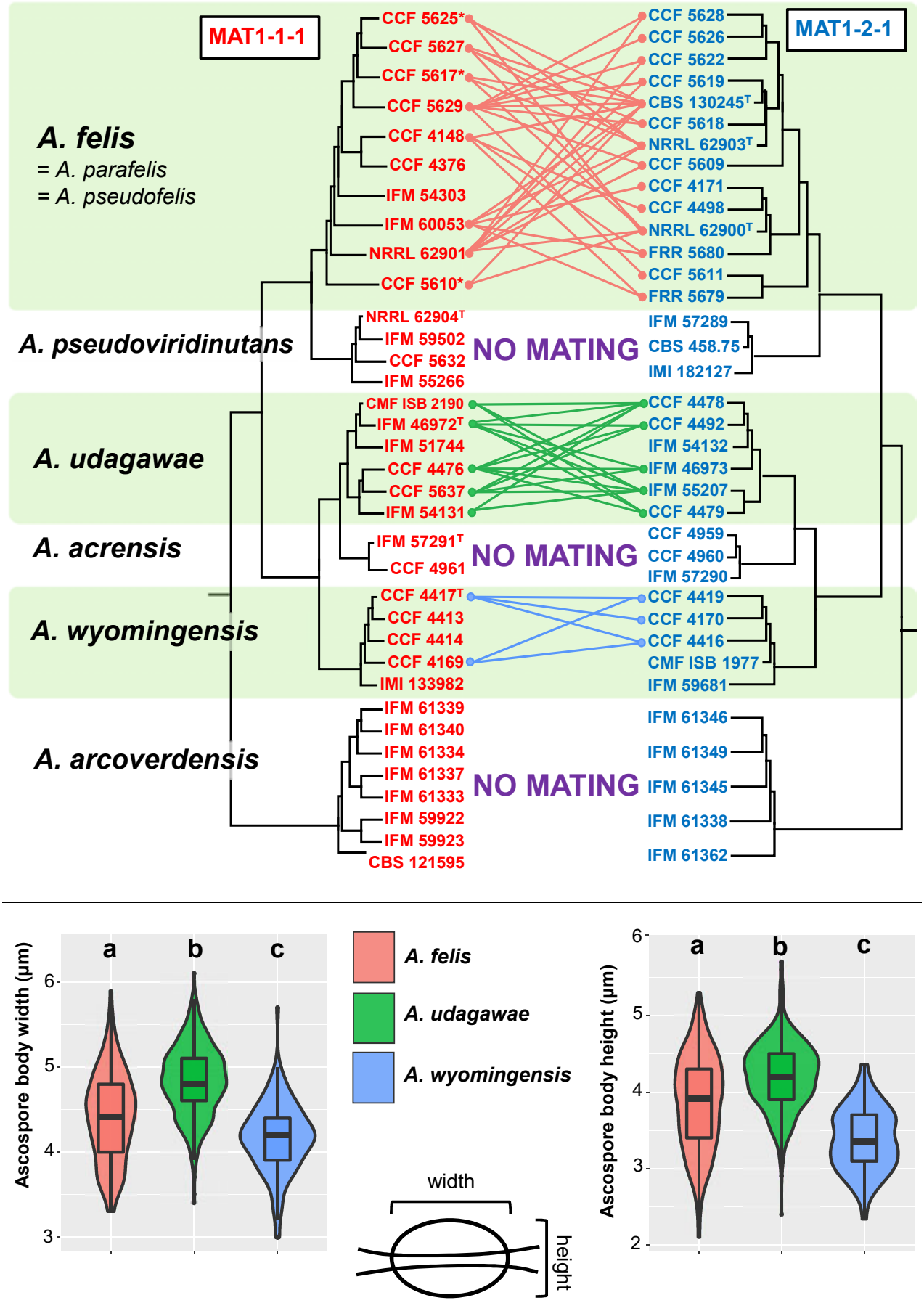

Fig. 6 Schematic depiction of results of intraspecific mating experiments between opposite mating type isolates of heterothallic members of the *Aspergillus viridinutans* species complex. Only successful mating experiments are displayed by connecting lines between opposite mating type isolates; remaining mating experiments were negative. Isolates marked by asterisk were only crossed with ex-type strains of *A. felis* (CBS 130245^{T}), *A. parafelis* (NRRL 62900^{T}) and *A. pseudofelis* (NRRL 62903^{T}). Boxplot and violin graphs were created in R 3.3.4 (R Core Team 2015) with package *ggplot2* (Wickham 2009) and show the differences between the width and height of ascospores of *A. udagawae*, *A. wyomingensis* and *A. felis*. Different letters above the plot indicate significant difference ($P < 0.05$) in the size of the ascospores between different species based on Tukey's HSD test. Boxplots show median, interquartile range, values within ± 1.5 of interquartile range (whiskers) and outliers.

The remaining species delimited in previous steps (Fig. 4), including *A. pseudoviridinutans* and *A. acrensis* (introduced in this study), were supported by *BEAST analysis. The species tree had identical topology with the trees inferred by ML and BI analyses of the concatenated and partitioned dataset (Fig. 5), and all species supported by *BEAST had 100 % ML bootstrap support (ML BS) and 1.00 BI posterior probabilities (BI PP). Several deep nodes in the species tree had only limited support similarly to ML and BI analyses. Thus clear positions of *A. wyomingensis* and *A. siamensis* within the clade also containing *A. udagawae*, *A. acrensis* and *A. aureolus* remains unresolved, while *A. acrensis* with *A. aureolus* form a sister clade to *A. udagawae* (this topology gained absolute support in all further analyses – see below). Another robust clade contained sister species *A. felis* and *A. pseudoviridinutans*. The remaining species, i.e., *A. viridinutans*, *A. frankstonensis* and *A. arcoverdensis*, formed a basal clade in the AVSC and their positions within the clade are fully resolved (Fig. 4).

Clustering of isolates by origin and mating-type idiomorph

In the phylogenetic analysis, 111 combined *benA*, *CaM*, *act* and *RPB2* sequences were assessed for members of AVSC. All species delimited by methods based on the coalescent model were fully supported by BI and ML analyses (Fig. 5).

The *A. udagawae* lineage included 25 isolates that clustered in three main clades. Mating type gene idiomorph MAT1-1-1 was detected in 10 isolates while 14 strains had MAT1-2-1 idiomorph (MAT idiomorph was not determined in one strain). The majority of North American isolates (10/14) clustered in clade 1 together with one strain from Australia; clade 2 comprised only three strains originating from Asia; isolates from four different continents were present in clade 3. There was no apparent clustering based on clinical or environmental origin of strains, or their MAT idiomorph. All three clinical isolates from Asia had an identical haplotype based on four studied protein-coding loci (Fig. 5) but one strain had MAT1-2-1 idiomorph in contrast to MAT1-1-1 idiomorph detected in the remaining two strains.

The *A. acrensis* lineage included five strains isolated from soil (Brazil) or cave sediment (Romania), two of which had MAT1-1-1 idiomorph and three had MAT1-2-1 idiomorph. This lineage is very closely related to a homothallic species *A. aureolus* represented by four strains in our analysis. The only known clinical isolate of *A. aureolus* (IHEM 22515) was isolated from the cornea of a patient in Peru. We were unable to source further information about this case and thus the clinical relevance of this isolate cannot be confirmed.

The mutual phylogenetic position of homothallic *A. siamensis* and heterothallic *A. wyomingensis* remains unresolved. *Aspergillus siamensis* was represented in our analysis by only two isolates from soil in Thailand, which were included in the original description (Eamvijarn et al. 2013). The *A. wyomingensis* lineage included 15 isolates; 12 of them came from Wyoming (USA) and were closely related to each other and to one isolate from China, while two isolates from Australia and Europe displayed a higher number of unique positions. The ratio of MAT1-1-1 isolates to MAT1-2-1 isolates was 8 : 7, and the majority of MAT1-1-1 isolates from the USA (6/7) clustered in a separate subclade that was only supported in the BI analysis.

The *A. felis* lineage comprised 35 isolates that clustered in three main clades. Mating type gene idiomorph MAT1-1-1 was detected in 12 isolates, while 20 strains had MAT1-2-1 idiomorph (MAT idiomorph was not determined in three strains). There was no clustering based on geographic origin as all three clades included isolates from two to four continents. Clade 3 contained only clinical isolates (n = 4). Clinical strains were predominant in clade 1 (18 : 2) whereas environmental strains dominated in clade 2 (7 : 4). The ratio of MAT1-1-1 isolates to MAT1-2-1 isolates in clade 1 was balanced (10 : 9) but was biased toward MAT1-2-1 idiomorph in clades 2 (1 : 7) and 3 (1 : 3). Eight isolates of *A. pseudoviridinutans*, a sister species of *A. felis*, were examined in this study; MAT1-1-1 idiomorph was determined in five of them and MAT1-2-1 idiomorph in three of them. There was no apparent clustering based on clinical or environmental origin of strains, or their MAT idiomorph (Fig. 5).

A basal clade of AVSC comprises three soil-borne species. Whilst *A. viridinutans* and *A. frankstonensis* are known only from one locality in Australia, 13 *A. arcoverdensis* strains included in the analysis were isolated on three continents, i.e., South America, Asia and Australia. Both, *A. viridinutans* and *A. frankstonensis* were represented only by one and two isolates, respectively, included in the original descriptions (McLennan et al. 1954, Talbot et al. 2017), and only isolates of one mating type are known for each of these species. Isolates of both mating types were present in *A. arcoverdensis* (MAT1-1-1 : MAT1-2-1 ratio, 8 : 5). A geographical clustering was apparent in *A. arcoverdensis* strains; two strains from China and one strain from Australia formed sublineages separate from the Brazilian strains (Fig. 5).

Mating experiments and morphology of spores

The MAT1-1-1 and MAT1-2-1 idiomorphs were determined for 100 of 104 isolates representing heterothallic species in AVSC (Table 1). Systematic mating experiments were first performed within major phylogenetic clades of the AVSC. Opposite mating type strains representing genetic and geographic diversity for each heterothallic species were selected for mating experiments and crossed in all possible combinations if not otherwise indicated (Fig. 6). Successful mating was observed in lineages of *A. felis*, *A. udagawae* and *A. wyomingensis*. At least some individuals representing all three phylogenetic subclades of *A. felis* (Fig. 3, 5) and *A. udagawae* (Fig. 2, 5) crossed successfully with individuals from the other subclades. The mating capacity of individual isolates was unequal. Whilst some isolates of a particular species were able to mate with a broad spectrum of opposite mating type strains of the same species, others produced fertile ascomata with only a limited set of strains or did not mate at all. The morphology of ascospores among different crosses in these three species was consistent (Fig. 7). The exception was great variability in the convex surface ornamentation of *A. wyomingensis* ascospores among and as well as within pairings of different isolates ranging from almost smooth, tuberculate to echinulate (Fig. 7). Although both the width and height of ascospores of *A. felis*, *A. udagawae* and *A. wyomingensis* overlapped significantly, their dimensions were statistically significantly different (Tukey's HSD test, p value < 0.05) (Fig. 6). No fertile cleistothecia were produced by crossing opposite mating type isolates of *A. pseudoviridinutans*, *A. acrensis* and *A. arcoverdensis*. Mating experiments were not performed in *A. viridinutans* and *A. frankstonensis* due to the absence of opposite mating type strains.

Opposite mating type isolates of each heterothallic species were also selected for interspecific mating assays and crossed in all possible combinations. Morphological characteristics of AVSC ascospores and induced hybrids are summarised in Table 5. Only three of 12 selected *A. udagawae* isolates produced fertile ascomata with some isolates of *A. felis*, *A. wyomingensis* or *A. acrensis* (Fig. 8). The highest mating capacity was observed in the ex-type strain of *A. udagawae* IFM 46972 that produced fertile ascomata when crossed with *A. felis* (CCF 5609, CCF 4171 and CCF 5611), *A. wyomingensis* (CCF 4416 and CCF 4411) and *A. acrensis* (IFM 57290). The width and height of ascospores of interspecific hybrids between *A. udagawae* and *A. acrensis* were significantly different (Tukey's HSD test,

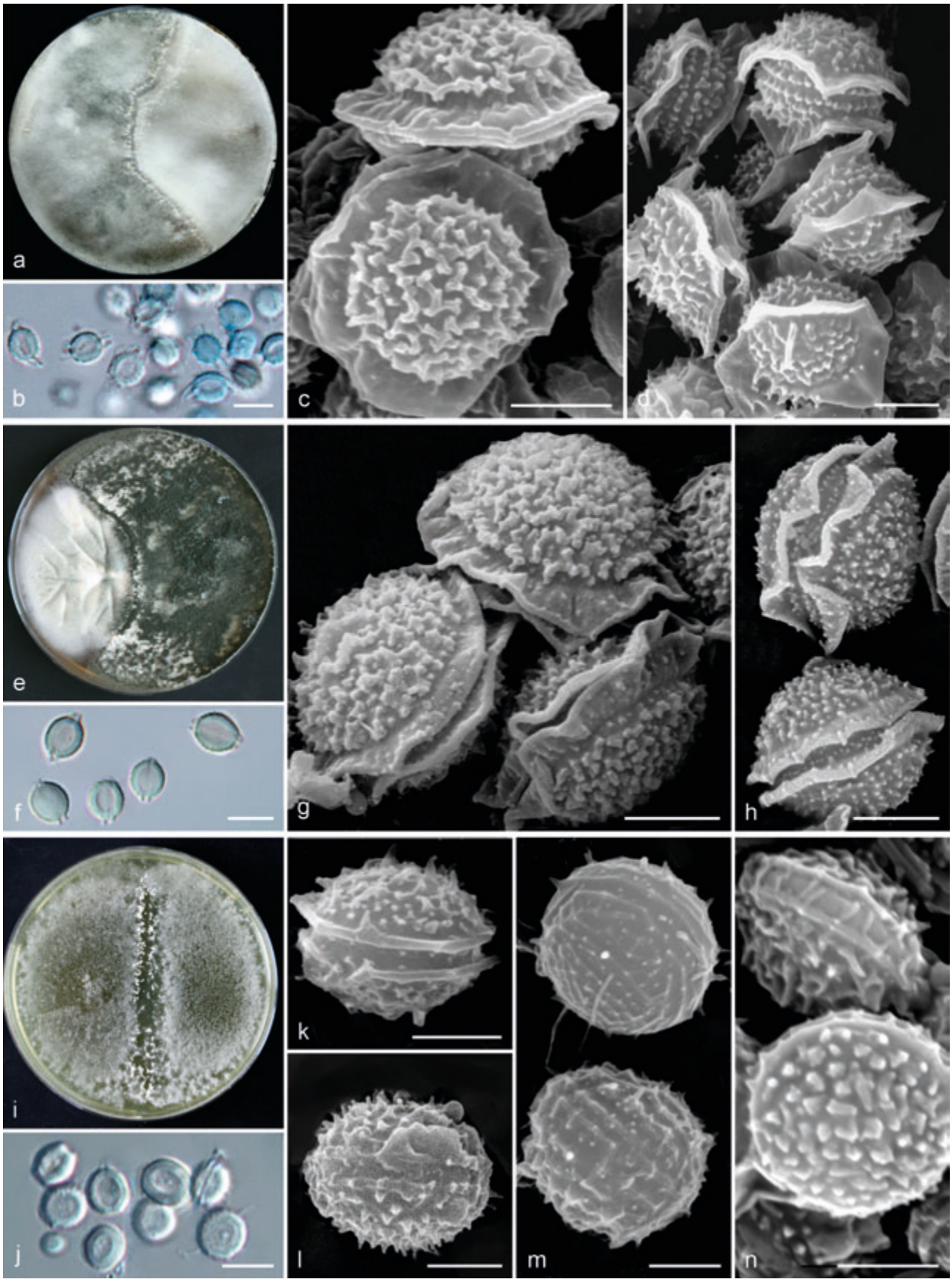

Fig. 7 Comparison of morphology of sexual morphs of *A. felis*, *A. udagawae* and *A. wyomingensis*. a. Fertile cleistothecia of *A. felis* as a result of crossing of isolates IFM 60053 × FRR 5680; b. ascospores in light microscopy; c–d. ascospores in scanning electron microscopy: CBS 130245^{T} × CCF 5627 (c), CBS 130245^{T} × IFM 60053 (d); e. fertile cleistothecia of *A. udagawae* as a result of crossing of isolates IFM 46972^{T} × IFM 46973; f. ascospores in light microscopy; g–h. ascospores in scanning electron microscopy; i. fertile cleistothecia of *A. wyomingensis* as a result of crossing of isolates CCF 4416 × CCF 4417^{T}; j. ascospores in light microscopy (CCF 4416 × CCF 4169); k–n. ascospores in scanning electron microscopy: CCF 4416 × CCF 4417^{T} (k–l), CCF 4417^{T} × CCF 4419 (m–n). — Scale bars: b, f, j = 5 µm; c–d, g–h, k–n = 2 µm.

Table 5 Ascospores characteristics of *Aspergillus viridinutans* complex species and interspecific hybrids.

Species / interspecific hybrid (×)	Ascospore body (mean ± standard deviation; µm)		Ornamentation of ascospores	
	width	height	length of crests (µm)[1]	surface ornamentation[2]
Aspergillus aureolus	4.8 ± 0.5	4.4 ± 0.4	(0.5–)1–1.5	crests present[3]; CS tuberculate to echinulate (SEM)
A. felis	4.4 ± 0.5	3.9 ± 0.6	0.5–1.5(–2)	crests present[3]; CS tuberculate to echinulate (SEM)
A. siamensis	4.5 ± 0.5	3.7 ± 0.4	(0.5–)1–1.5	crests present[3]; CS tuberculate, echinulate to reticulate (SEM)
A. udagawae	4.8 ± 0.4	4.2 ± 0.4	(0–)0.5(–1)	visible crests absent in < 10 % of ascospores (LM); CS tuberculate to reticulate (SEM)
A. wyomingensis	4.2 ± 0.4	3.4 ± 0.4	0–0.5	visible crests absent in > 50 % of ascospores (LM); CS almost smooth, tuberculate, echinulate (SEM)
A. felis × *A. pseudoviridinutans*	4.9 ± 0.4	4.2 ± 0.5	(0–)0.5–1	visible crests absent in 5–20 % of ascospores (LM) depending on parental isolates; CS tuberculate to echinulate (SEM)
A. felis × *A. wyomingensis*	4.8 ± 0.5	4.3 ± 0.3	(0–)0.5–1	visible crests absent in ~ 10 % of ascospores (LM); CS tuberculate (SEM)
A. felis × *A. udagawae*	5.1 ± 0.5	4.5 ± 0.5	0–0.5(–1)	visible crests absent in ~ 20 % of ascospores (LM); CS echinulate, tuberculate to reticulate (SEM)
A. udagawae × *A. wyomingensis*	5.0 ± 0.4	4.6 ± 0.3	0–1	visible crests absent in ~ 15 % of ascospores (LM); CS tuberculate (SEM)
A. udagawae × *A. acrensis*	5.2 ± 0.5	4.4 ± 0.5	0–0.5	visible crests absent in ~ 50 % of ascospores (LM) in CMF ISB 2190 × IFM 57290 and in 100 % of ascospores in IFM 46972 × IFM 57290; CS tuberculate to echinulate in CMF ISB 2190 × IFM 57290 (SEM) and glabrous in IFM 46972 × IFM 57290 (LM)

[1] Values in parentheses are less common (less than 10 % of measurements).
[2] LM = light microscopy; SEM = scanning electron microscopy; CS = convex surface.
[3] Crests may absent in < 1 % of ascospores in some isolates / crosses.

p value < 0.05) from *A. udagawae* (Fig. 8). Approximately 50 % of hybrid ascospores from mating CMF ISB 2190 with IFM 57290 lacked visible equatorial crests and if present, they were frequently interrupted or stellate (Fig. 9) in contrast to *A. udagawae* (visible crests present in > 90 % of ascospores, crests continuous). The ascomata from mating IFM 46972 with IFM 57290 contained only low numbers of ascospores that were globose or subglobose and glabrous (without crests and ornamentation on convex surface). This observation supported the hypothesis that *A. acrensis* is a separate species despite its close phylogenetic relationships to *A. udagawae*. The ascospore dimensions of hybrids between *A. udagawae* and *A. wyomingensis* were similar to those of *A. udagawae* and both width and height were significantly different (Tukey's HSD test, p value < 0.05) from *A. wyomingensis* (Fig. 8). These hybrid ascospores had well-defined equatorial crests that were most commonly 0.5–1 µm broad and similar to those of *A. udagawae* (Fig. 9). The hybrids of *A. udagawae* and *A. felis* had ascospores with similar equatorial crest length and body width to *A. udagawae* but were significantly different from *A. felis*, and their height was significantly different from both *A. felis* and *A. udagawae* (Fig. 8). The ascomata of hybrids between *A. udagawae* with *A. wyomingensis* and *A. felis*, respectively, usually contained only low numbers of ascospores. No mating or production of infertile ascomata only was observed between crosses of *A. udagawae* and the remaining heterothallic AVSC members (Fig. 8). Interestingly, the majority of interspecific hybrids produced approximately 1–10 % of globose or subglobose asco-spores with abnormally large dimensions, approximately 6.5–10.5 µm diam (their dimensions were not included for calculations of statistical measures in Fig. 8 and 10, and in Table 5). These cells had thick walls similar to normal ascospores, but lacked equatorial crests and had a glabrous or echinulate surface. Their dimensions were intermediate between normal ascospores and asci but their walls were dissimilar to those of thin-walled asci. These cells were not observed among progeny of the intraspecific crosses (intraspecific mating assay) and their presence probably indicates a defect in meiosis and ascospore development.

Two MAT1-1-1 isolates of *A. pseudoviridinutans* selected for interspecific mating assays, namely the ex-type strain NRRL 62904 and strain IFM 59502, were able to mate with a relatively high number of MAT1-2-1 isolates of *A. felis* (Fig. 10). The ascospores of these hybrids were statistically significantly different in their width and height from *A. felis*. Equatorial crests were absent in approximately 5–20 % hybrid ascospores and, if present, they were shorter than those of *A. felis* (Table 5). These observations suggest that *A. pseudoviridinutans* should be treated as a separate species as proposed by species delimitation methods despite the close phylogenetic relationships of both species and incomplete lineage sorting detected between these two species (Fig. 3). Only one interspecific hybrid was induced in our assay between *A. wyomingensis* CCF 4169 and *A. felis* NRRL 62900. The ascospore body width and height of this hybrid was significantly different from both parental species (Fig. 10). In contrast to *A. wyomingensis*, equatorial crests were present in the majority of hybrids and they were occasionally interrupted and stellate (Fig. 11). Infertile ascomata were observed in some crosses between *A. felis* and following species: *A. acrensis*, *A. wyomingensis* and *A. viridinutans*.

Aspergillus aureolus and *A. siamensis* are the only two homothallic species in the AVSC and readily produce ascomata on a broad spectrum of media and growth temperatures and are easily distinguishable from the eight heterothallic AVSC members. Most *A. aureolus* isolates produce distinctive yellow colonies in contrast to the whitish colonies of *A. siamensis* (Fig. 12). The ascospores of both species have similar dimensions, convex surface ornamentation and equatorial crest length (Table 5, Fig. 12) and most closely resemble those of *A. felis* from among heterothallic species.

The macromorphology of colonies, micromorphology of asexual morphs and physiology have only limited discriminatory power in AVSC members, as recognized in previous studies (Nováková et al. 2014, Matsuzawa et al. 2015). We compared surface ornamentation of conidia in all currently recognized species using SEM. The ornamentation showed a micro-tuberculate pattern and was broadly identical across all species (Fig. 13).

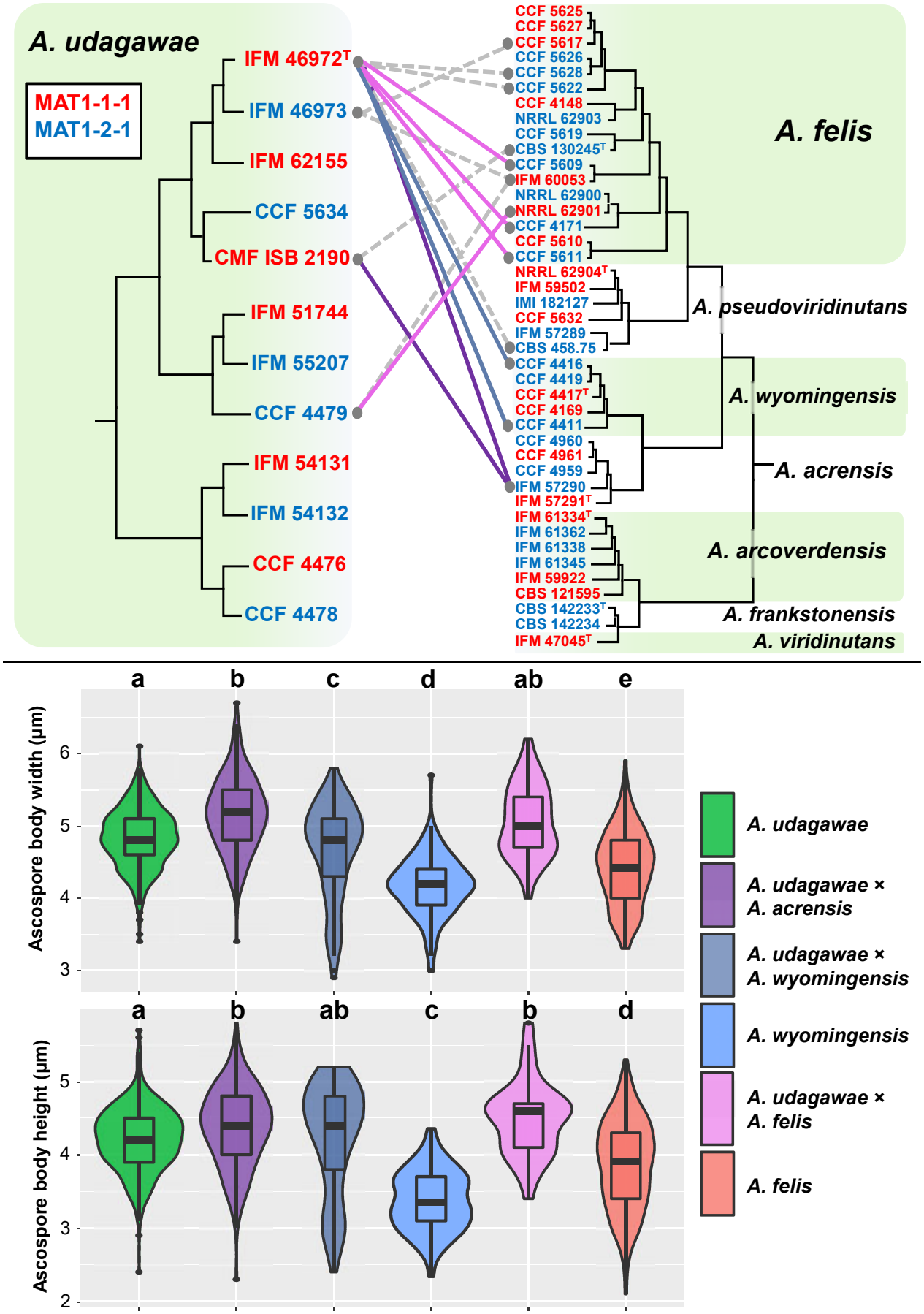

Fig. 8 Schematic depiction of results of interspecific mating experiments between opposite mating type isolates of *A. udagawae* and other heterothallic members of *Aspergillus viridinutans* species complex. Only successful mating experiments are displayed by coloured connecting lines between opposite mating type isolates (different colours correspond to hybrids between different species); grey dashed lines indicate production of infertile ascomata; remaining mating experiments were negative. Boxplot and violin graphs were created in R 3.3.4 (R Core Team 2015) with package *ggplot2* (Wickham 2009) and show the differences between the width and height of ascospores of particular species and their hybrids. Different letters above the plot indicate significant difference ($P < 0.05$) in the size of the ascospores based on Tukey's HSD test. Boxplots show median, interquartile range, values within ± 1.5 of interquartile range (whiskers) and outliers.

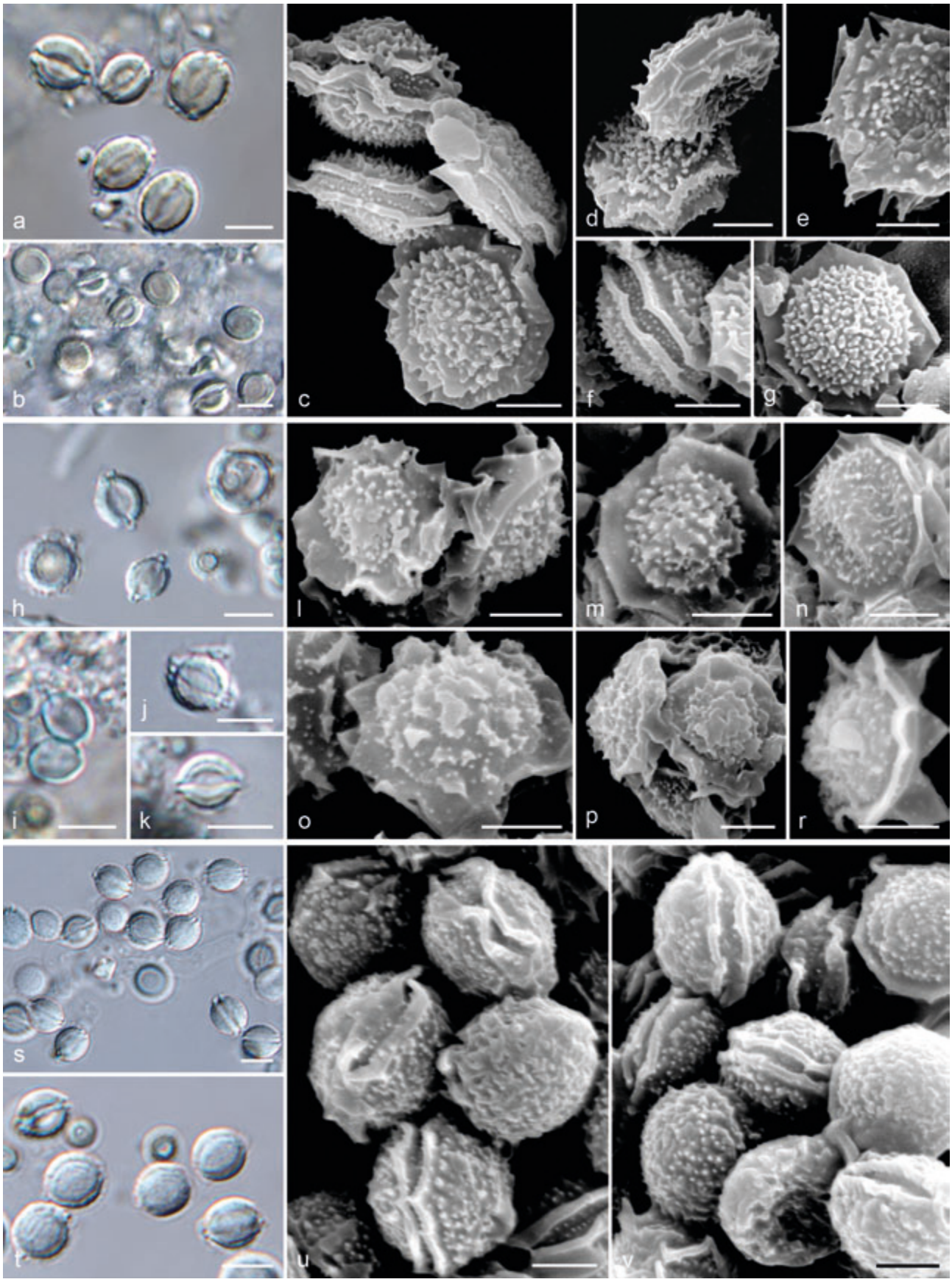

Fig. 9 Ascospore morphology of interspecific hybrids between *A. udagawae* and other species. a–g. Hybrid of *A. udagawae* CMF ISB 2190 × *A. acrensis* IFM 57290; a–b. ascospores in light microscopy; c–g. ascospores in scanning electron microscopy; h–r. hybrid of *A. udagawae* CCF 4479 × *A. felis* NRRL 62901; h–k. ascospores in light microscopy; l–r. ascospores in scanning electron microscopy; s–v. hybrid of *A. udagawae* IFM 46972^{T} × *A. wyomingensis* CCF 4411; s–t. ascospores in light microscopy; u–v. ascospores in scanning electron microscopy. — Scale bars: a–b, h–k, s–t = 5 µm; c–g, l–r, u–v = 2 µm.

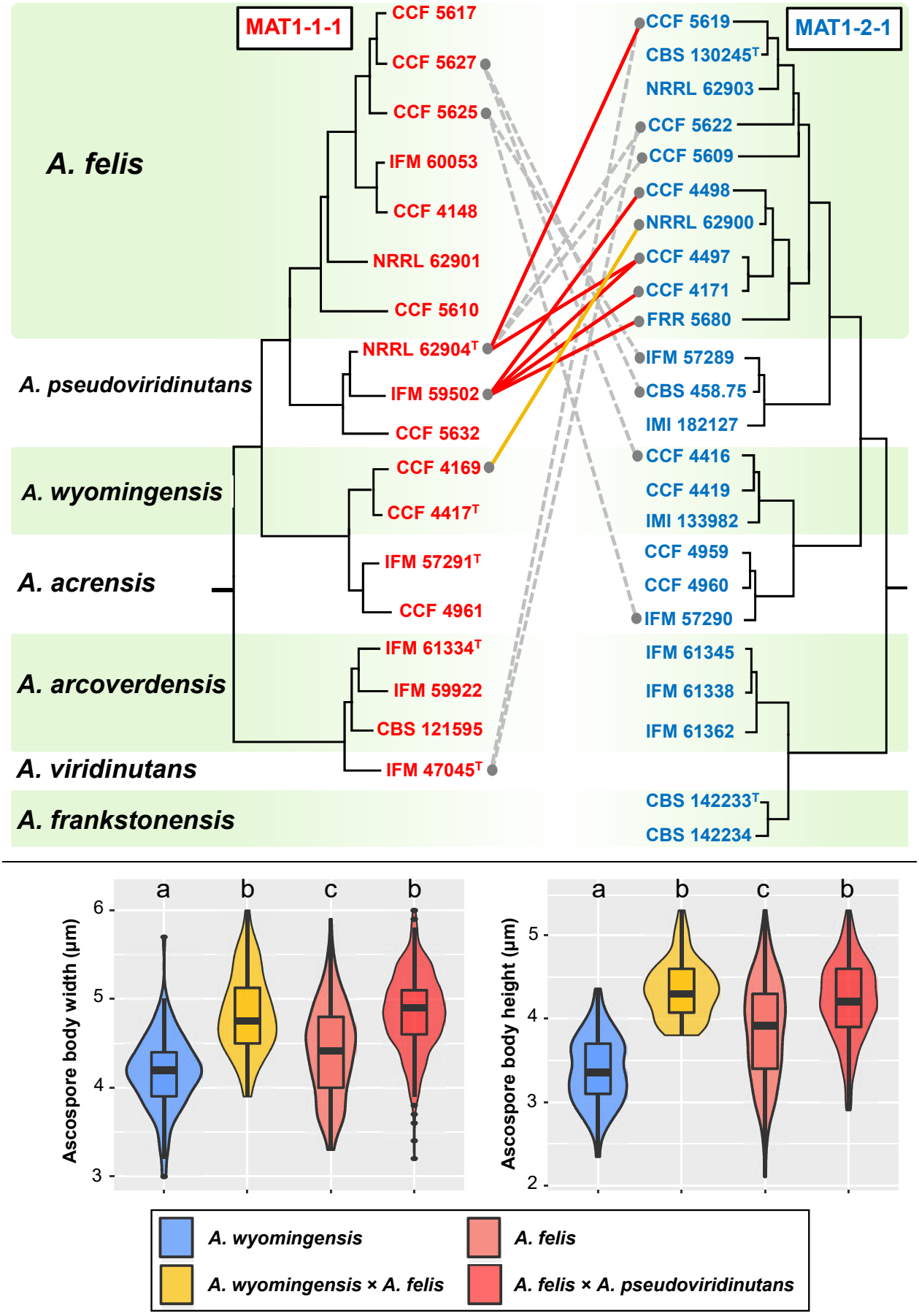

Fig. 10 Schematic depiction of results of interspecific mating experiments between opposite mating type isolates of heterothallic members of *Aspergillus viridinutans* species complex except of *A. udagawae*. Only successful mating experiments are displayed by coloured connecting lines between opposite mating type isolates (different colours correspond to hybrids between different species); grey dashed lines indicate production of infertile ascomata; remaining mating experiments were negative. Boxplot and violin graphs were created in R 3.3.4 (R Core Team 2015) with package *ggplot2* (Wickham 2009) and show the differences between the width and height of ascospores of particular species and their hybrids. Different letters above the plot indicate significant difference ($P < 0.05$) in the size of the ascospores based on Tukey's HSD test. Boxplots show median, interquartile range, values within ± 1.5 of interquartile range (whiskers) and outliers.

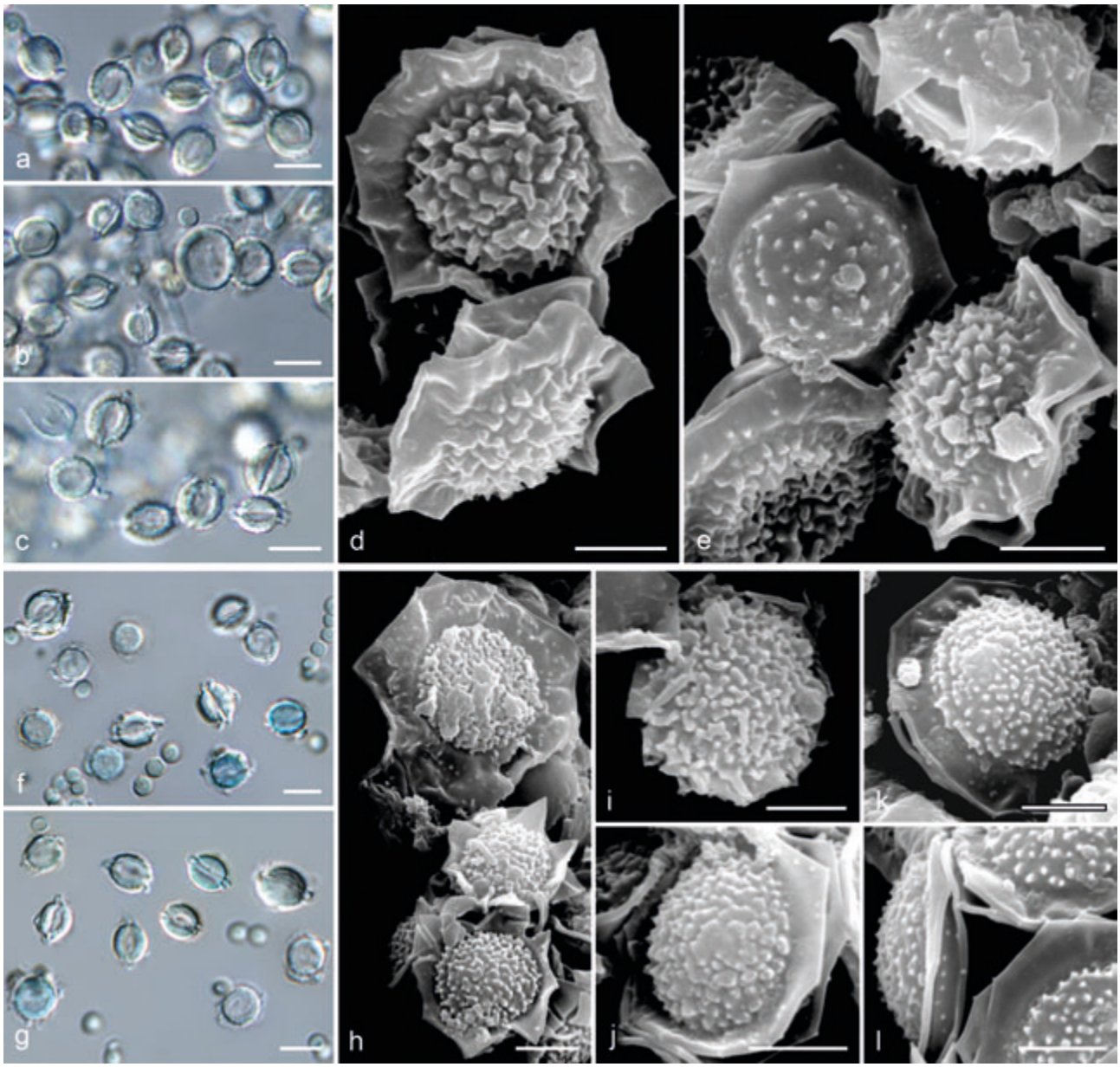

Fig. 11 Ascospore morphology of interspecific hybrids between *A. felis*, *A. pseudoviridinutans* and *A. wyomingensis.* a–e. Hybrid of *A. felis* × *A. pseudoviridinutans*; a–c. ascospores of hybrid CCF 4497 × IFM 59502 in light microscopy; d–e. ascospores in scanning electron microscopy: CCF 4497 × IFM 59502 (d), CCF 4171 × IFM 59502 (e); f–l. hybrid of *A. felis* NRRL 62900 × *A. wyomingensis* CCF 4169; f–g. ascospores in light microscopy; h–l. ascospores in scanning electron microscopy. — Scale bars: a–c, f–g = 5 µm; d–e, h–l = 2 µm.

TAXONOMY

Aspergillus acrensis Hubka, A. Nováková, Yaguchi, Matsuz. & Y. Horie, *sp. nov.* — MycoBank MB822542; Fig. 14

Etymology. Named after the region of origin of the ex-type strain – state Acre located in the northern Brazil.

Mycelium composed of hyaline, branched, septate, smooth-walled hyphae. Conidial heads greyish green, loosely columnar, up to 140 µm long, 15–25 µm diam. Conidiophores uniseriate, arising from aerial hyphae or the basal mycelium, hyaline to pale yellowish brown, frequently nodding, smooth, 150–600 µm long; stipes 3–5.5(–8) µm wide in the middle; vesicles hyaline to greyish green, pyriform, subclavate to clavate, (6–)9–16(–20) µm diam; phialides ampulliform, hyaline to greyish green, 4.5–6(–7.5) × 1.5–2.5(–3) µm, covering approximately the apical half of the vesicle. Conidia hyaline to greyish green, globose, subglobose to broadly ellipsoidal, smooth-walled to delicately roughened, microtuberculate in SEM, 2.5–3 × 2–2.5 µm (mean ± standard deviation, 2.8 ± 0.2 × 2.4 ± 0.2; length/width ratio 1.1–1.3, 1.2 ± 0.1). Heterothallic, sexual morph unknown.

Culture characteristics (7 d at 25 °C, unless otherwise stated) — Colonies on MEA attained 51–62 mm diam, sparsely lanose, slightly raised, flat, yellowish white (ISCC–NBS No. 92) to pale green (No. 149), no exudate, soluble pigment light greyish yellow (No. 101), reverse light greenish yellow (No. 101) to brilliant greenish yellow (No. 98). Colonies on CYA attained 33–48 mm diam, floccose, slightly raised, flat to slightly radially furrowed, yellowish white (No. 92) to greenish white (No. 153), sporulation in the colony centre pale green (No. 149) to greyish green (No. 150), no exudate, soluble pigment dark greyish yellow (No. 91), reverse deep yellow (No. 85), light olive brown (No. 94) to moderate olive brown (No. 95) with light yellow (No. 86) margin. Colonies on CYA at 37 °C grow more rapidly compared to 25 °C and attained 60–70 mm diam, lanose, slightly raised, flat to radially furrowed, white mycelium in margins, sporulation light olive grey (No. 112) to olive grey (No. 113), no exudate, no soluble pigment, reverse colourless, moderate yellow (No. 87) to greyish yellow (No. 90). Colonies on CZA attained 36–48 mm diam, lanose, slightly raised, flat, yellowish white (No. 92), no exudate, no or light greyish yellow (No. 101) soluble pigment, reverse light yellow (No. 86),

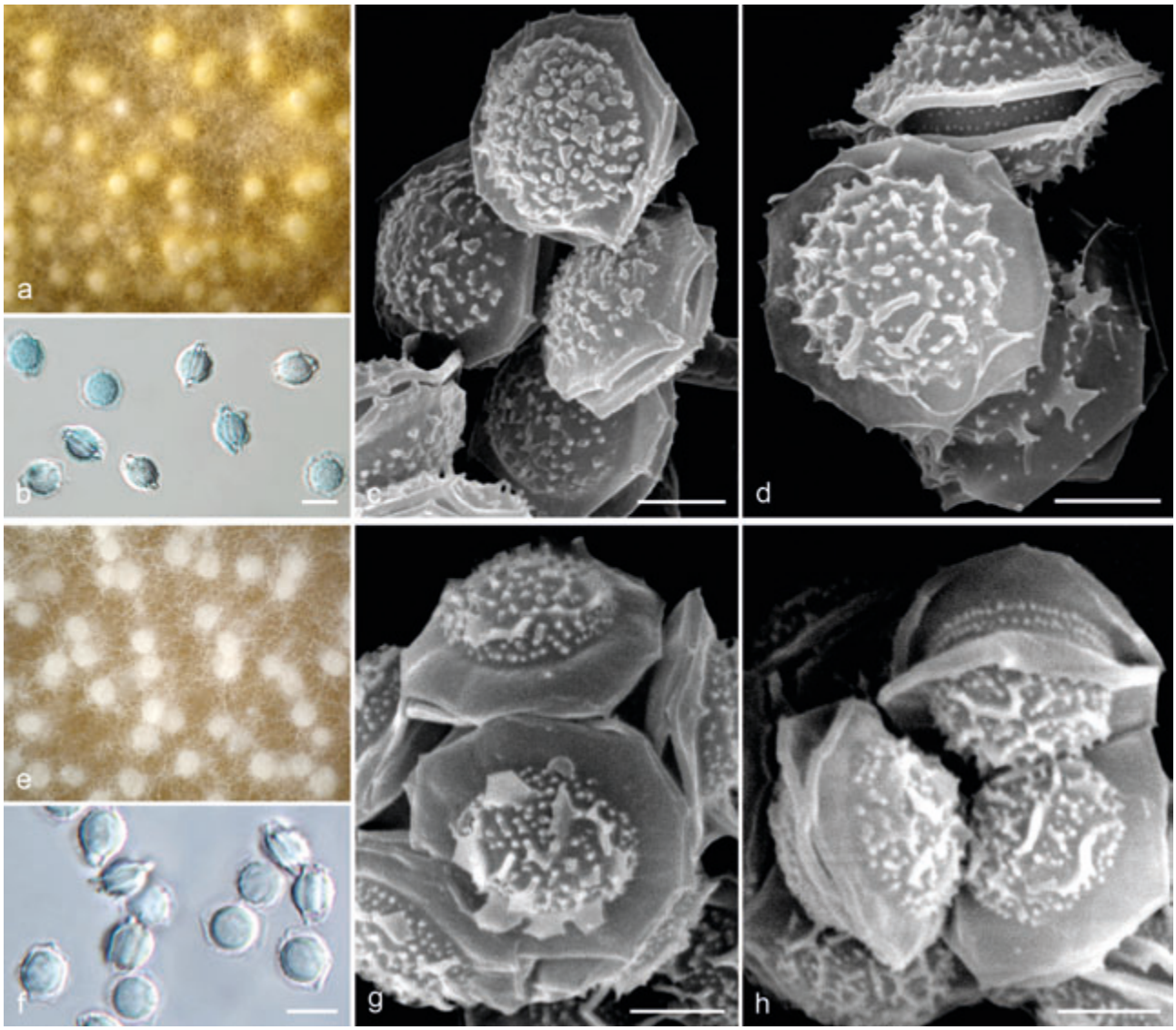

Fig. 12 Sexual morph morphology of homothallic species from *Aspergillus viridinutans* complex. a–d. *Aspergillus aureolus* isolates IFM 47021^{T} (a–b, d) and IFM 46584 (c); a. Macromorphology of ascomata after 3 wk of incubation on MEA at 37 °C; b. ascospores in light microscopy; c–d. ascospores in scanning electron microscopy; e–h. *Aspergillus siamensis* isolate IFM 59793^{T}; e. macromorphology of ascomata after 3 wk of incubation on MEA at 37 °C; f. ascospores in light microscopy; g–h. ascospores in scanning electron microscopy. — Scale bars: b, f = 5 µm; c–d, g–h = 2 µm.

light greenish yellow (101) to brilliant greenish yellow (No. 98). Colonies on YES lanose, yellowish white (No. 92), irregularly furrowed, no exudate, soluble pigment brilliant yellow (No. 83), reverse brilliant yellow (No. 83). Colonies on CY20S attained 58–65 mm diam, lanose, slightly raised, flat, yellowish white (No. 92), no exudate, no soluble pigment, reverse moderate brown (No. 58) to moderate reddish brown (No. 43). Colonies on CREA attained 32–35 mm diam, sparsely lanose, plane, mycelium yellowish white, no visible sporulation, reverse strong brown (No. 55), no acid production. Growth on MEA at 45 °C, no growth on MEA at 47 °C.

Exometabolites — Isolate IFM 57291 produced an aszonapyrone, a fumigatin, tryptoquivalines, tryptoquivalones; isolate IFM 57290 an aszonapyrone, fumagillin, fumigatins, helvolic acid, pseurotin A, tryptoquivalines, and a trytoquivalone; isolate CCF 4959 pseurotin A, viriditoxin and several potential naphtho-gamma-pyrones; CCF 4960 antafumicins, fumagillin, a fumigatin, helvolic acid, pseurotin A, and a tryptoquivalone; and CCF 4961 an aszonapyrone, fumagillin, fumigatins, pseurotin A, tryptoquivalines and tryptoquivalones. In general, similar metabolites are also produced by the two most closely related species, i.e., *A. aureolus* and *A. udagawae*. *Aspergillus aureolus* produces fumagillin, helvolic acid, pseurotin A, tryptoquivalines, tryptoquivalones and viriditoxin as well as several unique yellow secondary metabolites. *Aspergillus udagawae* produces fumagillin, fumigatins, tryptoquivalines and tryptoquivalones (Frisvad & Larsen 2015a).

Specimens examined. Brazil, State of Acre, Xapuri, grassland soil in a cattle farm, 6 Nov. 2001, *Y. Horie* (holotype IFM 57291H, isotypes PRM 935088 and PRM 935089, culture ex-type IFM 57291^{T} = CCF 4670^{T}); State of Amazonas, Manaus, forest soil in tropical rain forest, 11 Nov. 2001, *Y. Horie*, culture IFM 57290 (= CCF 4666). – Romania, Movile cave, above the Lake Room, cave sediment, 8 June 2014, *A. Nováková*, culture CCF 4959; Movile cave, cave corridor, cave sediment, 8 June 2014, *A. Nováková*, culture CCF 4960; Movile cave, Lake Room, cave sediment, 8 June 2014, *A. Nováková*, culture CCF 4961.

Notes — The morphology of *A. acrensis* strongly resembles that of several other *A. viridinutans* complex members. The closely related taxa *A. aureolus* and *A. siamensis* are readily distinguished from *A. acrensis* by the production of ascomata under standard cultivation conditions (both are homothallic). *Aspergillus viridinutans* and *A. frankstonensis* grow more slowly at 25 °C and have smaller vesicles. The macromorphology of colonies and micromorphology of the asexual morph does not distinguish *A. acrensis* reliably from *A. arcoverdensis*, *A. felis*, *A. pseudoviridinutans*, *A. udagawae* and *A. wyomingensis*.

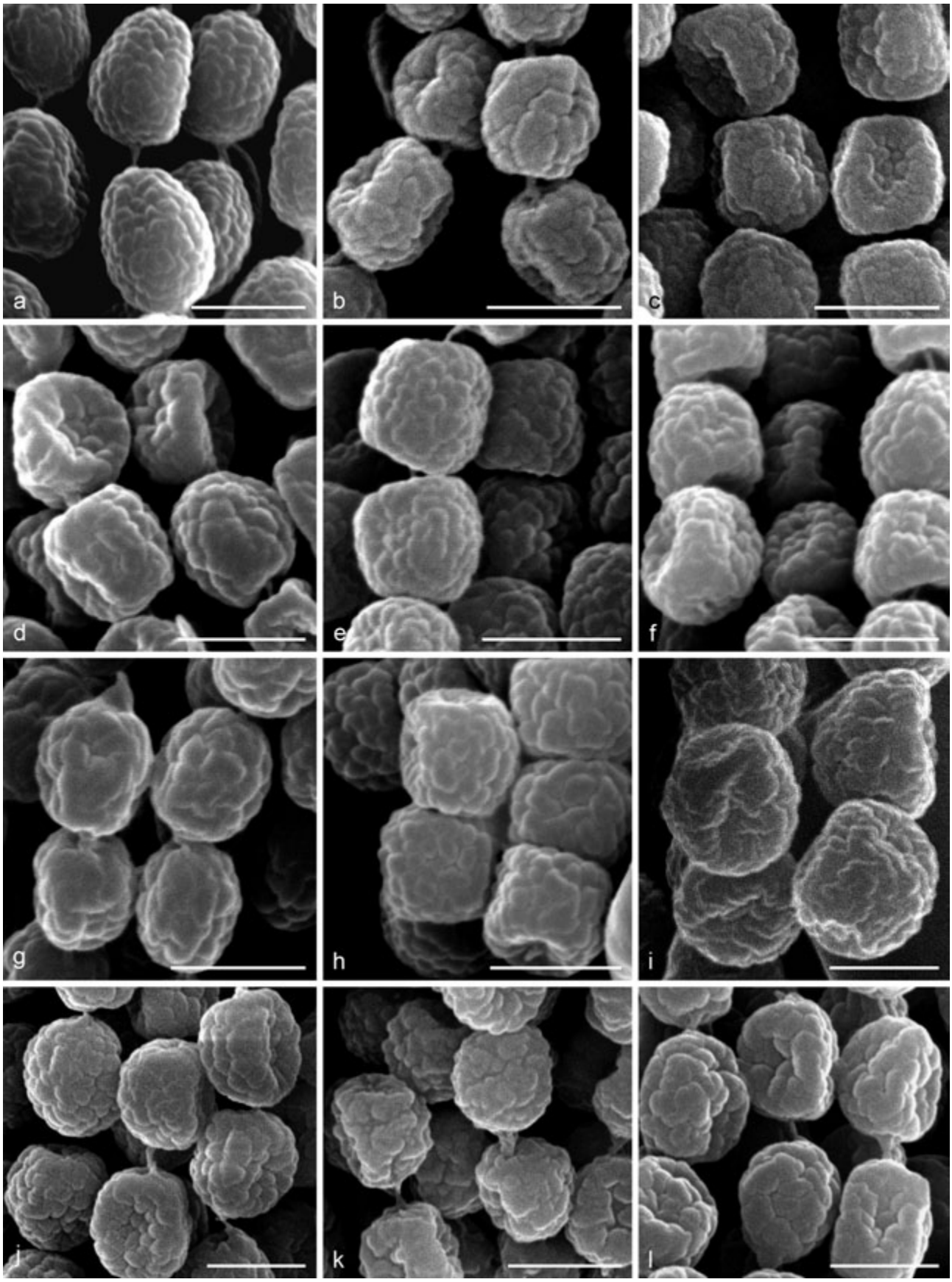

Fig. 13 Conidia with micro-tuberculate surface ornamentation pattern observed by scanning electron microscopy. a. *Aspergillus acrensis* IFM 57290; b. *A. arcoverdensis* IFM 61334^{T}; c. *A. aureolus* IFM 46584; d. *A. felis* CBS 130245^{T}; e. *A. felis* NRRL 62900 (ex-type of *A. parafelis*); f. *A. felis* NRRL 62903 (ex-type of *A. pseudofelis*); g. *A. frankstonensis* CBS 142234; h. *A. pseudoviridinutans* CBS 458.75; i. *A. siamensis* IFM 59793^{T}; j. *A. udagawae* IFM 46972^{T}; k. *A. viridinutans* IFM 47045^{T}; l. *A. wyomingensis* CCF 4414. — Scale bars = 2 µm.

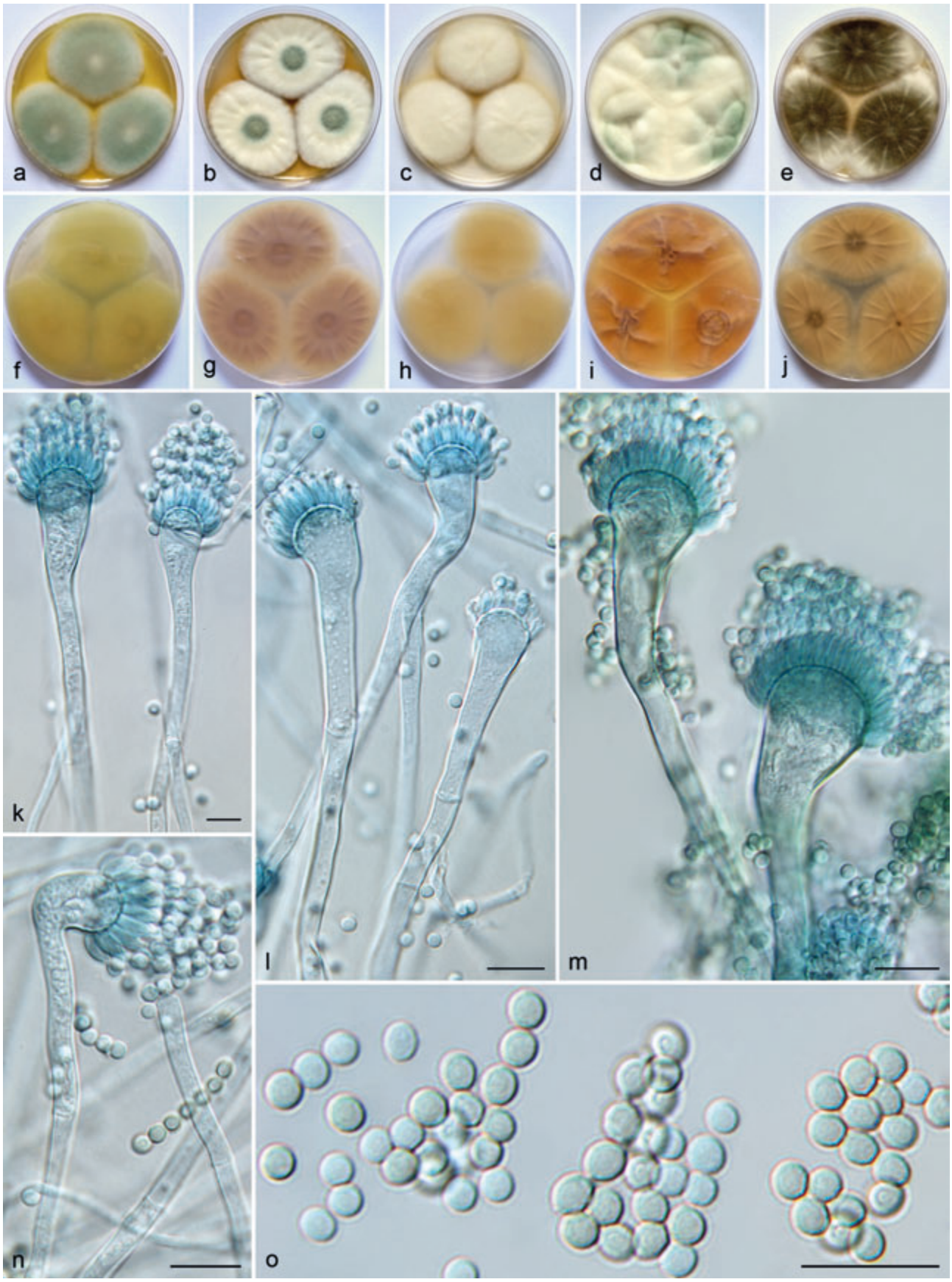

Fig. 14 Micromorphology and macromorphology of *Aspergillus acrensis*. a–e. Colonies of IFM 57291^{T} incubated 7 d at 25 °C on MEA, CYA, CZA, YES, and on CYA at 37 °C (from left to right); f–j. reverse of colonies of IFM 57291^{T} incubated 7 d at 25 °C on MEA, CYA, CZA, YES, and on CYA at 37 °C (from left to right); k–n. conidiophores; o. conidia. — Scale bars = 10 µm.

Some of these species can be differentiated each from the other by their characteristic sexual morph, but the production of ascomata was not induced in *A. acrensis* despite our attempts, similarly to *A. arcoverdensis* and *A. pseudoviridinutans*. Although isolate IFM 57290 was successfully crossed with isolates of *A. udagawae* IFM 46972 and CMF ISB 2190 *in vitro*, both the width and height of ascospores were statistically different from *A. udagawae*. Also, abnormalities in the shape and superficial ornamentation (Fig. 9) were present in a significant number of spores (equatorial crests were absent in ~ 50 % of ascospores). Reliable identification of *A. acrensis* can currently only be achieved by molecular methods.

Aspergillus udagawae Horie et al., Mycoscience 36: 199. 1995.

Epitypification. Brazil, São Paulo State, Botucatú, Lagoa Seka Avea, soil in a plantation, 23 Aug. 1993, *M. Takada* (holotype CBM-FA-0711, designated by Horie et al. (1995), epitype designated here PRM 945579, isoepitypes PRM 945580 and 945581, MycoBank MBT378451, culture ex-epitype IFM 46972 = CBS 114217 = DTO 157-D7 = CBM-FA 0702 = KACC 41155 = CCF 4558).

Notes — Horie et al. (1995) designated the specimen CBM-FA-0711 as a holotype of *A. udagawae*, a dried culture with ascomata created by crossing the isolates CBM-FA-0702 (MAT1-1-1) × CBM-FA-0703 (MAT1-2-1). Although this specimen demonstrates the sexual and asexual morph of the life cycle, it is not suitable for the purposes of the recent taxonomy for several reasons. First of all, it is not clear which of the two cultures contained within the type should be considered the ex-holotype culture. Additionally, interspecific hybrids can be induced by crossing opposite mating type strains of unrelated species *in vitro* as shown in this study and some previous studies (see Discussion), and deposition of a resultant 'hybrid' type could lead to ambiguities. Although this second argument does not apply to *A. udagawae* as both isolates included in the holotype are closely related phylogenetically, we believe that a more clearly defined type of this species will facilitate future taxonomic work. Because it is not possible to recognize which part of the holotype belongs to particular isolate, lectotype designation (in this case part of holotype specimen) is difficult. For this reason we decided to select an epitype PRM 945579 derived from the IFM 46972 (= CBM-FA 0702) culture.

DISCUSSION

Changing species concepts in the AVSC

The AVSC members show considerable phenotypic variability but usually share production of nodding heads (some vesicles borne at an angle to the stipe) and relatively poor sporulation with abundant aerial mycelium. All species have a maximum growth temperature of 42 or 45 °C and the macromorphology and diameter of their colonies are similar, except for *A. viridinutans* and *A. frankstonensis*, which grow more slowly than remaining species. In addition, the morphology of conidiophores and conidia is relatively uniform across species, including the superficial ornamentation of conidia as shown here (Fig. 13). For these reasons heterothallic AVSC members have resisted taxonomic classification and were only identified to a species complex level, until recently.

Due to the absence of taxonomically informative characters, most recently described species in the AVSC were delimited using the GCPSR rules. Using this approach, the species are recognized based on concordance between single-gene phylogenies and the absence of tree incongruities. The GCPSR has found wide application in the taxonomy of fungi (Dettman et al. 2006, Hubka et al. 2013a, Peterson et al. 2015, Visagie et al. 2017). Huge progress has been made recently in the development of statistical methods for multilocus species delimitation, driven by advances in the multispecies coalescent model (Bouckaert et al. 2014, Flot 2015, Fontaneto et al. 2015, Schwarzfeld & Sperling 2015, Jones 2017). Although the ideology of MSC delimitation methods is relatively similar to GCPSR, these methods are more robust because the species are delimited in three steps, i.e., species discovery, species tree construction and species validation (Carstens et al. 2013). The determination of species boundaries is more objective in contrast to GCPSR rules that are based on relatively subjective evaluation and comparison of single-gene trees. In addition, MSC methods are able to deal better with phenomena such as incomplete lineage sorting, recombination or non-reciprocal monophyly that lead to incongruences between single-gene trees. Compared to the phylogenetic analysis of concatenated gene datasets (including partitioned datasets) and in part also GCPSR, the MSC methods are less prone to over-delimitation of species (Degnan & Rosenberg 2006, Kubatko & Degnan 2007, Heled & Drummond 2010, Rosenberg 2013), especially when the results of multiple delimitation methods are compared in one analysis.

The GCPSR rules together with evaluation of limited phenotypic data were recently used for description of *A. felis*, *A. arcoverdensis* and *A. frankstonensis* in the AVSC (Barrs et al. 2013, Matsuzawa et al. 2015, Talbot et al. 2017). Genealogical analysis using five genetic loci was carried out for delimitation of *A. parafelis*, *A. pseudofelis* and *A. pseudoviridinutans*, three close relatives of *A. felis* (Sugui et al. 2014). Although the authors found no conflict between single-gene phylogenies, only two isolates of each of these four species were used in analysis, and sequences of *A. felis*, *A. parafelis* and *A. pseudofelis* strains included were almost invariable. These isolates did not cover sufficiently the genetic diversity of these species as shown here. Species delimitation results based on MSC in this study showed that *A. parafelis* and *A. pseudofelis* are included in the genetically diverse lineage of *A. felis* (Fig. 3).

Table 6 Highest intraspecific pairwise genetic distances in members of *Aspergillus viridinutans* complex (%).

Species (no. of isolates)	Highest genetic distances between two isolates according to different genetic loci					
	benA	*CaM*	*RPB2*	*act*	*mcm7*	*tsr1*
A. acrensis (5)	0.2	0.9	0.2	0	ND	ND
A. arcoverdensis (13)	0	0.9	0.5	1.4	ND	ND
A. aureolus (4)	0.4	0	0.1	0	ND	ND
A. felis (35)	4.2	2.4	0.6	2.5	1.3	3.3
A. frankstonensis (2)	0	0.2	0	0	0	ND
A. pseudoviridinutans (8)	2.6	2.2	1.9	2.1	0.7	1.4
A. siamensis (2)	0	0.1	0.1	0	ND	ND
A. udagawae (25)	1.1	2.8	1.2	4.9	ND	ND
A. wyomingensis (15)	0.4	0.9	0.4	0.9	ND	ND

ND, not determined.

The intraspecific pairwise genetic distances in *A. felis* (Table 6) range from 0.6 % (*RPB2*) to 4.2 % (*benA*). Similarly, pairwise genetic distances in *A. udagawae* (Table 6) are 1.1 % (*benA*) to 4.9 % (*act*). Such high intraspecific diversity in these genetic loci is unusual in *Aspergillus* and it reflects the intense recombination. Thus, when only limited number of strains from such species are selected for phylogenetic analysis, the results of species delimitation techniques may be biased and prone to overestimate the number of species. As we have shown here, this was clearly the case in the study of Sugui et al. (2014). This problem is probably widespread in current fungal taxonomy and limits possibilities of correct species boundaries delimitation. Also in this study, the number of strains of some closely related and phenotypically similar species is underrepresented, e.g., *A. viridinutans* and *A. frankstonensis*. In these cases, the species boundaries cannot be reliably defined using neither GCPSR rules nor MSC-based methods used in this study.

Clinically relevant species and their identification in clinical setting

Although sect. *Fumigati* harbours many important pathogenic species, members of the AVSC have been overlooked by both clinicians and mycologists until recently. The presence of these soil-borne species in clinical material was first reported by Katz et al. (2005) who examined phylogenetic positions of several 'atypical' (poorly sporulating) clinical isolates of *A. fumigatus*. The majority of these strains grouped with, but were not identical to, *A. viridinutans* and *A. aureolus* from the AVSC. Since then many similar epidemiological and clinical studies have reported the pathogenic role of AVSC members in humans and animals, as reviewed by Talbot & Barrs (2018). In humans the most common manifestation of disease is chronic invasive pulmonary aspergillosis in immunocompromised patients. AVSC species are also frequently reported as a cause of sino-orbital aspergillosis (SOA) in cats that is chronic, but frequently fatal. In contrast to humans and dogs, the disease usually affects ostensibly immunocompetent cats. This increasingly recognised clinical entity is most frequently caused by the AVSC species and less frequently by other cryptic species in sect. *Fumigati* (Barrs et al. 2012, 2013, 2014).

Based on the species boundaries redefined in this study, the AVSC encompasses four species that are confirmed opportunistic pathogens. According to a number of reported cases, in humans *A. udagawae* is the most important opportunistic pathogenic from the AVSC followed by *A. felis* and *A. pseudoviridinutans*. In contrast, SOA in cats is most commonly caused by *A. felis* and much less frequently by *A. udagawae* and *A. wyomingensis* (Barrs et al. 2013, 2014).

Medically important species from the AVSC demonstrate elevated minimum inhibitory concentrations (MICs) of itraconazole and voriconazole *in vitro*, and a variable susceptibility to amphotericin B, while posaconazole and echinocandins have potent *in vitro* activities (Lyskova et al. 2018). Since the intraspecific variation in MICs of particular antifungals is usually high, the use of reliable methods for MIC determinations takes precedence over correct identification to a species level. The latter may be challenging or even impossible in the clinical setting. However, identification to the level of species complex and differentiation from *A. fumigatus* is important due to strikingly different antifungal susceptibility patterns.

In contrast to *A. fumigatus*, the AVSC species do not grow at 47 and 50 °C, usually sporulate less and a proportion of their vesicles are borne at an angle to the stipe. In addition, some isolates produce acidic compounds detectable on CREA (Barrs et al. 2013, Nováková et al. 2014, Talbot & Barrs 2018). Despite the fact that ITS rDNA region sequences are not available for all AVSC members, this universal marker for fungal species identification and barcoding can be used to achieve identification to a species complex level. The sequences from all six protein-coding genes included in this study (Table 2) have sufficient discriminatory power for species level identification of all clinically relevant species. Among these genes, sequences of β-tubulin and calmodulin belong to the most commonly used in the clinical practice when correct identification is required (epidemiological studies, outbreak investigations or when dealing with infections refractory to antifungal therapy). However, the discrimination between *A. felis* and *A. pseudoviridinutans* can be limited when using the β-tubulin gene due to the incomplete lineage sorting phenomenon detected in this study (Fig. 3).

Additionally, the increasingly used method of matrix-assisted laser desorption/ionization time-of-flight mass spectrometry (MALDI-TOF MS) gives promising results for rapid and accurate discrimination between *A. fumigatus* and other clinically relevant aspergilli from sect. *Fumigati* (Alanio et al. 2011, Nakamura et al. 2017). The development of more robust, curated and accessible MALDI-TOF spectrum databases should enable the implementation of MALDI-TOF MS for routine identification of less common aspergilli in future. Several PCR assays targeting protein-coding or microsatellite loci have also been developed and show good efficiency in discrimination of less common pathogenic species in sect. *Fumigati* (Araujo et al. 2012, Fernandez-Molina et al. 2014, Chong et al. 2017).

Mating behaviour in the AVSC – heterothallic species

The increasing availability of PCR-based tools for identification of fungal genes responsible for sexual and somatic incompatibility has facilitated the ability to induce the sexual morph in fungi (Dyer & O'Gorman 2011). The characterisation of mating type (MAT) genes became routine when inducing the sexual morph of heterothallic species *in vitro*. Using this approach, the sexual morph has been induced recently in at least five members of sect. *Fumigati* (O'Gorman et al. 2009, Barrs et al. 2013, Swilaiman et al. 2013, Nováková et al. 2014, Hubka et al. 2017). The discovery of a sexual cycle in pathogenic and mycotoxigenic fungi has many important consequences, because fungi with a functional sexual cycle have greater potential to increase their virulence and to develop resistance to antifungals, fungicides, etc. (Kwon-Chung & Sugui 2009, Lee et al. 2010, Swilaiman et al. 2013).

Here, we induced the sexual morph with a relatively high rate of success in *A. felis*, *A. udagawae* and *A. wyomingensis* (Fig. 6). We demonstrated that ascospores of these three species have relatively stable morphology (Fig. 7) and that the size of their ascospores is significantly different from one another (Fig. 6) and can be differentiated by equatorial crest length (Table 5). However, not all opposite mating type strains of the same species are able to produce ascomata *in vitro* as demonstrated in all three mentioned species (Fig. 6). A similar decline in mating capacity was also demonstrated in previous studies on the AVSC (Sugui et al. 2010, Nováková et al. 2014), but also in *A. lentulus* (Swilaiman et al. 2013) and *A. fumigatus* (O'Gorman et al. 2009). These species require relatively rigid conditions to complete their sexual cycle and some crosses produce low numbers of or infertile ascomata or do not mate at all (Balajee et al. 2006, Yaguchi et al. 2007, Kwon-Chung & Sugui 2009, Sugui et al. 2010, Nováková et al. 2014). For instance, fertility between two opposite mating-type isolates may be influenced by the vegetative incompatibility genes (Olarte et al. 2015), regulators of cleistothecium development and hyphal fusion (Szewczyk & Krappmann 2010).

We were not able to induce the sexual morph in three heterothallic members of the AVSC, i.e., *A. acrensis*, *A. arcoverdensis* and *A. pseudoviridinutans*, despite the relatively high number of opposite mating-type strains that was available for the mating

Table 7 Genetic similarities between the ex-type isolates of *Aspergillus viridinutans* complex members based on identities from BLAST similarity search[1].

Species	Genetic similarities between species: *benA I CaM I RPB2* (%)									
	1.	2.	3.	4.	5.	6.	7.	8.	9.	10.
1. *A. acrensis*	–									
2. *A. arcoverdensis*	94.5/95.2/98.0	–								
3. *A. aureolus*	99.6/98.8/99.0	94.5/95.6/98.1	–							
4. *A. felis*	92.0/95.6/97.7	93.4/96.8/97.6	92.4/95.9/97.8	–						
5. *A. frankstonensis*	95.3/94.7/98.0	95.6/97.1/98.3	95.3/94.9/98.2	92.6/96.2/97.7	–					
6. *A. pseudoviridinutans*	94.7/95.2/97.6	95.7/96.0/97.4	94.9/95.5/97.8	95.5/97.6/98.1	96.0/95.3/97.5	–				
7. *A. siamensis*	96.6/95.8/98.9	95.5/95.6/98.5	96.7/96.0/98.9	93.0/95.7/98.2	95.6/94.7/98.0	95.5/95.4/97.9	–			
8. *A. udagawae*	97.4/96.8/99.0	94.7/95.6/98.2	97.4/97.1/99.1	92.0/95.9/97.9	95.3/95.1/98.1	94.5/95.6/97.7	96.2/96.3/99.1	–		
9. *A. viridinutans*	95.3/94.8/98.6	96.5/97.3/99.1	95.5/95.1/98.6	93.8/95.4/98.2	97.5/97.8/98.8	96.5/94.7/97.9	96.3/95.3/98.8	95.6/95.3/98.8	–	
10. *A. wyomingensis*	95.8/96.5/98.6	94.5/96.0/97.8	96.0/96.5/98.3	92.1/96.3/97.5	95.4/95.8/97.6	94.9/95.9/97.3	96.9/96.5/98.9	95.8/96.9/98.6	95.6/95.7/98.3	–

[1] nucleotide BLAST with default setting (http://blast.ncbi.nlm.nih.gov/Blast.cgi).

assays (Fig. 6). It is not clear if these species require different conditions for successful mating, if there are other unidentified pre-zygotic mating barriers between opposite mating type strains, or if they have lost the ability to complete their sexual cycle. The evidence that two of these species were able to mate with different species from AVSC makes the last possibility improbable (Fig. 8, 10). These hybrids can be differentiated from *A. udagawae* and *A. felis*, respectively, by their dimensions (Fig. 8, 10) and surface ornamentation (Fig. 9, 11; Table 5). It demonstrates that both *A. acrensis* and *A. pseudoviridinutans* should be treated as separate taxonomic entities from their related species. Similar deviations in size and surface ornamentation of ascospores were demonstrated in other interspecific hybrids (Fig. 8–11) when they were compared to parental species.

Mating behaviour in the AVSC – homothallic species

Although homothallic species prevail over heterothallic in sect. *Fumigati* (Fig. 1), only two homothallic species are present in the AVSC. It is supposed that heterothallism is ancestral to homothallism in fungi (Nauta & Hoekstra 1992), including *Aspergillus* (Rydholm et al. 2007, Lee et al. 2010). It is obvious from phylogenetic studies across different subgenera of *Aspergillus*, that reproductive strategy is evolutionary conservative and homothallic as well as heterothallic (or asexual) species are typically clustered in clades with a uniform reproductive strategy. For instance in subg. *Aspergillus*, the 31 currently accepted species of sect. *Aspergillus* are all homothallic (Chen et al. 2016a) while sister sect. *Restricti* encompasses 20 asexual and only one distantly related homothallic species, *A. halophilicus* (Sklenář et al. 2017). Similarly, subg. *Polypaecilum* harbours only asexual species (Martinelli et al. 2017, Tanney et al. 2017). Asexual species also predominate in subg. *Circumdati* (Jurjević et al. 2015) although most, if not all, probably have a cryptic sexual cycle as highlighted by sexual morph induction in *A. flavus*, *A. nomius*, *A. parasiticus*, *A. terreus* and *A. tubingensis* (Horn et al. 2009a, b, 2011, 2013, Arabatzis & Velegraki 2013). A strikingly different situation is present in subgenera *Nidulantes* (Chen et al. 2016a, Hubka et al. 2016a), *Fumigati* (Fig. 1) and *Cremei* (Hubka et al. 2016b) where heterothallic and homothallic species interchange like a mosaic along the phylogenetic tree.

Common genetic distances between closely related sister species across aspergilli usually range between 2–4 % in *benA* and *CaM* loci and 1–2 % in *RPB2* locus; the situation in AVSC is very similar (Table 7). Interestingly, there are only few examples of closely related homothallic and heterothallic/asexual species in *Aspergillus* despite their common origin. Genetic similarities between related couples of homothallic and heterothallic/asexual exceeding 95 % are rare, with only two examples in subg. *Circumdati* and one in subg. *Cremei* (Table 8). Section *Fumigati* is exceptional because it contains at least five pairs of highly related homothallic and heterothallic species (Table 8; Fig. 1). *Aspergillus acrensis*, described here, and *A. aureolus* represent the most closely related pair across genus *Aspergillus* (Table 8) and thus could be an ideal model for studying the evolution of reproductive modes. If we accept the hypothesis about the derived origin of homothallic species, it is probable that *A. aureolus* evolved in the lineage of *A. acrensis* relatively recently, due to the extremely low genetic distances of both species. This is also likely the reason why the multilocus species delimitation method STACEY and also some single-locus methods failed to segregate *A. acrensis* from *A. aureolus* (Fig. 2) in this study.

Interspecific hybridization in fungi and its consequences

Interspecific hybridization is an important process affecting speciation and adaptation of micro- and macroorganisms, however,

Table 8 Genetic similarities between selected homothallic species and their most closely related heterothallic / anamorphic relatives across diversity of the genus *Aspergillus*.

Homothallic species (section) – closest heterothallic / anamorphic species	Genetic similarities (%): *benA* / *CaM* / *RPB2*[1]
subg. *Aspergillus*	
A. halophilicus (*Restricti*) – any species	≤ 89
A. montevidensis (*Aspergillus*) – any species	≤ 88
subg. *Circumdati*	
A. alliaceus (*Flavi*) – *A. lanosus*	96.4 / 95.7 / 99.1
A. muricatus (*Circumdati*) – *A. ochraceus*	≤ 91
A. neoflavipes (*Flavipedes*) – *A. micronesiensis*	94.8 / 91.9 / 97.5
A. neoniveus (*Terrei*) – any species	≤ 90
subg. *Cremei*	
A. chrysellus (*Cremei*) – *A. wentii*	97.1 / 97.2 / 97.7
A. cremeus (*Cremei*) – any species	≤ 91
A. stromatoides (*Cremei*) – any species	≤ 93
subg. *Fumigati*	
A. acanthosporus (*Clavati*) – *A. clavatus*	≤ 93
A. aureolus (*Fumigati*) – *A. acrensis*	99.6 / 98.8 / 99.0
A. cejpii (*Clavati*) – any species	≤ 88
A. fischeri (*Fumigati*) – *A. fumigatus*	94.3 / 94.5 / 97.9
A. posadasensis (*Clavati*) – *A. clavatus*	95.1 / 92.6 / 93.5
A. quadricinctus (*Fumigati*) – *A. duricaulis*	92.6 / 95.0 / 99.1
A. siamensis (*Fumigati*) – *A. wyomingensis*	97.1 / 96.5 / 98.9
A. waksmanii (*Fumigati*) – *A. nishimurae*	97.8 / 98.4 / 96.6
subg. *Nidulantes*	
A. discophorus (*Nidulantes*, *A. aeneus* clade) – *A. karnatakaensis*	≤ 92
A. falconensis (*Nidulantes*, *A. nidulans* clade) – *A. recurvatus*	≤ 93
A. monodii (*Usti*) – any species	≤ 90
A. nidulans (*Nidulantes*, *A. nidulans* clade) – any species	≤ 92
A. pluriseminatus (*Nidulantes*, *A. multicolor* clade) – any species	≤ 92
A. purpureus (*Nidulantes*, *A. spelunceus* clade) – any species	≤ 90
A. undulatus (*Nidulantes*, *A. stellatus* clade) – any species	≤ 89

[1] If none of three genetic similarities exceed 95 %, the values are replaced by only one highest value (usually *RPB2* locus).

relatively little is still known about the frequency of hybridization in fungi and its role in evolution of fungal species. Fungal hybrids may form either by a partial or complete sexual cycle or by a parasexual process. Mating between two species may be prevented by pre-zygotic barriers (e.g., gamete recognition) and various post-zygotic barriers (developmental problems, hybrid viability and ability to reproduce, etc.). The disagreement between phylogenetic/morphological species concepts and biological species compatibilities has been repeatedly described in fungi. Phylogenetic divergence in some fungal groups might have preceded development of reproductive barriers as shown by interspecific hybrids induced *in vitro* between primary human and animal pathogenic *Trichophyton* species (Kawasaki et al. 2009, 2010, Anzawa et al. 2010, Kawasaki 2011), opportunistic pathogenic *Candida albicans* and *C. dubliniensis* (Pujol et al. 2004), members of *Aspergillus* sect. *Fumigati* (Sugui et al. 2014, Talbot et al. 2017), mycotoxigenic *A. flavus* and *A. parasiticus* (Olarte et al. 2015), *A. flavus* and *A. minisclerotigenes* (Damann & DeRobertis 2013), phytopathogenic species from the *Fusarium graminearum* complex (Bowden & Leslie 1999) and species of *Neurospora* (Dettman et al. 2003). Natural interspecific hybrids resulting from recombination between species or parasexual reproduction are most commonly reported and have been extensively studied in saprophytic yeasts (González et al. 2008, Sipiczki 2008, Nakao et al. 2009, Louis et al. 2012), the plant endophyte *Epichloë* (Cox et al. 2014, Charlton et al. 2014, Shymanovich et al. 2017) and in various plant pathogenic fungi including species of *Fusarium graminearum* complex (O'Donnell et al. 2004, Starkey et al. 2007), *Ophiostoma* (Brasier et al. 1998, Solla et al. 2008), *Microbotryum* (Gladieux et al. 2010), *Melampsora* (Spiers & Hopcroft 1994, Newcombe et al. 2000), *Botrytis* (Staats et al. 2005), *Verticillium* (Inderbitzin et al. 2011) and *Heterobasidion* (Gonthier et al. 2007, Lockman et al. 2014).

Considering that *in vitro* induction of hybrids is relatively successful, it is surprising that reports on the isolation of naturally occurring hybrids are infrequent in human and animal pathogenic fungi. It suggests that post-zygotic mating barriers play a fundamental role in the maintenance of species boundaries. Naturally occurring hybrids have been detected in yeasts and dimorphic fungi, including between *Candida* spp. (Schröder et al. 2016), *Malassezia* spp. (Wu et al. 2015), *Cryptococcus neoformans* and *C. gattii* (Bovers et al. 2006, 2008, Kwon-Chung & Varma 2006, Aminnejad et al. 2012) and *Coccidioides immitis* and *C. posadasii* (Johnson et al. 2015). However, to date, reports on these hybrids in filamentous fungi are restricted to the *Neocosmospora solani* complex (Short et al. 2013, 2014). Species definition has become a controversial issue in some of these species complexes with naturally occurring hybrids because of differing opinions on species concepts among taxonomists (Kwon-Chung & Varma 2006, Kawasaki 2011, Kwon-Chung et al. 2017).

Even in cases where interspecific hybrids with high fitness and fertility can be demonstrated, the intensity of gene flow between natural populations must be sufficient to oppose genetic drift in order to have a significant impact on genetic isolation of species. In fungi, these processes cannot be evaluated rigorously by *in vitro* mating assays, as these cannot be extrapolated fully to a natural setting (Starkey et al. 2007, Sugui et al. 2014, Hubka et al. 2015a). Indeed, natural interspecific hybrids have never been reported for the majority of species that readily produce hybrids *in vitro*, including *Aspergillus*, dermatophytes and *Neurospora*. The MSC and GCPSR approaches provide practical tools for evaluating the significance of gene flow between natural populations and for assessing species limits. The interpretation of *in vitro* mating assays without a robust phylogeny is thus controversial, because a number of clearly phylogenetically, morphologically and ecologically distinct species lack effective

reproductive barriers. In addition, the evaluation of biological species limits using mating assays requires determination of the fitness and fertility of progeny, which is demanding in both time and cost.

In general, mating success between different species under laboratory conditions is much lower compared to intraspecific mating, suggesting strong reproductive isolation between species and adherence to the biological species concept. In agreement with this, only a limited number of strains with exceptional mating capacity are usually capable of interspecific hybridization with strains of different species, e.g., *A. udagawae* strain IFM 46972 (Fig. 8) or *A. pseudoviridinutans* strain IFM 59502 (Fig. 10).

Several studies demonstrated that interspecific hybrids express genetic abnormalities or have decreased fertility and viability. Genetic analysis of the progeny of a cross between *F. asiaticum* × *F. graminearum* detected multiple abnormalities that were absent in intraspecific crosses of *F. graminearum*, i.e., pronounced segregation distortion, chromosomal inversions, and recombination in several studied linkage groups (Jurgenson et al. 2002, Gale et al. 2005). Matings between *C. neoformans* × *C. gattii* produced only a low percentage of viable progeny. It has been suggested that *C. neoformans* and *C. gattii* produce only stable diploid hybrids, but not true recombinants (Kwon-Chung & Varma 2006). Although Olarte et al. (2015) obtained hybrid progeny of *A. flavus* and *A. parasiticus*, fertile crosses were rare and involved only one parental strain of *A. flavus*. Viable ascospores were extremely rare, suggesting extensive genetic incompatibility and post-zygotic incompatibility mechanisms. Morphologically, the progeny differed from parental strains in growth rate, sclerotium production, stipe length, conidial head seriation and conidial features (Olarte et al. 2015). Decreased viability of hybrid ascospores was also detected among *Neurospora* spp. (Dettman et al. 2003) and in *Aspergillus* sect. *Fumigati*, in addition to abnormalities in their surface ornamentation visualised by SEM (Sugui et al. 2014), which is in agreement with the present study (Fig. 9, 11). Apart from ascospore ornamentation, we also found significant differences in hybrid ascospore dimensions from parental species (Fig. 8, 10).

The relatively recent globalization of trade in horticultural and agricultural plants, and introduction of non-native plant species has resulted in the inadvertent introduction of alien plant pathogens into non-endemic areas, contributing to the emergence of some devastating plant diseases (Brasier 2001, Mehrabi et al. 2011, Dickie et al. 2017). Anthropogenic activities or changes in the distribution of fungi (e.g., in response to climate changes) may bring together related, previously allopatric pathogenic species. Subsequent interspecific hybridization could give rise to pathogens with new features, including adaptation to new niches and host species, and varying degrees of virulence, as evidenced in *Verticillium longisporum*, *Zymoseptoria pseudotritici*, *Blumeria graminis* f. sp. *triticale*, and hybrids between *Ophiostoma novo-ulmi* and *O. ulmi* (Brasier 2001, Schardl & Craven 2003, Depotter et al. 2016).

As far as we know, the occurrence of *Aspergillus* interspecific hybrids in nature has not been proven despite successful hybridization of some species *in vitro*. However, there is no reason to assume that this phenomenon does not occur occasionally. Genetic recombination similar to that found in intraspecific mating occurred in half of the progeny produced by mating *A. fumigatus* with *A. felis*, while the other half were probably diploids or aneuploids (Sugui et al. 2014). Progeny resulting from mating between *A. flavus* and *A. minisclerotigenes* was fertile when crossed with parental strains and the frequency of successful matings was similar to that within pairs of *A. flavus* and *A. minisclerotigenes* strains, respectively (Damann & DeRobertis 2013). Ultimately, the viable hybrid must present some characteristics that promotes its survival (Turner et al. 2010, Mixão & Gabaldón 2018). For instance Olarte at al. (2015) showed that some F_1 progeny of *A. flavus* × *A. parasiticus* produced higher aflatoxin concentrations compared to midpoint parent aflatoxin levels, and some hybrids synthesized G aflatoxins that were not produced by the parents. This suggested that hybridization is an important diversifying force generating novel toxin profiles (Olarte et al. 2015). Although interspecific hybridization in aspergilli is a relatively newly discovered phenomenon, it is likely to have played an important role in the evolution of the genus.

The relationship between hybridization and changes in virulence potential is not well understood in human and animal fungal pathogens but its role in the emergence of novel plant fungal pathogens is well documented, as discussed. The evidence of biological compatibility between major pathogens in *Aspergillus* sect. *Fumigati* sheds new light on possible interspecific transfer of virulence genes, genes responsible for antifungal resistance, and other genes influencing adaptation of these fungi to a changing environment. Further studies should elucidate to what extent interspecific hybridization shaped the evolution of these opportunistic pathogens.

CONCLUSIONS

Based on consensus results of species delimitation methods and after evaluation of mating assay results and phenotypic data, we now recognise 10 species within the AVSC. This number comprises nine previously recognised and one new species proposed here. *Aspergillus pseudofelis* and *A. parafelis* are placed in synonymy with *A. felis*. All four genetic loci used for phylogenetic analysis across the AVSC have sufficient variability for reliable species identification and can be used as DNA barcodes. Though more laborious, the MSC are a suitable tool for delimitation of genetically diverse cryptic species in cases where classical phylogenetic, morphological and mating compatibility data do not yield satisfactory results.

Acknowledgements This research was supported by the project of the Charles University Grant Agency (GAUK 1434217), Czech Science Foundation (No. 17-20286S), Charles University Research Centre program No. 20406, the project BIOCEV (CZ.1.05/1.1.00/02.0109) provided by the Ministry of Education, Youth and Sports of CR and ERDF, and by a Thompson Research Fellowship from the University of Sydney. We thank Milada Chudíčková and Alena Gabrielová for their invaluable assistance in the laboratory, CCF collection staff (Ivana Kelnarová and Adéla Kovaříčková) for lyophilization of the cultures, Miroslav Hyliš for assistance with scanning electron microscopy, Stephen W. Peterson, Kyung J. Kwon-Chung, Adrian M. Zelazny, Maria Dolores Pinheiro and Dirk Stubbe for providing important cultures for this study. Vit Hubka is grateful for support from the Czechoslovak Microscopy Society (CSMS scholarship 2016).

REFERENCES

Alanio A, Beretti J-L, Dauphin B, et al. 2011. Matrix-assisted laser desorption ionization time-of-flight mass spectrometry for fast and accurate identification of clinically relevant Aspergillus species. Clinical Microbiology and Infection 17: 750–755.

Alastruey-Izquierdo A, Mellado E, Peláez T, et al. 2013. Population-based survey of filamentous fungi and antifungal resistance in Spain (FILPOP Study). Antimicrobial Agents and Chemotherapy 57: 3380–3387.

Alcazar-Fuoli L, Mellado E, Alastruey-Izquierdo A, et al. 2008. Aspergillus section Fumigati: Antifungal susceptibility patterns and sequence-based identification. Antimicrobial Agents and Chemotherapy 52: 1244–1251.

Aminnejad M, Diaz M, Arabatzis M, et al. 2012. Identification of novel hybrids between Cryptococcus neoformans var. grubii VNI and Cryptococcus gattii VGII. Mycopathologia 173: 337–346.

Anzawa K, Kawasaki M, Mochizuki T, et al. 2010. Successful mating of Trichophyton rubrum with Arthroderma simii. Medical Mycology 48: 629–634.

Arabatzis M, Velegraki A. 2013. Sexual reproduction in the opportunistic human pathogen Aspergillus terreus. Mycologia 105: 71–79.
Araujo R, Amorim A, Gusmão L. 2012. Diversity and specificity of microsatellites within Aspergillus section Fumigati. BMC Microbiology 12: 154.
Balajee SA, Gribskov J, Brandt M, et al. 2005a. Mistaken identity: Neosartorya pseudofischeri and its anamorph masquerading as Aspergillus fumigatus. Journal of Clinical Microbiology 43: 5996–5999.
Balajee SA, Gribskov JL, Hanley E, et al. 2005b. Aspergillus lentulus sp. nov., a new sibling species of A. fumigatus. Eukaryotic Cell 4: 625–632.
Balajee SA, Kano R, Baddley JW, et al. 2009. Molecular identification of Aspergillus species collected for the transplant-associated infection surveillance network. Journal of Clinical Microbiology 47: 3138–3141.
Balajee SA, Nickle D, Varga J, et al. 2006. Molecular studies reveal frequent misidentification of Aspergillus fumigatus by morphotyping. Eukaryotic Cell 5: 1705–1712.
Barrs V, Beatty J, Dhand NK, et al. 2014. Computed tomographic features of feline sino-nasal and sino-orbital aspergillosis. The Veterinary Journal 201: 215–222.
Barrs VR, Halliday C, Martin P, et al. 2012. Sinonasal and sino-orbital aspergillosis in 23 cats: Aetiology, clinicopathological features and treatment outcomes. The Veterinary Journal 191: 58–64.
Barrs VR, Van Doorn TM, Houbraken J, et al. 2013. Aspergillus felis sp. nov., an emerging agent of invasive aspergillosis in humans, cats and dogs. PLoS One 8: e64871.
Bouckaert RR. 2010. DensiTree: making sense of sets of phylogenetic trees. Bioinformatics 26: 1372–1373.
Bouckaert R[R], Heled J, Kühnert D, et al. 2014. BEAST 2: a software platform for Bayesian evolutionary analysis. PLoS Computational Biology 10: e1003537.
Bovers M, Hagen F, Kuramae EE, et al. 2006. Unique hybrids between the fungal pathogens Cryptococcus neoformans and Cryptococcus gattii. FEMS Yeast Research 6: 599–607.
Bovers M, Hagen F, Kuramae EE, et al. 2008. AIDS patient death caused by novel Cryptococcus neoformans × C. gattii hybrid. Emerging Infectious Diseases 14: 1105–1108.
Bowden RL, Leslie JF. 1999. Sexual recombination in Gibberella zeae. Phytopathology 89: 182–188.
Brasier CM. 2001. Rapid evolution of introduced plant pathogens via interspecific hybridization. Bioscience 51: 123–133.
Brasier CM, Kirk SA, Pipe ND, et al. 1998. Rare interspecific hybrids in natural populations of the Dutch elm disease pathogens Ophiostoma ulmi and O. novo-ulmi. Mycological Research 102: 45–57.
Carbone I, Kohn LM. 1999. A method for designing primer sets for speciation studies in filamentous ascomycetes. Mycologia 91: 553–556.
Carstens BC, Pelletier TA, Reid NM, et al. 2013. How to fail at species delimitation. Molecular Ecology 22: 4369–4383.
Charlton ND, Craven KD, Afkhami ME, et al. 2014. Interspecific hybridization and bioactive alkaloid variation increases diversity in endophytic Epichloë species of Bromus laevipes. FEMS Microbiology Ecology 90: 276–289.
Chen A, Frisvad J, Sun B, et al. 2016a. Aspergillus section Nidulantes (formerly Emericella): polyphasic taxonomy, chemistry and biology. Studies in Mycology 84: 1–118.
Chen A, Varga J, Frisvad JC, et al. 2016b. Polyphasic taxonomy of Aspergillus section Cervini. Studies in Mycology 85: 65–89.
Chen AJ, Hubka V, Frisvad JC, et al. 2017. Polyphasic taxonomy of Aspergillus section Aspergillus (formerly Eurotium), and its occurrence in indoor environments and food. Studies in Mycology 88: 37–135.
Chong GM, Vonk, AG, Meis JF, et al. 2017. Interspecies discrimination of A. fumigatus and siblings A. lentulus and A. felis of the Aspergillus section Fumigati using the AsperGenius® assay. Diagnostic Microbiology and Infectious Disease 87: 247–252.
Coelho D, Silva S, Vale-Silva L, et al. 2011. Aspergillus viridinutans: an agent of adult chronic invasive aspergillosis. Medical Mycology 49: 755–759.
Cox MP, Dong T, Shen G, et al. 2014. An interspecific fungal hybrid reveals cross-kingdom rules for allopolyploid gene expression patterns. PLoS Genetics 10: e1004180.
Damann K, DeRobertis C. 2013. Mating of Aspergillus flavus × Aspergillus minisclerotigenes hybrids: are they functionally mules? Phytopathology 103: S2.32–S2.33.
Degnan JH, Rosenberg NA. 2006. Discordance of species trees with their most likely gene trees. PLoS Genetics 2: e68.
Depotter JR, Seidl MF, Wood TA, et al. 2016. Interspecific hybridization impacts host range and pathogenicity of filamentous microbes. Current Opinion in Microbiology 32: 7–13.
Dettman JR, Jacobson DJ, Taylor JW. 2006. Multilocus sequence data reveal extensive phylogenetic species diversity within the Neurospora discreta complex. Mycologia 98: 436–446.
Dettman JR, Jacobson DJ, Turner E, et al. 2003. Reproductive isolation and phylogenetic divergence in Neurospora: Comparing methods of species recognition in a model eukaryote. Evolution 57: 2721–2741.
Dickie IA, Bufford JL, Cobb RC, et al. 2017. The emerging science of linked plant-fungal invasions. New Phytologist 215: 1314–1332.
Domsch KH, Gams W, Anderson T-H. 2007. Compendium of soil fungi, 2nd taxonomically revised edition. IHW-Verlag, Eching.
Dyer PS, O'Gorman CM. 2011. A fungal sexual revolution: Aspergillus and Penicillium show the way. Current Opinion in Microbiology 14: 649–654.
Eamvijarn A, Manoch L, Chamswarng C, et al. 2013. Aspergillus siamensis sp. nov. from soil in Thailand. Mycoscience 54: 401–405.
Fernandez-Molina JV, Abad-Diaz-de-Cerio A, Sueiro-Olivares M, et al. 2014. Rapid and specific detection of section Fumigati and Aspergillus fumigatus in human samples using a new multiplex real-time PCR. Diagnostic Microbiology and Infectious Disease 80: 111–118.
Flot J-F. 2015. Species delimitation's coming of age. Systematic Biology 64: 897–899.
Fontaneto D, Flot J-F, Tang CQ. 2015. Guidelines for DNA taxonomy, with a focus on the meiofauna. Marine Biodiversity 45: 433–451.
Frisvad JC, Larsen TO. 2015a. Extrolites of Aspergillus fumigatus and other pathogenic species in Aspergillus section Fumigati. Frontiers in Microbiology 6: 1485.
Frisvad JC, Larsen TO. 2015b. Chemodiversity in the genus Aspergillus. Applied Microbiology and Biotechnology 99: 7859–7877.
Frisvad JC, Thrane U. 1987. Standardized high-performance liquid chromatography of 182 mycotoxins and other fungal metabolites based on alkylphenone retention indices and UV-VIS spectra (diode array detection). Journal of Chromatography A 404: 195–214.
Frisvad JC, Thrane U. 1993. Liquid column chromatography of mycotoxins. In: Betina V (eds), Chromatography of mycotoxins: techniques and applications. Journal of Chromatography Library 54: 253–372.
Fujisawa T, Barraclough TG. 2013. Delimiting species using single-locus data and the Generalized Mixed Yule Coalescent approach: a revised method and evaluation on simulated data sets. Systematic Biology 62: 707–724.
Gale LR, Bryant J, Calvo S, et al. 2005. Chromosome complement of the fungal plant pathogen Fusarium graminearum based on genetic and physical mapping and cytological observations. Genetics 171: 985–1001.
Gautier M, Normand A-C, Ranque S. 2016. Previously unknown species of Aspergillus. Clinical Microbiology and Infection 22: 662–669.
Gladieux P, Vercken E, Fontaine MC, et al. 2010. Maintenance of fungal pathogen species that are specialized to different hosts: allopatric divergence and introgression through secondary contact. Molecular Biology and Evolution 28: 459–471.
Glass NL, Donaldson GC. 1995. Development of primer sets designed for use with the PCR to amplify conserved genes from filamentous ascomycetes. Applied and Environmental Microbiology 61: 1323–1330.
Gonthier P, Nicolotti G, Linzer R, et al. 2007. Invasion of European pine stands by a North American forest pathogen and its hybridization with a native interfertile taxon. Molecular Ecology 16: 1389–1400.
González SS, Barrio E, Querol A. 2008. Molecular characterization of new natural hybrids of Saccharomyces cerevisiae and S. kudriavzevii in brewing. Applied and Environmental Microbiology 74: 2314–2320.
Heled J, Drummond AJ. 2010. Bayesian inference of species trees from multilocus data. Molecular Biology and Evolution 27: 570–580.
Horie Y, Miyaji M, Nishimura K, et al. 1995. New and interesting species of Neosartorya from Brazilian soil. Mycoscience 36: 199–204.
Horn BW, Moore GG, Carbone I. 2009a. Sexual reproduction in Aspergillus flavus. Mycologia 101: 423–429.
Horn BW, Moore GG, Carbone I. 2011. Sexual reproduction in aflatoxin-producing Aspergillus nomius. Mycologia 103: 174–183.
Horn BW, Olarte RA, Peterson SW, et al. 2013. Sexual reproduction in Aspergillus tubingensis from section Nigri. Mycologia 105: 1153–1163.
Horn BW, Ramirez-Prado JH, Carbone I. 2009b. The sexual state of Aspergillus parasiticus. Mycologia 101: 275–280.
Hothorn T, Bretz F, Westfall P. 2008. Simultaneous inference in general parametric models. Biometrical Journal 50: 346–363.
Houbraken J, Spierenburg H, Frisvad JC. 2012. Rasamsonia, a new genus comprising thermotolerant and thermophilic Talaromyces and Geosmithia species. Antonie van Leeuwenhoek 101: 403–421.
Hubka V, Dudová Z, Kubátová A, et al. 2017. Taxonomic novelties in Aspergillus section Fumigati: A. tasmanicus sp. nov., induction of sexual state in A. turcosus and overview of related species. Plant Systematics and Evolution 303: 787–806.
Hubka V, Kolařík M. 2012. β-tubulin paralogue tubC is frequently misidentified as the benA gene in Aspergillus section Nigri taxonomy: primer specificity testing and taxonomic consequences. Persoonia 29: 1–10.
Hubka V, Kolařík M, Kubátová A, et al. 2013a. Taxonomical revision of Eurotium and transfer of species to Aspergillus. Mycologia 105: 912–937.

Hubka V, Kubatova A, Mallatova N, et al. 2012. Rare and new aetiological agents revealed among 178 clinical Aspergillus strains obtained from Czech patients and characterised by molecular sequencing. Medical Mycology 50: 601–610.

Hubka V, Nissen C, Jensen R, et al. 2015a. Discovery of a sexual stage in Trichophyton onychocola, a presumed geophilic dermatophyte isolated from toenails of patients with a history of T. rubrum onychomycosis. Medical Mycology 53: 798–809.

Hubka V, Nováková A, Jurjević Ž, et al. 2018. Polyphasic data support the splitting of Aspergillus candidus into two species; proposal of A. dobrogensis sp. nov. International Journal of Systematic and Evolutionary Microbiology 68: 995–1011. doi: https://doi.org/10.1099/ijsem.0.002583.

Hubka V, Nováková A, Kolařík M, et al. 2015b. Revision of Aspergillus section Flavipedes: seven new species and proposal of section Jani sect. nov. Mycologia 107: 169–208.

Hubka V, Nováková A, Peterson SW, et al. 2016a. A reappraisal of Aspergillus section Nidulantes with descriptions of two new sterigmatocystin producing species. Plant Systematics and Evolution 302: 1267–1299.

Hubka V, Nováková A, Samson R, et al. 2016b. Aspergillus europaeus sp. nov., a widely distributed soil-borne species related to A. wentii (section Cremei). Plant Systematics and Evolution 302: 641–650.

Hubka V, Peterson SW, Frisvad JC, et al. 2013b. Aspergillus waksmanii sp. nov. and Aspergillus marvanovae sp. nov., two closely related species in section Fumigati. International Journal of Systematic and Evolutionary Microbiology 63: 783–789.

Inderbitzin P, Davis RM, Bostock RM, et al. 2011. The ascomycete Verticillium longisporum is a hybrid and a plant pathogen with an expanded host range. PLoS One 6: e18260.

Johnson SM, Carlson EL, Pappagianis D. 2015. Coccidioides species determination: does sequence analysis agree with restriction fragment length polymorphism? Mycopathologia 179: 373–379.

Jones G. 2017. Algorithmic improvements to species delimitation and phylogeny estimation under the multispecies coalescent. Journal of Mathematical Biology 74: 447–467.

Jurgenson J, Bowden R, Zeller K, et al. 2002. A genetic map of Gibberella zeae (Fusarium graminearum). Genetics 160: 1451–1460.

Jurjević Ž, Kubátová A, Kolařík M, et al. 2015. Taxonomy of Aspergillus section Petersonii sect. nov. encompassing indoor and soil-borne species with predominant tropical distribution. Plant Systematics and Evolution 301: 2441–2462.

Kapli P, Lutteropp S, Zhang J, et al. 2017. Multi-rate Poisson tree processes for single-locus species delimitation under maximum likelihood and Markov chain Monte Carlo. Bioinformatics 33: 1630–1638.

Katoh K, Standley DM. 2013. MAFFT multiple sequence alignment software version 7: improvements in performance and usability. Molecular Biology and Evolution 30: 772–780.

Katz ME, Dougall AM, Weeks K, et al. 2005. Multiple genetically distinct groups revealed among clinical isolates identified as atypical Aspergillus fumigatus. Journal of Clinical Microbiology 43: 551–555.

Kawasaki M. 2011. Verification of a taxonomy of dermatophytes based on mating results and phylogenetic analyses. Medical Mycology Journal 52: 291–295.

Kawasaki M, Anzawa K, Mochizuki T, et al. 2009. Successful mating of a human isolate of Arthroderma simii with a tester strain of A. vanbreuseghemii. Medical Mycology Journal 50: 15–18.

Kawasaki M, Anzawa K, Wakasa A, et al. 2010. Matings among three teleomorphs of Trichophyton mentagrophytes. Japanese Journal of Medical Mycology 51: 143–152.

Kelly KL. 1964. Inter-Society Color Council – National Bureau of Standards color name charts illustrated with centroid colors. US Government Printing Office, Washington DC.

Klich MA. 2002. Biogeography of Aspergillus species in soil and litter. Mycologia 94: 21-27.

Kocsubé S, Perrone G, Magistà D, et al. 2016. Aspergillus is monophyletic: evidence from multiple gene phylogenies and extrolites profiles. Studies in Mycology 85: 199–213.

Kretzer A, Li Y, Szaro T, Bruns TD. 1996. Internal transcribed spacer sequences from 38 recognized species of Suillus sensu lato: phylogenetic and taxonomic implications. Mycologia 88: 776–785.

Kubatko LS, Degnan JH. 2007. Inconsistency of phylogenetic estimates from concatenated data under coalescence. Systematic Biology 56: 17–24.

Kwon-Chung KJ, Bennett JE, Wickes BL, et al. 2017. The case for adopting the "species complex" nomenclature for the etiologic agents of cryptococcosis. mSphere 2: e00357-16.

Kwon-Chung KJ, Sugui JA. 2009. Sexual reproduction in Aspergillus species of medical or economical importance: why so fastidious? Trends in Microbiology 17: 481–487.

Kwon-Chung KJ, Varma A. 2006. Do major species concepts support one, two or more species within Cryptococcus neoformans? FEMS Yeast Research 6: 574–587.

Lanfear R, Frandsen PB, Wright AM, et al. 2017. PartitionFinder 2: new methods for selecting partitioned models of evolution for molecular and morphological phylogenetic analyses. Molecular Biology and Evolution 34: 772–773.

Leaché AD, Fujita MK. 2010. Bayesian species delimitation in West African forest geckos (Hemidactylus fasciatus). Proceedings of the Royal Society of London B: Biological Sciences 277: 3071–3077.

Lee SC, Ni M, Li W, et al. 2010. The evolution of sex: a perspective from the fungal kingdom. Microbiology and Molecular Biology Reviews 74: 298–340.

Liu F, Wang M, Damm U, et al. 2016. Species boundaries in plant pathogenic fungi: a Colletotrichum case study. BMC Evolutionary Biology 16: 81.

Liu YJ, Whelen S, Hall BD. 1999. Phylogenetic relationships among ascomycetes: evidence from an RNA polymerse II subunit. Molecular Biology and Evolution 16: 1799–1808.

Lockman B, Mascheretti S, Schechter S, et al. 2014. A first generation Heterobasidion hybrid discovered in Larix lyalli in Montana. Plant Disease 98: 1003.

Louis VL, Despons L, Friedrich A, et al. 2012. Pichia sorbitophila, an interspecies yeast hybrid, reveals early steps of genome resolution after polyploidization. G3: Genes, Genomes, Genetics 2: 299–311.

Lyskova P, Hubka V, Svobodova L, et al. 2018. Antifungal susceptibility of the Aspergillus viridinutans complex: comparison of two in vitro methods. Antimicrobial Agents and Chemotherapy 62: e01927-17. doi: https://doi.org/10.1128/AAC.01927-17.

Martinelli L, Zalar P, Gunde-Cimerman N, et al. 2017. Aspergillus atacamensis and A. salisburgensis: two new halophilic species from hypersaline/arid habitats with a phialosimplex-like morphology. Extremophiles 21: 755–773.

Matsuzawa T, Takaki GMC, Yaguchi T, et al. 2015. Aspergillus arcoverdensis, a new species of Aspergillus section Fumigati isolated from caatinga soil in State of Pernambuco, Brazil. Mycoscience 56: 123–131.

Mayr A, Lass-Flörl C. 2011. Epidemiology and antifungal resistance in invasive aspergillosis according to primary disease-review of the literature. European Journal of Medical Research 16: 153.

McLennan EI, Tucker S, Thrower L. 1954. New soil fungi from Australian heathland: Aspergillus, Penicillium, Spegazzinia. Australian Journal of Botany 2: 355–364.

Mehrabi R, Bahkali AH, Abd-Elsalam KA, et al. 2011. Horizontal gene and chromosome transfer in plant pathogenic fungi affecting host range. FEMS Microbiology Reviews 35: 542–554.

Meyer V, Wu B, Ram AF. 2011. Aspergillus as a multi-purpose cell factory: current status and perspectives. Biotechnology Letters 33: 469–476.

Mixão V, Gabaldón T. 2018. Hybridization and emergence of virulence in opportunistic human yeast pathogens. Yeast 35: 5–20.

Nakamura S, Sato H, Tanaka R, et al. 2017. Ribosomal subunit protein typing using matrix-assisted laser desorption ionization time-of-flight mass spectrometry (MALDITOF MS) for the identification and discrimination of Aspergillus species. BMC Microbiology 17: 100.

Nakao Y, Kanamori T, Itoh T, et al. 2009. Genome sequence of the lager brewing yeast, an interspecies hybrid. DNA Research 16: 115–129.

Nauta M, Hoekstra R. 1992. Evolution of reproductive systems in filamentous ascomycetes. I. Evolution of mating types. Heredity 68: 405–410.

Negri C, Gonçalves S, Xafranski H, et al. 2014. Cryptic and rare Aspergillus species in Brazil: prevalence in clinical samples and in vitro susceptibility to triazoles. Journal of Clinical Microbiology 52: 3633–3640.

Newcombe G, Stirling B, McDonald S, et al. 2000. Melampsora × columbiana, a natural hybrid of M. medusae and M. occidentalis. Mycological Research 104: 261–274.

Nguyen L-T, Schmidt HA, Von Haeseler A, et al. 2015. IQ-TREE: A fast and effective stochastic algorithm for estimating maximum-likelihood phylogenies. Molecular Biology and Evolution 32: 268–274.

Nielsen KF, Månsson M, Rank C, et al. 2011. Dereplication of microbial natural products by LC-DAD-TOFMS. Journal of Natural Products 74: 2338–2348.

Nováková A, Hubka V, Dudová Z, et al. 2014. New species in Aspergillus section Fumigati from reclamation sites in Wyoming (USA) and revision of A. viridinutans complex. Fungal Diversity 64: 253–274.

O'Donnell K. 1993. Fusarium and its near relatives. In: Reynolds DR, Taylor JW (eds), The fungal holomorph: mitotic, meiotic and pleomorphic speciation in fungal systematics: 225–233. CAB International, Wallingford.

O'Donnell K, Ward TJ, Geiser DM, et al. 2004. Genealogical concordance between the mating type locus and seven other nuclear genes supports formal recognition of nine phylogenetically distinct species within the Fusarium graminearum clade. Fungal Genetics and Biology 41: 600–623.

O'Gorman CM, Fuller HT, Dyer PS. 2009. Discovery of a sexual cycle in the opportunistic fungal pathogen Aspergillus fumigatus. Nature 457: 471–474.

Olarte RA, Worthington CJ, Horn BW, et al. 2015. Enhanced diversity and aflatoxigenicity in interspecific hybrids of Aspergillus flavus and Aspergillus parasiticus. Molecular Ecology 24: 1889–1909.
Peterson SW. 2008. Phylogenetic analysis of Aspergillus species using DNA sequences from four loci. Mycologia 100: 205–226.
Peterson SW, Jurjević Ž, Frisvad JC. 2015. Expanding the species and chemical diversity of Penicillium section Cinnamopurpurea. PLoS One 10: e0121987.
Pitt JI, Hocking AD. 2009. Spoilage of stored, processed and preserved foods. In: Pitt JI & Hocking AD (eds), Fungi and food spoilage. Springer, London: 401–421.
Posada D. 2008. jModelTest: phylogenetic model averaging. Molecular Biology and Evolution 25: 1253–1256.
Pujol C, Daniels KJ, Lockhart SR, et al. 2004. The closely related species Candida albicans and Candida dubliniensis can mate. Eukaryotic Cell 3: 1015–1027.
R Core Team. 2015. R: A language and environment for statistical computing. R Foundation for Statistical Computing, Vienna.
Réblová M, Hubka V, Thureborn O, et al. 2016. From the tunnels into the treetops: new lineages of black yeasts from biofilm in the Stockholm metro system and their relatives among ant-associated fungi in the Chaetothyriales. PLoS One 11: e0163396.
Reid NM, Carstens BC. 2012. Phylogenetic estimation error can decrease the accuracy of species delimitation: a Bayesian implementation of the general mixed Yule-coalescent model. BMC Evolutionary Biology 12: 196.
Ronquist F, Teslenko M, Van der Mark P, et al. 2012. MrBayes 3.2: efficient Bayesian phylogenetic inference and model choice across a large model space. Systematic Biology 61: 539–542.
Rosenberg NA. 2013. Discordance of species trees with their most likely gene trees: a unifying principle. Molecular Biology and Evolution 30: 2709–2713.
Rydholm C, Dyer P, Lutzoni F. 2007. DNA sequence characterization and molecular evolution of MAT1 and MAT2 mating-type loci of the self-compatible ascomycete mold Neosartorya fischeri. Eukaryotic Cell 6: 868–874.
Sabino R, Veríssimo C, Parada H, et al. 2014. Molecular screening of 246 Portuguese Aspergillus isolates among different clinical and environmental sources. Medical Mycology 52: 519–529.
Samson RA, Visagie CM, Houbraken J, et al. 2014. Phylogeny, identification and nomenclature of the genus Aspergillus. Studies in Mycology 78: 141–173.
Schardl C, Craven K. 2003. Interspecific hybridization in plant-associated fungi and oomycetes: a review. Molecular Ecology 12: 2861–2873.
Schmitt I, Crespo A, Divakar PK, et al. 2009. New primers for promising single-copy genes in fungal phylogenetics and systematics. Persoonia 23: 35–40.
Schröder MS, De San Vicente KM, Prandini TH, et al. 2016. Multiple origins of the pathogenic yeast Candida orthopsilosis by separate hybridizations between two parental species. PLoS Genetics 12: e1006404.
Schwarzfeld MD, Sperling FA. 2015. Comparison of five methods for delimitating species in Ophion Fabricius, a diverse genus of parasitoid wasps (Hymenoptera, Ichneumonidae). Molecular Phylogenetics and Evolution 93: 234–248.
Shigeyasu C, Yamada M, Nakamura N, et al. 2012. Keratomycosis caused by Aspergillus viridinutans: an Aspergillus fumigatus-resembling mold presenting distinct clinical and antifungal susceptibility patterns. Medical Mycology 50: 525–528.
Short DP, O'Donnell K, Geiser DM. 2014. Clonality, recombination, and hybridization in the plumbing-inhabiting human pathogen Fusarium keratoplasticum inferred from multilocus sequence typing. BMC Evolutionary Biology 14: 91.
Short DP, O'Donnell K, Thrane U, et al. 2013. Phylogenetic relationships among members of the Fusarium solani species complex in human infections and the descriptions of F. keratoplasticum sp. nov. and F. petroliphilum stat. nov. Fungal Genetics and Biology 53: 59–70.
Shymanovich T, Charlton ND, Musso AM, et al. 2017. Interspecific and intraspecific hybrid Epichloë species symbiotic with the North American native grass Poa alsodes. Mycologia 109: 459–474.
Singh G, Dal Grande F, Divakar PK, et al. 2015. Coalescent-based species delimitation approach uncovers high cryptic diversity in the cosmopolitan lichen-forming fungal genus Protoparmelia (Lecanorales, Ascomycota). PLoS One 10: e0124625.
Sipiczki M. 2008. Interspecies hybridization and recombination in Saccharomyces wine yeasts. FEMS Yeast Research 8: 996–1007.
Sklenář F, Jurjević Ž, Zalar P, et al. 2017. Phylogeny of xerophilic aspergilli (subgenus Aspergillus) and taxonomic revision of section Restricti. Studies in Mycology 88: 161–236.
Solla A, Dacasa M, Nasmith C, et al. 2008. Analysis of Spanish populations of Ophiostoma ulmi and O. novo-ulmi using phenotypic characteristics and RAPD markers. Plant Pathology 57: 33–44.
Spiers A, Hopcroft D. 1994. Comparative studies of the poplar rusts Melampsora medusae, M. larici-populina and their interspecific hybrid M. medusae-populina. Mycological Research 98: 889–903.
Staats M, Van Baarlen P, Van Kan JA. 2005. Molecular phylogeny of the plant pathogenic genus Botrytis and the evolution of host specificity. Molecular Biology and Evolution 22: 333–346.
Stamatakis A, Hoover P, Rougemont J. 2008. A rapid bootstrap algorithm for the RAxML web servers. Systematic Biology 57: 758–771.
Starkey DE, Ward TJ, Aoki T, et al. 2007. Global molecular surveillance reveals novel Fusarium head blight species and trichothecene toxin diversity. Fungal Genetics and Biology 44: 1191–1204.
Stewart JE, Timmer LW, Lawrence CB, et al. 2014. Discord between morphological and phylogenetic species boundaries: incomplete lineage sorting and recombination results in fuzzy species boundaries in an asexual fungal pathogen. BMC Evolutionary Biology 14: 38.
Sugui JA, Kwon-Chung KJ, Juvvadi PR, et al. 2015. Aspergillus fumigatus and related species. Cold Spring Harbor Perspectives in Medicine 5: a019786.
Sugui JA, Peterson SW, Figat A, et al. 2014. Genetic relatedness versus biological compatibility between Aspergillus fumigatus and related species. Journal of Clinical Microbiology 52: 3707–3721.
Sugui JA, Vinh DC, Nardone G, et al. 2010. Neosartorya udagawae (Aspergillus udagawae), an emerging agent of aspergillosis: How different is it from Aspergillus fumigatus? Journal of Clinical Microbiology 48: 220–228.
Swilaiman SS, O'Gorman CM, Balajee SA, et al. 2013. Discovery of a sexual cycle in Aspergillus lentulus, a close relative of A. fumigatus. Eukaryotic Cell 12: 962–969.
Szewczyk E, Krappmann S. 2010. Conserved regulators of mating are essential for Aspergillus fumigatus cleistothecium formation. Eukaryotic Cell 9: 774–783.
Talbot JJ, Barrs VR. 2018. One-health pathogens in the Aspergillus viridinutans complex. Medical Mycology 56: 1–12.
Talbot JJ, Houbraken J, Frisvad JC, et al. 2017. Discovery of Aspergillus frankstonensis sp. nov. during environmental sampling for animal and human fungal pathogens. PLoS One 12: e0181660.
Tanney JB, Visagie CM, Yilmaz N, et al. 2017. Aspergillus subgenus Polypaecilum from the built environment. Studies in Mycology 88: 237–267.
Turner E, Jacobson D, Taylor JW. 2010. Reinforced postmating reproductive isolation barriers in Neurospora, an Ascomycete microfungus. Journal of Evolutionary Biology 23: 1642–1656.
Vinh DC, Shea YR, Jones PA, et al. 2009. Chronic invasive aspergillosis caused by Aspergillus viridinutans. Emerging Infectious Diseases 15: 1292–1294.
Visagie CM, Yilmaz N, Renaud JB, et al. 2017. A survey of xerophilic Aspergillus from indoor environment, including descriptions of two new section Aspergillus species producing eurotium-like sexual states. MycoKeys 19: 1–30.
White TJ, Bruns T, Lee S, et al. 1990. Amplification and direct sequencing of fungal ribosomal RNA genes for phylogenetics. In: Innis MA, et al. (eds), PCR protocols: a guide to methods and applications: 315–322. Academic Press, San Diego.
Wickham H. 2009. ggplot2: Elegant Graphics for Data Analysis. Springer-Verlag, New York.
Wu G, Zhao H, Li C, et al. 2015. Genus-wide comparative genomics of Malassezia delineates its phylogeny, physiology, and niche adaptation on human skin. PLoS Genetics 11: e1005614.
Xia X. 2017. DAMBE6: new tools for microbial genomics, phylogenetics, and molecular evolution. Journal of Heredity 108: 431–437.
Yaguchi T, Horie Y, Tanaka R, et al. 2007. Molecular phylogenetics of multiple genes on Aspergillus section Fumigati isolated from clinical specimens in Japan. Japanese Journal of Medical Mycology 48: 37–46.
Yang Z, Rannala B. 2010. Bayesian species delimitation using multilocus sequence data. Proceedings of the National Academy of Sciences 107: 9264–9269.
Yu G, Smith DK, Zhu H, et al. 2017. ggtree: an R package for visualization and annotation of phylogenetic trees with their covariates and other associated data. Methods in Ecology and Evolution 8: 28–36.
Zhang J, Kapli P, Pavlidis P, et al. 2013. A general species delimitation method with applications to phylogenetic placements. Bioinformatics 29: 2869–2876.